12-1-2014

Ore Classification and Breccia Formation in the 144 Zone Gold Deposit: A Chemical Replacement Model, Bare Mountain Range, Nevada

William Thomas Fischer
University of Nevada, Las Vegas, fischerw@unlv.nevada.edu

ORE CLASSIFICATION AND BRECCIA FORMATION IN THE 144 ZONE GOLD DEPOSIT: A CHEMICAL REPLACEMENT MODEL, BARE MOUNTAIN RANGE, NEVADA

By

William T. Fischer

Bachelor of Science in Geology
St. Norbert College
2012

A thesis submitted in partial fulfillment
of the requirements for the

Master of Science - Geoscience

Department of Geoscience
College of Sciences
The Graduate College

University of Nevada, Las Vegas
December 2014

UNLV | GRADUATE COLLEGE

We recommend the thesis prepared under our supervision by

William Thomas Fischer

entitled

Ore Classification and Breccia Formation in the 144 Gold Deposit: A Chemical Replacement Model, Bare Mountain, Nevada

is approved in partial fulfillment of the requirements for the degree of

Master of Science - Geoscience

Department of Geoscience

Jean S. Cline, Ph.D., Committee Chair

Rodney M. Metcalf, Ph.D., Committee Member

Ganqing Jiang, Ph.D., Committee Member

Barbara Luke, Ph.D., Graduate College Representative

Kathryn Hausbeck Korgan, Ph.D., Interim Dean of the Graduate College

December 2014

ABSTRACT

Ore Classification and Breccia Formation in the 144 Zone Gold Deposit: A Chemical Replacement Model Bare Mountain Range, Nevada

By

William T. Fischer

Dr. Jean S. Cline, Examination Committee Chair

Professor

University of Nevada, Las Vegas

The 144 Zone is an oxidized, breccia-hosted, disseminated gold deposit that formed along the contact between Early Cambrian Carrara Formation limestone and overlying Bonanza King Formation dolomite within the Bare Mountain range in southern Nevada. Gold mineralization occurs within a breccia body that contains a variety of breccia types. Research goals of this project included classifying clay, oxide and other minerals as well as breccia types to identify the habits of gold mineralization and the minerals associated with gold. Research was also aimed at determining the paragenesis of Au mineralization and brecciation in the 144 Zone. Underground mapping provided spatial relationships between breccia types, host rocks and alteration assemblages. Clay minerals and the effects of a post-ore oxidation event have made it difficult to identify primary mineral assemblages; however, samples of different breccia types collected along transects from low to no Au to high grade were analyzed using transmitted and reflected light petrography, applied reflectance spectroscopy, secondary electron microscopy, and electron probe microanalysis to characterize mineral assemblages, identify clay and oxide minerals, and locate gold.

Two main breccia types have been identified. Breccia type 1 (BT1) has clasts composed of dolomite, phengitic dolomite and quartz with goethite cemented by a quartz-rich matrix; breccia type 2 (BT2) has clasts consisting of dolomite, phengitic dolomite and quartz with goethite cemented by a matrix of dominant phengite and goethite and minor quartz. Neither breccia type has a preferred association with high gold grades.

Clast and matrix compositions and textures show that both breccia types formed simultaneously by selective replacement of the lower-most Bonanza King dolomite. Fluid-rock reactions transformed the dolomite into having the appearance of clasts. Quartz replacement of dolomite and precipitation of pyrite, Au and phengite produced the matrices of BT1 and BT2.

Gold is most closely associated with cubic goethite that replaced pyrite, but is also closely related to anhedral goethite. Gold is located in pitted zones of goethite and along the contact of goethite with quartz. Quartz is typically associated with and encloses Au-bearing goethite.

Clay minerals include relatively common high-temperature phengite with minor to trace kaolinite, montmorillonite, smectite, and phengitic illite. Although phengite is the most abundant clay, it is not consistently spatially associated with gold at the sample scale, though it may be at the deposit scale.

The geologic constraints that characterize gold mineralization in the 144 Zone can be applied to exploration throughout Bare Mountain for additional gold that formed under similar conditions. This study suggests that the important geological controls were the Carrara-Bonanza King contact, the presence of reactive lowermost Bonanza King dolomite, and the presence of a quartz latite dike. Locating other localities of this contact at fault or dike intersections that could have provided conduits for gold-bearing fluids can provide future drill targets.

ACKNOWLEDGEMENTS

First and foremost, I would like to thank my advisor, Dr. Jean Cline, for always making herself available to entertain and answer questions, discuss my ideas, advise me, and for taking on this project. Thank you, Jean for taking me on as one of your students and for making me a better geologist and a more proficient scientific writer.

A special thanks must also be given to Patrick McAndless, former Vice President of Exploration for Imperial Metals Corporation, for the time he dedicated to assisting me throughout this project. Pat made frequent visits to UNLV in order to assist me in collecting, interpreting and organizing the data I collected. Without Pat, this research project would not exist. Thank you for making this project possible and for sharing your passion and wisdom with me.

I am also grateful to the Imperial Metals Corporation for funding this project, and Imperial Metals engineer Greg Gillstrom for assisting me in developing cross-sections and maps for this project. I also thank Sterling Gold Corporation, specifically Chuck Stevens for backing this project. Kevin Garceau and Jetzen Loo are also thanked for assisting in so many aspects of this study including sample collection, accompanying me in the underground workings of the mine, and for generating digital images that assisted in making figures and underground maps. I would also like to thank all the miners at the Sterling Gold mine for their assistance.

In addition, I would like to acknowledge Corvus Gold Incorporated and the entire North Bullfrog team, especially Russell Meyers, Leisa Meitl, Chris Brown, and Mark Reischman for teaching me about applied SWIR spectroscopy and providing me with TerraSpec analyses and interpretation. I would also like to thank Dick Tosdal and Scott Halley for their interpretation of the TerraSpec data.

Special thanks must also be given to Minghua Ren at the UNLV EMiL lab for assisting me with collecting SEM and EPMA data, Bryan Eleogram for assisting me with underground

mapping, and the Society of Economic Geologists (SEG) and the UNLV Graduate and Professional Student Association (GPSA) for the grants and scholarships that I was awarded throughout my graduate study.

Finally I would like to thank my family and friends. Thank you for all the love and support you have provided me throughout this journey. You provided me with the emotional encouragement that was critical in the completion of this project. I will be eternally thankful for your support.

TABLE OF CONTENTS

LIST OF TABLES

LIST OF FIGURES

CHAPTER 1

INTRODUCTION

The state of Nevada is a known locality for gold mineralization, currently accounting for more than 76% of US gold production, making it the 4th largest gold producer in the world (Nevada Bureau of Mines and Geology, 2012). The Bare Mountain district, located in southern Nevada approximately 15 km southwest of Beatty, Nevada, has produced more than 200,000 ounces of gold (Gillstrom, 2006) making it an intriguing location for further gold exploration.

The 144 Zone, a breccia-hosted gold deposit, was discovered in 2001 in the Bare Mountain district. The deposit is located on the east side of the Bare Mountain range (Fig. 1). The 144 Zone breccia is entirely oxidized and occurs along the contact of the Bonanza King and Carrara Formations, two carbonate-dominated formations. Previous work completed by Taylor et al. (2011) established the extent of the ore body and defined the 144 Zone as a hydrothermal breccia. Although defined as a hydrothermal breccia, no detailed breccia formation model was proposed. Taylor et al., (2011) proposed that brecciation was caused by high- and low-angle Tertiary normal faulting. Two different breccia types were characterized by Taylor et al. (2011) based on variations in alteration. One breccia was described as having a silica matrix and the other breccia was described as being clay-rich. Taylor et al. (2011) proposed that the silica matrix breccia pre-dated the clay-rich breccia based on cross-cutting relationships between the silica matrix and the clay-rich matrix.

This study expands on the preliminary observations and research on the 144 Zone deposit to determine how gold was deposited, where gold is located, to identify the breccia types of the 144 Zone, to determine the alteration minerals associated with gold deposition and different breccia types, and to identify the relationship between gold deposition and formation of the 144 Zone breccia. Methods employed included characterizing the ore, gangue, and alteration minerals and identifying features related to gold mineralization through optical petrography, spectral reflectance data, scanning electron microscopy, and electron probe microanalysis on a large suite of samples collected from drill core, surface outcrop, and the underground workings of the 144 Zone. By determining the location of native Au and confirming the minerals associated with Au, we identified minerals that are indicators for high Au concentrations. In addition, breccia types were classified based on physical and mineralogical characteristics in an attempt to identify breccia types associated with gold grade and to determine the processes that formed the breccia and the 144 zone gold deposit. This study generated a model for 144 Zone breccia formation that expands the understanding of breccia formation and will guide future exploration for similar deposits within the district.

This study determined that alteration minerals comprise both breccia clasts and matrix and confirmed the presence of secondary quartz, phengite, and pyrite, which are common minerals associated with other epithermal gold deposits. Native Au within the 144 Zone occurs as submicrometer particles, undetectable with the naked eye, and which are spatially related to microscopic goethite after pyrite. Additionally, this study confirmed the presence of two distinct breccia types, both of which formed by

hydrothermal alteration of Bonanza King dolomite. Both breccia formations were coincident with gold deposition.

CHAPTER 2

BACKGROUND GEOLOGY

Stratigraphy

Stratigraphic units within Bare Mountain date from Late Proterozoic carbonate and siliciclastic formations (Fig. 2) to Early Tertiary volcanic rocks (Fig. 3) and conglomerates. A passive margin sequence is composed of Late Proterozoic Sterling Quartzite, Late Proterozoic to Early Cambrian Wood Canyon Formation, and Early Cambrian Zabriskie Quartzite, Carrara Formation, and Bonanza King Formation (Stewart, 1970). The timing of passive margin deposition has been interpreted as during the Late Proterozoic and Early Cambrian (600 to 555 Ma) (Stewart, 1970).

The Sterling Quartzite was described by Stewart (1970) and was divided into 5 members (A, B, C, D, E). Members A, C, D, and E (587.2 meters thick) are present within Bare Mountain and are predominantly composed of yellowish-gray to purplish quartzite and conglomerate with minor siltstone and trace dolomite. Interbedded dolomite is found in the upper members of the Sterling quartzite (Stewart, 1970; Monsen et al., 1991).

The Wood Canyon Formation was described and divided into three members by Stewart (1970) and Monsen et al., (1991). The formation is a westward thickening wedge predominately composed of siliciclastic rocks (Cornwall and Kleinhampl, 1964). The three members consist of greyish-green siltstone, lesser yellowish-grey quartzite, greyish-green siltstone and shale, and light brown-weathering dolomite and limestone beds.

Dolomite and limestone beds are present in the lower and upper members (Stewart, 1966).

The Cambrian Zabriskie Quartzite (347.7 meters thick) is defined by Stewart (1970) as a cliff-forming, pale-red, fine- to medium-grained orthoquartzite that is thick-bedded, laminated and cross-stratified (Fig. 2). The basal contact grades down from quartzite to pelitic rocks of the Wood Canyon Formation. A sharp break in slope marks the contact between these two formations in the field (Stewart, 1970).

The Cambrian Carrara Formation was named, described and mapped by Cornwall and Kleinhampl (1961, 1964) and mapped by Monsen et al. (1991). A detailed description of the Carrara Formation within Bare Mountain was published by Palmer and Halley (1979). The Carrara Formation is heterogeneous, consisting primarily of marine sediments comprised of interstratified thin- to medium-bedded shale and dark-grey limestone with minor sandstone and siltstone. This formation represents the transition between dominantly quartzitic Lower Cambrian rocks and predominantly calcareous Middle and Upper Cambrian rocks. The Carrara Formation has been divided into nine members, three of which have been identified at Bare Mountain (Cornwall and Kleinhampl, 1961; Palmer and Halley, 1979). The Lower Carrara (87 meters thick) contains alternating beds of sandstone, siltstone, shale, phyllite, schist, micaceous quartzite and limestone (Cornwall and Kleinhampl 1961; 1964). Its lower contact with the Zabriskie Quartzite is defined in the field by a transition from orthoquartzite to limestone (Cornwall and Kleinhampl, 1961; Palmer and Halley, 1979). The Middle Carrara (62 meters thick) is equivalent to the Gold Ace Limestone Member of the Carrara Formation (Palmer and Halley, 1979). The Middle Carrara is a cliff-forming, thick-

bedded, dark grey limestone with pelitic slope-forming sequences. The contact of the Middle Carrara with the lower Carrara is sharp (Palmer and Halley, 1979). The Upper Carrara (200 meters thick) is a slope-forming succession of intercalated thin- to medium-bedded, dark greenish-grey phyllite, schist, micaceous quartzite, and medium to dark grey limestone with orange bands of chert. Terrigenous rocks decrease in abundance in the upper part of this section. The basal contact of the Upper Carrara with the Middle Carrara is sharp and is indicated by the lowermost dark grey limestone with orange bands of chert. Intervals of medium-bedded algal limestone form resistant sequences at the top and near the middle of the Upper Carrara (Palmer and Halley, 1979).

The Bonanza King Formation was measured, mapped and described in Bare Mountain by Cornwall and Kleinhampl (1961) and mapped by Monsen et al., (1991). The measured thickness is 1,159 meters. The Bonanza King Formation is divided into two members: The lower Papoose Lake Member and the overlying Banded Mountain Member. The Papoose Lake Member (579.5 meters thick) consists of cliff-forming, white to dark grey dolomite and limestone intercalated with sparse but distinctive yellowish, silty-sandy intervals. The basal contact of the Papoose Lake Member with the Carrara Formation is defined as the base of white, silty dolomite and limestone above dark grey limestone. The lower Papoose Lake Member is typically white dolomite and limestone with yellowish-orange silty laminae of phengite. The upper Papoose Lake Member consists of silty and sandy dolomite, which grades downward into an interval consisting of medium- to thick-bedded dolomite and limestone with interspersed silty sandy beds.

The overlying Banded Mountain Member (579.5 meters) is divided into two parts. The lower Banded Mountain Member (396.5 meters) consists of cliff-forming dolomite and limestone that is distinctively striped in alternating light to dark grey bands. The basal contact is sharp and is defined by a pale orange band. The upper Banded Mountain Member (183 meters) is composed of cliff-forming, crystalline, thickly bedded dolomite varying in color from light to dark grey. The basal contact is sharp and mapped at a dark-grey band (Monsen et al., 1991).

Igneous Rocks

Quartz latite flows and intrusive rocks within Bare Mountain and the surrounding area are interpreted to be products of the Southwest Nevada Volcanic Field (SWNVF) (Mills et al., 1997) (Fig. 3). The SWNVF is a silicic multi-caldera volcanic field that formed during the eruption of the Crater Flat, Paintbrush, and Timber Mountain Group tuffs that formed from approximately 4500 km^3 of metaluminous magma that erupted in three stages from 15.1 to 7.5 Ma (Sawyer et al., 1990). The main magmatic stage erupted from 15.1 to 12.7 Ma and was responsible for the emplacement of the Crater Flat Tuff Group. The timber mountain volcanic eruptive sequence began at 12.7 Ma and ceased by 9.5 Ma. The late magmatic stage began shortly after 9.4 Ma and lasted until 7.5 Ma. The rocks of the Timber Mountain and Paintbrush Tuff Groups were deposited during timber mountain volcanic stage and the late magmatic stage, respectively (Sawyer et al., 1990; Mills et al., 1997). The SWNVF is comprised mainly of felsic ash flow tuffs and lesser rhyolite flows. Volcanism in the SWNVF coincided with peak Basin and Range extensional deformation (Sawyer et. al., 1994). Although regional extension was

concurrent with volcanism associated with the SWNVF, the two events have not been genetically linked (Sawyer et. al., 1994).

Quartz latite flows and intrusive bodies of the Crater Flat Group are scarce throughout Bare Mountain and, where present, consistently trend north-south. Carr (1984) described the quartz latite intrusions. Weathered quartz latite surfaces appear greyish-orange to pale yellowish orange while fresh surfaces are whitish-red to pale grey-pink silicic porphyries. Quartz latite porphyries consist of phenocrysts as large as 2 mm of sanidine, quartz, plagioclase and biotite. The groundmass is predominantly fine crystalline sanidine, plagioclase and quartz with sparse oxide minerals. Dikes can range up to 20 meters wide and intrude Proterozoic and Paleozoic rocks. Biotite from this unit has yielded a K-Ar age of 13.9 Ma +/- 0.1 Ma (Carr, 1984). The Crater Flat Group is interpreted to have erupted from the Crater Flat-Prospector Pass caldera complex. The caldera is located within Crater Flat valley, east of Bare Mountain (Noble et al., 1991).

Regional Tectonic History

Late Proterozoic rifting of the western margin of North America is described by Stewart (1970) and Levy and Christie-Blick (1991). Proterozoic rifting led to the deposition of siliciclastic and carbonate rocks that host the 144 Zone gold deposit (Stewart, 1970). Based on subsidence analysis and geologic observations in the field, initiation of rifting, which led to westward thickening of the shallow marine miogeocline (Stewart, 1970), is proposed to be older than 700 Ma. Rifting ceased at approximately 545 Ma. The lack of preserved upper crustal rifting evidence and a poor fossil record in the latest Proterozoic and Lower Cambrian strata have made the age of rifting difficult to constrain (Levy & Christie-Blick 1991).

Regional compression during the Late Permian to Early Triassic, associated with the Golconda thrust, established a coeval belt of compressional deformation that extended through Death Valley and Bare Mountain (Snow, et. al., 1991). Compressional tectonism caused thrusting of Late Proterozoic siliciclastic rocks over early Cambrian carbonate rocks within Bare Mountain, along the Sterling thrust (Fig. 4). The Sterling thrust was responsible for uplifting and placing the Sterling Quartzite and Wood Canyon Formation on top of Bonanza King and Carrara Formations (Snow, et. al., 1991).

A transition from compression to extension began in North America in the mid-Eocene (45 Ma) as a result of decoupling of the Farallon plate from the North American plate. This decoupling event allowed hot asthenospheric mantle to interact with the North American plate, resulting in high K calc-alkaline magmatism in Nevada that swept from north to south (Armstrong and Ward, 1991). Magmatism associated with this decoupling event occurred between 15.1 Ma and 7.5 Ma in Bare Mountain (Sawyer et al., 1990).

At approximately 15 Ma, Basin and Range style extension initiated in the Bare Mountain range (Hoisch, 2000) resulted in high-angle normal faults, low-angle detachment faults, and tilted fault blocks separated by Late Miocene to Quaternary alluvium (Stewart, 1980; Wernike et al., 1988). High-angle normal faults in Bare Mountain typically trend north-south and bound the eastern and western flanks of the range. The north end of the range has been terminated by the Fluorspar Canyon detachment fault (Fig. 4). The detachment fault dips moderately to the north at 40° (Morealli and Anderson, 2008) and separates Precambrian and Paleozoic rocks to the south from the Miocene volcanic rocks related to the SWNVF to the north.

Thermochronology data completed by Hoisch (2000) indicate a final unroofing age of 12.6 to 11.1 Ma along the fault. Basin and Range faulting in Bare Mountain is thought to have continued into the Quaternary. These young faults represent the final stages of the Basin and Range extensional regime (Carr, 1984; Hamilton, 1988).

Dextral motion along the Pacific and North American plate boundaries at approximately 8 to10 Ma began to be accommodated by the Walker Lane tectonic belt, which is located at the western extent of the Basin and Range along the California-Nevada border (Fig. 1) (Anderson, et. al., 2011). The Walker Lane exhibits dextral strike-slip movement and extensional movement that has been documented in Basin and Range-related normal faults (Wesnousky, 2005). Taylor et al. (2011) interpreted dextral strike-slip movement along faults within Bare Mountain as associated with movement along the Walker Lane. Several Au-Ag epithermal deposits have formed within the Walker Lane (Faulds and Henry, 2008).

Bare Mountain Geology

The Late Precambrian to Late Paleozoic sedimentary rocks of Bare Mountain have been deformed by large-scale folding. Folding may have been caused by low-angle thrust faults and right-lateral faulting during the late Paleozoic or Mesozoic (Cornwall and Kleinhampl, 1961). The majority of the rocks dip to the north in successive blocks that are separated by thrust and tear faults (Longwell, 1961) (Fig. 4).

Bare Mountain District Ore Deposit Geology

Several gold deposits, including the 144 Zone, have been discovered within Bare Mountain and in the nearby Bullfrog Hills (Fig. 5). Gold was first discovered between

1904 and 1905 (Ransome, 1910; Lincoln, 1923) at the original Bullfrog mine. The Bare Mountain district, also known as the Fluorine district, has produced a variety of materials including fluorite (Daisy, Goldspar and Mary mines), ceramic silica (Silicon mine), mercury (Thompson and Telluride mines) and volcanic cinders from 1918 until 1989. Gold occurrences in Bare Mountain share similar host rocks, secondary minerals, and gold mineralization styles.

Sterling Deposit

The Sterling deposit, located along the eastern flank of the Bare Mountain range, is a sediment-hosted disseminated Au deposit that is located stratigraphically above the 144 Zone (Fig. 5). The deposit occurs within the Sterling thrust, which has placed the Wood Canyon Formation over the Bonanza King Formation. Mineralization is located along the intersection of normal faults that intersect the Sterling thrust fault (Odt, 1983; Tingley, 1984; Jackson, 1988). Native gold is associated with kaolinite, illite, sericite, jarosite, and alunite in the Bonanza King Formation, Wood Canyon Formation and hydrothermally altered porphyry dikes (Odt, 1983). Gold is microscopic, reaching 4 micrometers in diameter and is associated with pyrite, oxide minerals, clay, or calcite and is located within breccias (Odt, 1989).

Goldspar Deposit

The Goldspar deposit is an historic subeconomic gold and fluorite prospect located north of the 144 Zone (Fig. 5). Native gold is located within a high-angle breccia pipe that has developed within the Nopah Formation. The Nopah Formation is Cambrian to Ordovician in age and is located stratigraphically above the Bonanza King Formation.

The breccia pipe consists of Tertiary volcanic clasts exclusively (Tingley, 1984; Jackson, 1988). Fluorite in the deposit is located within a felsic intrusion that has intruded the carbonate host rock. This deposit has not been well characterized and has never been developed into a producing gold mine (Horton, 1961).

Telluride Mine

Gold mineralization in the Telluride mine is associated with quartz, opal, alunite and pyrite along the Fluorspar Canyon detachment fault (Figs. 4, 5). Gold occurs in altered quartz latite porphyry dikes that intrude Cambrian-Ordovician carbonate rocks of the Nopah Formation, located stratigraphically above the Bonanza King Formation in the footwall of the detachment fault (Jackson, 1988). Mercury was also mined from pipe-like breccia bodies (Tingley, 1984).

Mother Lode Mine

The Mother Lode gold mine is situated north of the Telluride mine, near the most northeastern exposure of the Fluorspar Canyon detachment fault (Figs. 4, 5). Disseminated gold mineralization is present in felsic porphyry dikes and in adjacent interbedded sandstone, siltstone and limestone of the Mississippian Eleana Formation. Alteration is primarily illite+/-sericite+/-calcite with pyrite in unoxidized rocks and with jarosite in oxidized rocks (Mapa, 1990; Castor and Weiss, 1992).

Secret Pass Deposit

Disseminated gold in the Secret Pass deposit is hosted in altered ash-flow tuff of the Bullfrog Member of the Crater Flat Tuff Group. The deposit is bounded by the underlying Fluorspar Canyon detachment fault (Figs. 4, 5) that dips to the north at 40°

(Morealli and Anderson, 2008). Alteration and gangue minerals associated with gold include quartz, adularia, calcite and pyrite (Greybeck and Wallace, 1991).

Gold Ace Property

Gold was discovered at the Gold Ace property in 1913 but the claim was abandoned in 1936 (Figs. 4, 5). Production of an unknown amount of gold is suggested by the presence of a small mill and a tailings pile. Gold mineralization was reported in bedding plane shear zones and veins within the Sterling Quartzite (Cornwall, 1972).

Bullfrog District

The Bullfrog district is located in the Bullfrog Hills, north of the town of Beatty, Nevada (Fig. 5). The district contains gold-silver veins and disseminated mineralization that accounts for the largest known precious metal resource in the SWNVF (Sawyer, et al., 1990). The Bullfrog Hills district accounted for approximately 112,000 ounces of gold and 869,000 ounces of silver from 1904 until 1921 (Ransome et. al., 1910, Cornwall, 1972; Castor and Weiss, 1992).

Deposits are hosted within rhyolite ash-flow tuff units that date between 14 and 11 Ma (Carr et al., 1986). Mineralization is located within low- and high-angle faults associated with Basin and Range extension. Alteration assemblages associated with Au-Ag mineralization include adularia, sericite/illite, and quartz replacing calcite (Castor and Weiss, 1992). Mineralization is interpreted to be associated with the Late and Timber Mountain Magmatic stages of the SWNVF at approximately 9-10 Ma (Jackson; 1988; Marvin, et. al., 1989; Noble, et. al., 1991).

Exploration north of the Bullfrog Hills, in the North Bullfrog property, was re-initiated in 2005 and drilling has identified two styles of low-sulfidation epithermal mineralization. These are defined as potentially high-grade, structurally controlled fissure veins, and associated stockwork zones, and low-grade disseminated or replacement deposits within altered volcanic rocks (Meyers and Reichmann, 2014).

144 Zone Deposit Geology

Gold mineralization within the 144 Zone (Fig. 6) is hosted by a breccia that formed along the contact between the overlying Bonanza King Formation and the underlying Carrara Formation (Gillstrom, 2006). The 144 Zone breccia is thickest adjacent to the dike, where it is approximately 50 meters thick. The breccia extends along the contact between the Bonanza King and Carrara Formations for approximately 228 meters from north to south and approximately 260 meters from east to west (Gillstrom, 2006) (Fig. 6). The majority of the breccia formed within the overlying Bonanza King Formation and the overall shape of the breccia is irregular (Fig. 6). Breccia thickness decreases from top to bottom as shown in level plan maps (Fig. 7) (Taylor, et al., 2011). The breccia extends west of a quartz latite dike that is a member of the Crater Flat Tuff Group of the Main Magmatic Stage of the SWNVF, based on a K/Ar age date of 13.9 Ma +/- 0.1 Ma (Carr, 1984). The quartz latite dike appears to intercept the mineralization (Fig. 6). Castor and Weiss (1992) interpreted that dike emplacement occurred prior to the mineralization based on alteration and anomalous gold values found locally in the quartz latite dikes in Bare Mountain. These quartz latite swarms have been affected by potassium feldspar, sericitic, and argillic alteration that replaced sanidine and plagioclase (Castor and Weiss, 1992).

The ore and gangue minerals within the 144 Zone are oxidized, making it difficult to determine the original ore mineralogy. Brecciated rocks, clay-altered rock, limestone, and dolomite are moderately to intensely oxidized. Iron oxide minerals less than 1 mm in diameter are observed in hand samples and with microscopy (10 um to 500 um) (Taylor, et al., 2011).

Taylor et al. (2011) described the 144 Zone breccia as a hydrothermal breccia, but no genetic model was provided. They concluded that there were two main stages of brecciation related to two alteration assemblages, and that brecciation and alteration minerals were related to extensional faulting. The first alteration stage produced a silicified breccia with a siliceous matrix, interpreted to be associated with little to no gold. The second brecciation and alteration stage contains clay alteration that cross-cuts the siliceous breccia. Higher gold grades were determined to be associated with this second brecciation event.

Structures and faults within the 144 Zone have not been clearly identified, with the exception of the West fault. This fault, identified in drill core, strikes 341° and dips 72° to the SW. Gold mineralization and breccia textures terminate at the West fault (Fig. 6).

Taylor et al. (2011) recognized an antiform-like feature along the contact of the Bonanza King and Carrara Formations (Fig. 6), but were unable to determine its origin. Bedding within the Carrara Formation spatially associated with the 144 Zone and the antiform dips consistently north from 45° to 65°. Bedding and orientation of the Bonanza King Formation was not determined within the 144 Zone due to its massive nature. The

consistent dip of the Carrara Formation indicates that the feature is not a fold and was not generated by compressional tectonic regimes.

CHAPTER 3
METHODS

Geologic Mapping

Field studies included compiling the geology of several drifts of the 144 Zone. The 3292', 3260' 3220' and 3180' levels of the 144 Zone were mapped using a modified version of the Anaconda mapping approach (Einaudi, 1997). Mine generated base maps displaying the location and geometry of drifts on each level at a 1:20 scale were used as base maps for the mapping project. Completed maps were input into the three-dimensional mining software Minesite and the maps were digitized. Where the breccia was not constrained by mapping, drill core logs were used to identify breccia contacts.

Sample Collection

Samples were collected from underground workings and drill core, with a focus on collecting transects of samples from locations where Au grade changes from low- to high-grade. Samples were collected from underground workings near the quartz latite dike in documented areas of high-grade Au. Samples were also collected from drill core from the ST02-21 and SU13-177 drill holes because the rock showed unique textures in different types of brecciated rock, different host rock, and rocks that varied in grade. Samples were collected along transects that transition from low-grade Au or undetectable Au to high-grade Au and from unaltered or slightly altered rock to rock with textures and mineralogies that appeared to be related to the mineralization process. The best transects, selected for detailed analytical work, exhibit: (1) a range of grade from no/low to high-grade Au, (2) a range of breccia textures from unaltered or slightly altered rock to highly altered rock, and (3) a change in grade or alteration style over distances no more than 6 meters.

Geochemistry

Two unaltered samples of Bonanza King (DC02-21-670') and Carrara Formation (DC02-21-9) were analyzed using multi-element whole rock oxide and trace multi-element analyses by AcmeLabs. $LiBO_2$ fusion followed by X-ray fluorescence analysis was used to quantified major oxides: SiO_2, Al_2O_3, Fe_2O_3, CaO, MgO, Na_2O, K_2O, TiO_2, P_2O_5, SO_3, V_2O_5 and Cr_2O_3 (AcmeLabs, 2013, p. 16). Loss on Ignition (LOI) and elemental concentrations of Sr, Ba, Cu, Ni, Pb, Zn, and Zr were also determined from whole-rock analysis.

Trace elements were quantified using a 4-acid digestion followed by Inductively Coupled Plasma Mass Spectrometry (ICP-MS) (AcmeLabs, 2013, p. 12). Quantified elements include: Ag, Al, As, Au, Ba, Be, Bi, Ca, Cd, Ce, Co, Cr, Cu, Fe, Hf, In, K, La, Li, Mg, Mn, Mo, Na, Nb, Ni, P, Pb, Rb, Re, S, Sb, Sc, Se, Sn, Sr, Ta, Te, Th, Ti, Tl, U, V, W, Y, Zn, and Zr. Trace element analysis of the host rocks provides background information about the host rocks.

Petrographic Analysis

Thirty-nine polished sections were analyzed using transmitted and reflected light petrography to identify textural relationships of breccia types, characterize the ore, identify alteration minerals in high- to low-grade samples, and determine the location of gold within the samples. A Nikon OPTIPHOT-POL optical microscope was used to characterize mineral assemblages, determine mineral paragenesis, presence of oxidation, mineralogy, porosity, and textural relationships.

Scanning Electron Microscopy

A JEOL-5600 Scanning Electron Microscope (SEM) located in the Electron Microanalysis and Imaging Laboratory (EMiL) at the University of Nevada, Las Vegas (UNLV) was used to obtain semi-quantitative chemical compositions that aided in the identification of clay and calcareous minerals. Polished sections used in the SEM were carbon coated. High-resolution microscopy was conducted by using the SEM to observe and document textural and spatial relationships between clay, quartz, carbonate minerals, oxide, and Au-bearing iron oxide minerals.

Electron Probe Microanalysis

A JEOL-8900 Electron Probe Microanalyzer (EPMA) at the UNLV EMiL was used to quantify the major, minor and trace element chemistry of texturally and spatially diverse minerals. EPMA analysis focused on confirming the presence of native gold and the chemistry of Au-bearing goethite. The suite of elements quantified and detection limits are provided in Table 1.

Spectral Reflectance Data

An ASD TerraSpec 4 Standard-Resolution Mineral Analyzer was used to identify clay, oxide and other unknown minerals. The wavelength range for the TerraSpec 4 analyzer during data collection was from 350 nm to 2500 nm with an accuracy of 0.5 nm and a resolution of 3 nm at 700 nm and 10 nm at 1400/2100 nm. A scanning duration of 150 milliseconds was used to analyze all samples, including darker-colored samples that have a lower reflectance, making them more difficult to analyze (ASD Inc., 2013).

The TerraSpec 4 mineral analyzer analyzed 224 coarse reject samples contained in RC-chip trays. Prior to each spectral read-out, chip trays were turned upside-down and shaken to remix the samples and position sample material at the top of the sample compartment, so that the spectral lens contacted maximum sample material during analysis. Visible and near infrared (VNIR) and shortwave infrared (SWIR) absorption data were interpreted using The Spectral Geologist 7 (TSG 7) processing and spectrometer analysis software.

White mica crystallinity was also determined from spectral data for each sample by determining the ratio of the AlOH absorption feature at 2208 nm to the interlayer water absorption feature at 1900 nm. The depth of these absorption features was recorded with the TerraSpec 4 mineral analyzer and interpreted by TSG 7 software. White mica crystallinities were then described as excellent, good, moderate, or poor based on the value of the ratio. The higher the value, the better the crystallinity.

CHAPTER 4
HOST ROCKS, BRECCIA TYPES, AND ALTERATION

Host Rocks

Unaltered and unmineralized samples of the Bonanza King and Carrara Formations were collected from surface outcrop (Fig. 8; Fig. 9A). Samples containing no or trace gold were also collected within and along the periphery of the deposit from the Bonanza King and Carrara Formations (Fig. 9B-E). Unmineralized samples of Bonanza King Formation collected from surface outcrop are composed of dolomite (90 to 100%), minor detrital phengite (0 to 10%), rare quartz (1 to 3%) and goethite (1 to 5%) (Fig. 8A). Dolomite crystals within the samples range from 10 um to 300 um and are anhedral to subhedral (Fig. 8B). Detrital phengite crystals exhibit a bladed texture, are 10 um to 100 um in length, and are located along margins of dolomite crystals (Figs. 8C, 8D). Rare anhedral quartz crystals range from 40 um to 150 um and contains birefringent solid inclusions of dolomite, indicative of replacement of dolomite. Rare anhedral to euhedral goethite crystals are spatially associated with quartz and are 10 to 150 um in diameter. Geochemical analyses of unaltered and unmineralized Bonanza King dolomite (Tables 2, 3) confirm that the Bonanza King Formation sample is dominantly dolomite. Low concentrations of Al, Fe, and Si are consistent with the presence of observed trace to minor detrital phengite, quartz and goethite in hand samples.

A minor percentage of unaltered and unmineralized Bonanza King Formation exhibits breccia textures (Fig. 8E). Clasts range from 3 mm to 5 cm and are composed of dolomite and lesser calcite crystals that range from 50 um to 300 um. The matrix is

composed of dolomite and lesser calcite crystals that are anhedral and range from 10 um to 30 um (Fig. 8F).

Unaltered and unmineralized Carrara Formation is composed almost entirely of calcite (95 to 100%). Crystals are 10 to 200 um in diameter (Figs. 9A, 9B). Rare quartz (<5%) and goethite (<5%) are also present. Quartz and goethite crystals are no larger than 150 um. Tan bands crosscutting the gray rock are observed locally in Carrara Formation hand samples collected along the periphery of the deposit; however, these bands are not mineralogically distinct and are composed of calcite (Figs. 9C, 9D). Geochemical analyses of an unaltered and unmineralized Carrara Formation (Tables 2, 3) are consistent with abundant calcite, rare quartz, and a lack of Au.

Breccias

Samples collected from drill core and underground workings in the 144 Zone deposit were examined to characterize the breccias, and two types of breccia were distinguished based on physical characteristics (Table 4). Breccias were classified using the following criteria: matrix mineralogy, alteration of matrix, vug abundance in matrix, oxide minerals in matrix, clast mineralogy, clast geometry (angular or rounded), clast size, abundance of alteration minerals within clasts, abundance of vugs, oxide minerals in clasts, and matrix- versus clast-supported. Breccia Type 1 (BT1) can be either monolithic or heterolithic with one or more clast types (Figs. 10A, 10F) and a blackish-brown quartz dominant matrix (Fig. 11). Breccia Type 2 (BT2) can be either monolithic or heterolithic with one or more clast types (Figs. 12A, 12E) and an orange-red to yellow, phengite- and goethite-dominant matrix with minor quartz.

Breccia Type 1

BT1 contains dominantly tan phengitic dolomite clasts and may or may not also contain lesser white dolomite clasts, black quartz-rich clasts, and/or red goethite clasts. A combination of SEM EDS, ASD TerraSpec 4, and petrography were used to determine the composition and chemistry of phengitic dolomite clasts and mineral textures within the clasts. Phengitic dolomite clasts (Figs. 10A, 10B, 10C) contain anhedral dolomite crystals (75 to 85%) that range from 10 um to 75 um in diameter and thin phengite crystals (25 – 35%) 5 to 25 um in diameter and up to 200 um long are present along dolomite crystal contacts. Phengitic dolomite clasts range from < 1 mm to 8 cm and are rounded to angular. Very small phengitic dolomite clasts, < 300 um in diameter that can only be distinguished by optical petrography, are also present. Dolomite clasts (10 to 15%) are white to grey in color (Fig. 10D), range from <1 mm to 8 cm (Fig. 10E) and are rounded to angular. Very coarse-grained dolomite clasts (4 cm to 8 cm) exhibit small fractures less than 1 mm in diameter that are filled by goethite and quartz. Rare red goethite clasts (<3%) are <1 mm to 8 mm and rounded to subangular (Fig. 10F). Goethite clasts are entirely composed of goethite. Black quartz clasts or quartz-rich clasts range from <1 mm to 5 mm and are rounded to subangular (Fig. 10F). Quartz-rich clasts are composed mainly of quartz (65 to 100%) with variable amounts of goethite (0 to 35%). Quartz clasts are difficult to distinguish from the matrix of BT1 in hand sample and at the micrometer-scale due to their identical mineralogies.

The matrix of BT1 is very fine grained. Crystals within the matrix range from 10 um to 600 um in diameter and are composed predominantly of quartz with variable abundances of phengite and goethite. Quartz (Figs. 11B, 11D, 11F) comprises 55 to 90

vol% of the matrix composition. All quartz crystals within the matrix are anhedral and range from 10 um to 100 um (Fig. 11B).

Phengite abundance in the matrix of BT1 varies from sample to sample, ranging from 5 to 35 vol%. Phengite is bladed, occurs as laths between quartz crystals or has sheaf-like textures, and individual crystals of phengite range from 1 um to 100 um. Phengite is always enclosed by quartz (Figs. 11B, 11D).

Goethite (1 to 30%) is typically the least abundant mineral in the matrix of BT1 samples (Figs. 11B, 11C, and 11F). Where present, it varies from anhedral to cubic in form and ranges from 10 um to 600 um. In rare occurrences, goethite crystals no more than 0.5 mm can be identified with a hand lens.

The matrix of BT1 exhibits variable porosity. Rounded to angular vugs range from absent to abundant. Where BT1 is fractured, white calcite may fill fractures. BT1 samples exhibit either a brown or a black matrix in hand sample. Although the matrix color varies in hand sample (Fig. 11A), there is no recognizable mineral difference between the brown and black matrix.

The textural relationships between the matrix and clasts were also determined for BT1. Samples are matrix-supported and can be both matrix- (Figs. 11A, 11B) and clast-dominant (Fig. 11C). The contact between clasts and matrix is commonly sharp and varies from straight to wavy. “Crackle” breccia textures that transition from competent rock to breccia are rare. Instead, small clasts up to 300 um across are present in the matrix and form a transition from clast to matrix (Figs. 10D, 10E). Quartz crystals along the boundaries of clasts of all sizes contain or encompass birefringent solid inclusions of

dolomite and lesser calcite, indicating replacement of carbonate minerals. Adjacent clasts within a single sample have geometries that vary from angular to rounded.

Breccia Type 2

BT2 is comprised predominantly of black, quartz-rich clasts (75 to 100%) with no or few white dolomite (0 to 15%) and tan phengitic dolomite clasts (0 to 5%). Black, quartz-rich clasts are dominantly quartz with minor goethite (Fig. 12A, 12C, 12E). The clasts are rounded to subangular and range from < 1 mm to 6 cm (Fig. 12A). Anhedral quartz crystals (60 to 100%) within the clasts range from 10 um to 100 um (Fig. 12B), and contain very fine birefringent solid inclusions of dolomite. Goethite crystals (0 to 40%) are 10 um to 50 um in diameter and are anhedral to cubic in shape (Fig. 12B).

Light grey to white clasts are composed of dolomite (100%). The clasts range from 2 mm to 155 mm and are rounded to angular (Figs. 12E, 12F). Dolomite clasts are the second-most dominant clast type in BT2.

Tan phengitic dolomite clasts are the least abundant clast type in BT2 and are identical to the phengitic dolomite clasts present in BT1 (Figs. 12C, 12D). Phengitic dolomite clasts are 1 mm to 2 mm in length and are subrounded. They are typically contained within black quartz-rich clasts.

The matrix of BT2 is very fine grained, composed predominantly of phengite (35 to 90%) and goethite (1 to 70%) with minor quartz (3 to 20%), is orange-red to yellow in color, and is friable. Individual phengite, goethite, and quartz crystals are difficult to distinguish in hand sample and with transmitted light (Figs. 13A, 13B, 13C). Reflected light, however, allows for these individual crystals to be identified (Figs. 13D, 13E).

Phengite was confirmed using SEM EDS and spectral reflectance analysis (Fig. 14D). Phengite crystals most commonly are bladed or elongated laths ranging from 10 um – 50 um by no more than 10 um (Figs. 14A, 14C). Goethite crystals are irregular to cubic, reach 300 um in diameter, and are the brightest minerals under reflected light (Figs. 13D, 13E). Quartz crystals in the matrix are anhedral, medium grey, have a good polish under reflected light, and range from 10 um to 300 um. Clasts apparent only at the microscopic scale are common. In hand samples, BT2 appears to be both matrix- and clast-supported.

Highly altered, phengite-rich samples of BT2 appear composed entirely of phengite in hand sample (Figs. 15A, 15D). However, at high magnification, goethite crystals (1 to 10%) and quartz crystals (1 to 5%) no larger than 20 um can be identified (Figs. 15B, 15C, 15E), indicating that these samples are a phengite-rich end member of BT2. Phengite (80 to 99%) crystals in phengite-rich samples are bladed and elongated and are no larger than 50 um. Phengite-rich samples also have abundant pore space.

Alteration

Alteration within the 144 Zone breccia can be recognized by comparing unmineralized surface rocks with altered and mineralized breccia samples, specifically, the minerals within these rocks. Host rock and breccia sample comparisons indicated different alteration types associated with the Au mineralization. These alteration types include: silicification, clay and phengite alteration, and decarbonatization.

Silicification

Silicification is the most common alteration associated with the 144 Zone, and quartz has variably replaced primary sedimentary minerals in both breccia types. Quartz

is present in clasts in BT1 and BT2 and in the matrix of BT1 (Figs. 16A, 16C). Euhedral comb texture quartz is present rimming vugs and fractures, indicating open space deposition of quartz (Fig. 16F). Quartz crystals along quartz-dolomite contacts and in quartz-rich clasts commonly contain solid inclusions of dolomite and lesser calcite, indicating progressive quartz replacement of dolomite and calcite (Figs. 16B, 16D). Quartz is spatially associated with goethite and phengite (Figs. 16A, 16B, 16D).

Clay and Phengite Alteration

Clay alteration, dominated by phengite that was confirmed by ASD Mineral and SEM EDS analysis, is also present within the 144 Zone breccias. Trace kaolinite, montmorillonite, phengitic-illite and muscovite were also identified by ASD mineral analysis. However, owing to their rare presence, these minerals are not a significant component of the alteration and have not been described.

In addition to the breccias, altered, phengite-rich samples that do not have a breccia texture are common within the 144 Zone. These samples consist of massive sheaf-like, bladed and lathlike phengite (Figs. 15B, 15C). BEI analyses show that this rock type is dominated by phengite with minor anhedral quartz and goethite, and relatively abundant pore space (Figs. 15E, 15F, 15G, 15H).

Decarbonatization

Decarbonatization is a significant alteration type within the 144 Zone. It is indicated by the replacement of dolomite by quartz and by the presence of vugs or cavities in BT1 and BT2 where dolomite was removed. Vugs and cavities are rounded, range from less than 1 mm to greater than 10 cm in length (Fig. 17A), and can be rimmed

by euhedral quartz crystals (Fig. 17D), minor goethite (Fig. 17C), or phengitic dolomite and quartz (Fig. 17B).

Post-Ore Stage Minerals

Carbonate minerals and minerals that formed by oxidation of earlier minerals have also been identified within the 144 Zone and formed after gold mineralization and breccia formation events. White calcite and rare brown siderite and ankerite fill some fractures, forming veins (Fig. 18C). Additionally, white calcite fills small vugs from 2 mm to 6 meter diameter cavities (Fig. 18D).

Oxide minerals within the 144 Zone, identified through Terraspec 4 mineral analysis, include goethite and rare hematite, identified in only four samples. The entire deposit is moderately to intensely oxidized and goethite is present in both breccia types and within unmineralized host rock.

In BT1 samples, goethite is commonly located along the contact between dolomite or phengitic dolomite clasts and the matrix (Fig. 19D). Crystals are also regularly found isolated within the matrix of BT1 (Fig. 19A). Goethite crystals less commonly rim vugs (Fig. 17C) and occur within phengitic dolomite clasts (Figs. 19B, 19C). In rare occurrences, goethite crystals rim phengitic dolomite, dolomite and quartz-rich clasts (Figs. 18A, 18B).

In BT2 samples, goethite is located in the matrix (Fig. 13E) and quartz-rich clasts (Fig. 12B; Fig. 13D). Rarely, goethite is located along the contact between quartz-rich clasts and phengitic dolomite clasts (Fig. 12D). In highly altered, phengite-rich samples

of BT2, goethite crystals are located in the groundmass, are no more than 60 um, and are associated with quartz and phengite (Fig. 15E).

Goethite crystals were separated into two types based on their form. Type 1a goethite crystals are euhedral and isolated from one another by at least 1 mm (Fig. 19A). They are near perfect cubes or triangular sections of a cubic goethite crystal. Pitted regions no larger than 5 microns are present on all faces. Individual goethite crystals range from 0.25 mm to 1 mm. The majority of type 1a crystals range from 100 um to 400 um and are not detectable in hand sample. Type 1a goethite crystals are exclusively encompassed by anhedral quartz (Fig. 19A).

Type 1b goethite crystals are subhedral to anhedral crystals (Figs. 19B, 19D) that are isolated from one another by at least 1 mm or are in clusters with other goethite crystals. Clusters of type 1b goethite are defined as having more than 5 crystals no larger than 50 um that are less than 100 um away from other goethite crystals (Fig. 19C). Isolated type 1b goethites commonly range between 200 um to 700 um and are not detectable in hand sample. Less common type 1b goethites are visible with a hand lens and range from 0.25 mm to 1 mm.

Type 2 goethite is anhedral and forms veins. These veins range from 25 um to 40 um and are no longer than 2 cm. Type 2 goethite is spatially associated with silicified areas along fractured carbonate rock, within the matrix of BT1 (Fig. 19F), rimming vugs (Fig. 19E), and rimming phengitic dolomite clasts and dolomite clasts.

Gold Mineralization

Microscopic native gold is located within pitted areas in all goethite types within BT1 and BT2 samples (Figs. 20C, 20D). Gold was also identified along the rims of goethite crystals in BT1 samples (Figs. 21A, 21B, 21C). Based on EPMA, goethite containing Au also contains Sb, As, and Hg plus Fe, but not Ag and Bi (Figs. 21A, 21B, 21C).

Trace Silver and Monazite

During EPMA analysis, Ag concentrations as high as 4,735 ppm were confirmed in goethite (Fig. 22A). Silver, ranging from 48.2 to 4,735 ppm, was found in pitted areas up to 5 um in width and along the rims of goethite. EPMA indicates that silver values do not commonly coexist with Au in analyzed spots in goethite (Appendix C).

Rare earth elements including Ce, La and Nd were confirmed within monazite that was present in one sample that contains 6 oz/st Au. The sample is primarily composed of phengite. Monazite crystals reach 10 um in diameter and were confirmed with SEM EDS analysis (Fig. 22B). Monazite contains elevated or significant concentrations of Ce, La and Nd (Figs. 22C, 22D). Monazite is spatially associated with phengite and quartz.

Sample Transects

Figure 23 displays a sample transect with hand samples, polished sections, and photomicrographs, from low- to high-grade Au, and coincident with decreasing host rock dolomite and increasing quartz and goethite alteration. This transect also illustrates the

transition from dolomite to BT2. Low-grade samples in the sample transect consist primarily of dolomite (85 to 90%), trace pore space fractures (5%), and minor wavy veinlets (3%) (Fig. 23A). The veinlets have parallel vein walls no more than 20 um wide, and consist of quartz with trace to minor goethite. Inclusions of dolomite 1 to 5 um across enclosed by quartz crystals are shown in the far right photomicrograph). The presence of both parallel vein walls and solid inclusions of dolomite in quartz indicates both open space filling by quartz and replacement of dolomite by quartz.

Sample B (Fig. 23B) has elevated Au and is more fractured than sample A. The rock is still primarily dolomite (75 to 80%); however, quartz (5 to 10%) and goethite (3 to 5%) are more abundant than in sample A, owing to replacement of dolomite along increasingly abundant wavy veinlets. Moreover, the irregular nature of the vein walls in the photomicrograph indicate replacement, which is confirmed in the photomicrograph with the higher magnification.

An increase in gold grade to 0.188 oz/st in sample C (Fig. 23C), 0.8 meters from sample B, coincides with an increase in quartz and goethite. This high-grade rock is composed primarily of dolomite (60 to 70%). However, large areas of quartz (20 to 30%) and goethite (5 to 10%) are relatively common (Fig. 23C). Locations of dolomite and quartz can be distinguished in hand sample C where white areas are composed of dolomite and black areas consist of quartz. An increase in goethite abundance and fracturing of dolomite is readily noticeable in polished section. At the micrometer scale, apparent dolomite “clasts” are beginning to form as a result of replacement of dolomite by quartz. Goethite, spatially associated with quartz, is also increasing with quartz abundance. The sample in Figure 23C signifies the transition from dolomite to BT1, as

the quartz-dominant matrix and phengitic dolomite and dolomite clasts of BT1 begin to take form.

The highest grade sample D consists primarily of quartz (40 to 45%), phengite (40 to 50%) and goethite (5 to 15%). The sample was collected 1 meter from sample C (Fig. 23C) and contains 0.617 oz/st Au. Abundant, low relief phengite with goethite and trace quartz (Fig. 23D) comprise the matrix that cements quartz-rich clasts. Abundant goethite (30- 35%) is present in quartz-rich clasts. Furthermore, inclusions of dolomite, no larger than 3 microns, are present in quartz crystals that constitute quartz–rich clasts. The transition from Fig. (23A) to Fig. (23D) demonstrates the transition from host rock dolomite to BT2. This change in rock type was accomplished by the removal of dolomite by quartz replacement, which is supported by the presence of micron-sized inclusions of dolomite encapsulated by quartz.

Figure 24 displays a sample transect that exhibits little variation in mineralogy or hand sample texture; however, Au concentrations vary from 0.065 oz/st to 1.886 oz/st over a distance of 3.5 meters. Au occurs exclusively in goethite and all goethite is spatially associated with quartz. Breccia sample A (Fig. 24A) contains 0.065 oz/st Au and is composed of quartz-rich matrix (55 to 60%) and phengitic dolomite clasts (40 to 45%). Phengitic dolomite clasts contain isolated quartz and bladed phengite and exhibit a diffuse boundary as shown in the photomicrograph (Fig. 24A). Minor goethite is indicated by the lack of black minerals in the polished section.

High-grade samples B and C were collected no more than 3.5 meters from low-grade sample A. High-grade samples exhibit textures and mineralogy nearly identical to the low grade sample, but clast-matrix boundaries are not diffuse. Polished sections of

these samples exhibit increased goethite and porosity. Goethite in high grade samples is located rimming phengitic dolomite clasts or within phengitic dolomite clasts encapsulated by quartz. In both occurrences Au-bearing goethite is spatially associated with quartz.

Figure 25 displays a 2.5-meter transect across highly altered and mineralized phengite-rich samples of BT2 that, in hand sample, appear to vary little in mineralogy, though Au increases significantly. Polished section examination shows that the lowest grade sample A is composed primarily of phengite with minor goethite and quartz and is highly porous. Higher grade hand samples B and C (Figs. 25B, 25C) share identical textures, a similar mineralogy, and a comparable porosity with sample A; however, goethite is more abundant in higher-grade samples B and C than in sample A.

Breccia samples in Figure 26 examine the correlation between porosity, Au grade, and goethite over a 1.5-meter transect. Low-grade BT1 sample A (Fig. 26A) is composed of quartz-rich matrix (85%) with phengitic dolomite clasts (10%) and low goethite (<5%) and porosity (1%). Vugs are irregular to cubic in shape and reach 600 um in diameter (Fig. 26A). BT1 samples B and C (Fig. 26B, 26C) were collected from within one meter of sample A. Both samples have nearly identical mineralogy and textures compared to low-grade sample A, including a quartz-rich matrix (55 to 60%) cementing phengitic dolomite clasts (40 to 45%); however, goethite, porosity, and Au are more abundant in samples B and C. Both samples contain vugs that that are commonly rimmed with goethite. Moreover, goethite is more abundant in samples B and C than lower grade sample A. Alternatively, highest grade BT2 sample D is primarily composed of phengite and abundant goethite, and minor quartz. In hand sample, the sample appears

to be entirely composed of phengite. However, in the polished section, white, quartz-rich clasts (10 to 15%) can be distinguished within the low-relief phengite (70 to 80%) and goethite (20 to 30%) matrix. This sample exhibits the greatest porosity, and contains the most abundant goethite and Au compared to other samples in the sample transect. Goethite is spatially associated with quartz and pore space (Fig. 26D).

Map Relationships

Underground maps along with a three-dimensional model of geology based on drilling illustrate the spatial relationships of the breccia types to the Bonanza King and Carrara Formations and the quartz latite dike, and how these relationships vary at different elevations in the mine. These relationships contribute to establishing a breccia formation mechanism and a model for the formation of alteration minerals.

The petrographic study has established that the 144 Zone formed through fluid-rock reaction and replacement, rather than collapse brecciation. Underground mapping and cross sections have produced no evidence of the dissolution of carbonate rock that later collapses in on itself to form a collapse breccia (Laznicka, 1988). Such breccias consist of a concentric zonation that exhibits a progressive increase in brecciation and mineralization towards the center of the breccia body. Moreover, collapse breccias commonly exhibit dome or cone shapes (McCormick, 1971). The 144 Zone displays none of these features. Instead, the geologic maps produced from underground mapping (Fig. 29) and the cross-sections based on a 3D mine model show that the breccia has largely formed adjacent to the carbonate rock-latite dike contact, and that it extends away from this contact along the Carrara and Bonanza King Formation contacts. Moreover, the Bonanza King-Carrara contact is straight and not disrupted by collapse.

The thickest section of the 144 Zone breccia, which formed along the Bonanza King-Carrara Formation contact, is located adjacent to the quartz latite dike (Fig. 6B) as shown on a three-dimensional mine model based on drilling. This model shows that the base of the breccia is in contact with Carrara limestone, the Bonanza King dolomite occurs above the breccia, and the breccia is narrowest at lower elevation (Fig. 7). Figure 27 displays the map view relationship of the drifts and levels of the underground workings in the 144 Zone. Figure 28 illustrates the geology of the 3292', 3260', 3220', and 3180' levels, based on geologic mapping in these drifts, and can be compared to the mine model shown in Figures 6A and 7.

The geologic maps (Fig. 28) show that BT1 is bounded by the quartz latite dike or BT2 to the east, and by Carrara limestone to the west on the 3292', 3260', and 3220' levels. BT1 is the dominant breccia type on the 3292' level (70 vol%) (Fig. 28A). At greater depth, on the 3260' and 3220' levels, the relative volume of BT1 to BT2 decreases (Figs. 28B, 28C).

On several levels, narrow irregularly shaped blocks of Bonanza King dolomite from 1.5 m – 9.1 m across and that have a sharp contact with the breccia are contained within BT1. The dolomite blocks are most abundant on the uppermost 3292' level, and they are cross-cut by vein-like textures of BT1, 5 – 45 cm in diameter (Figs. 29A, 29B, 29C, 29D) crosscutting the dolomite. Blocks of Bonanza King dolomite are also present in BT1 on the 3260' and 3220' level (Figs. 28B, 28C).

BT2 occurs on all levels of the 144 Zone and most commonly occurs between BT1 and the latite dike, though it also can be found within BT1. BT2 is localized mainly along the contact of the quartz latite dike, suggesting that abundant phengite in BT2 is

possibly related to proximity of the quartz latite dike. The largest volume of BT2 occurs on the 3260’ level (28B). BT2 is also present on the 3180’ level adjacent to the dike (Fig. 28D).

CHAPTER 5

BRECCIA FORMATION

Observations made during petrography and underground mapping have demonstrated that the 144 Zone breccia developed from ongoing chemical replacement of the lowermost Bonanza King Formation. The presence of minor dolomite and trace calcite solid inclusions in quartz in BT1 and BT2 is indicative of replacement. Dolomite blocks that range from 1.5 – 9 meters in width appear to be surrounded by BT1 and BT2 (Figs. 28, 29B). Additionally, dolomite commonly contains BT1 that has vein-like textures (Figs. 29A - C). Dolomite blocks surrounded by BT1 at map scale are analogous to dolomite inclusions in quartz crystals at the microscopic scale.

Limestone of the Carrara Formation was not altered and the presence of a sharp contact with Carrara limestone with overlying breccia, observed during mapping, indicates that the Carrara Formation did not contribute to breccia formation. Hand sample and petrographic descriptions confirm that rare calcite is only present in low-grade Bonanza King dolomite samples collected within the deposit. Low abundances of calcite can be expected in dolomite rock based on descriptions completed by Cornwall and Kleinhampl (1961) and Monsen et al. (1991).

Breccia Type 1 Formation

Geologic relationships, underground map patterns, and examination of sample transects have led to the following model for the formation of BT1. Hydrothermal fluids ascended along the contact between the quartz latite dike and the Carrara Formation and moved laterally along the Bonanza King-Carrara contact, altering the Bonanza King

Formation and eventually forming an apparent breccia. In some instances, dolomite was not altered to either breccia type, resulting in relic dolomite surrounded by BT1 and BT2.

BT1 formed in response to hydrothermal fluid penetration along microfractures and mineral grain boundaries (Figs. 32A, C-F). Quartz initially precipitated in open space indicated by the presence of small minor veins with parallel vein walls. Veins contain dolomite fragments that likely formed during microfracturing, and that were encapsulated by quartz. Hydrothermal fluids reacted with the host rock, replacing dolomite with quartz. Continued fluid-rock reaction reduced the abundance of dolomite while increasing the abundance of quartz (Figs. 32G, 32H).

At the same time, Au-bearing pyrites precipitated with quartz either by sulfidation of the host rock, by replacing other minerals through ion diffusion or by fluid cooling, along fluid-rock reaction fronts. Alternatively, hydrothermal fluids reacting with pre-ore stage diagenetic or detrital pyrites within the Bonanza King Formation could have also caused Au precipitation (Figs. 32H-J).

Goethite is interpreted to be a pseudomorph of pyrite. However, no relic pyrite has been documented. Goethite replacement of pyrite is based on the crystal morphology of goethite within the 144 Zone and the presence of Au-bearing pyrites in other deposits within Bare Mountain. Goethite within the 144 Zone commonly displays a cubic crystal morphology, indicative of pyrite's isometric crystal form, as opposed to the orthorhombic crystal structure of primary goethite. If goethite did not replace pyrite, botryoidal textures, common in goethite, would be present. Additionally, the presence of Au-bearing pyrite throughout the Bare Mountain district, especially in the near-by

Sterling deposit (Odt, 1989), suggests that pyrite precipitated with Au in the 144 Zone and that the alteration to goethite was a post-ore alteration process.

Continuous dolomite dissolution transformed dolomite rock into apparent phengitic dolomite and dolomite clasts (Fig. 32I). As dolomite and phengitic dolomite rock became "clasts," the simultaneous precipitation of quartz, pyrite, and Au plus concentration of phengite along quartz crystal boundaries formed the BT1 matrix (Fig. 32I), resulting in the formation of BT1 (Fig. 32B). Sometime after the hydrothermal system ended, post-ore oxidizing fluids altered pyrite to goethite and removed sulfur. The location of goethite, especially along matrix-clast boundaries, records not only the location of pyrite precipitation, but also the location of relic fluid-rock reaction fronts that were responsible for BT1 formation (Figs. 10B, 32J).

Breccia Type 2 Formation

BT2 derives from dolomite rock that was subjected to hydrothermal alteration and fluid-rock reaction that removed almost all dolomite through extensive decarbonatization, precipitated minor quartz compared to BT1, and both concentrated and precipitated phengite, producing a phengite-rich rock. Hydrothermal fluids invaded dolomite rock along microcracks and grain boundaries (Figs. 33A, C, D). Fluid-rock reaction and/or fluid cooling led to precipitation of pyrite and gold (Fig. 33E). Fluid-rock reaction removed significant dolomite through decarbonatization, and quartz replaced nearly all remaining dolomite and phengitic dolomite clasts forming quartz-rich clasts (Fig. 33F). At the same time, fluids that had reacted with and altered plagioclase and sanidine in the latite dike, precipitated secondary phengite proximal to the dike, producing the BT2 matrix (Figs. 33B, F). The abundant micropore space and minor quartz in the matrix of

BT2 indicates that BT2 formation was dominated by decarbonatization of dolomite, formation of phengite by ion diffusion (Turpault et al., 1992) related to alteration of the dike, plus likely physical transport of phengite particles by the ore fluid from the dike. Phengite-rich rock, from which all dolomite was removed, represents fluid-rock alteration that has gone to completion.

Phengite Precipitation

The majority of secondary phengite in BT2 likely formed by ionic diffusion related to hydrothermal alteration of the latite dike during mineralization. Figure 34A, modified from Turpault et al. (1992), illustrates a model for phengite precipitation. Hydrothermal fluids transporting silica, S^{3-} and Au^{2+} moved upward along the quartz latite dike Carrara Formation contact, and reacted with the quartz latite dike. Fluid-rock reaction altered plagioclase and sanidine (Castor and Weiss, 1992), facilitating ionic diffusion of Al^{3+} and K^{+} laterally along the Cararra - Bonanza King contact. As fluid-rock reaction removed dolomite, Fe^{2+} and Mg^{2+} were released and, along with Al^{3+}, K^{+}, and silica in the fluid, were consumed by precipitation of secondary phengite (Turpault et al., 1992). The presence of BT2, and especially phengite-rich rock, indicate localities of pervasive hydrothermal fluid flow and alteration. This interpretation is consistent with the close spatial relationship between BT2 and dike margins.

The physical transport of phengite particles away from the dike could also have contributed to the presence of phengite some distance from the dike. In this scenario, phengite is a product of alteration of sanidine and plagioclase along the margin of the dike, which after formation, was physically moved laterally along the Cararra - Bonanza

King contact by the ore fluid. Phengite accumulated in pore spaces and became encapsulated during the replacement of dolomite to quartz.

CHAPTER 6

INDICATORS OF GOLD

One goal of this project was to identify features in the rock that correlate with gold grade. This study has determined that goethite is the best mineral indicator of gold, while quartz, phengite, and dolomite are poor indicators of gold. It was also determined that porosity in BT1 correlates with gold, while porosity in BT2 does not. Finally, it was determined that there is no preferred correlation between breccia type and gold.

Breccia Type

BT1 and BT2 samples exhibit a wide range of Au values from low- to high-grade, and neither breccia type has a stronger correlation with Au. Gold in BT1 samples ranges from 0.041 to 1.869 oz/st with a mean of 0.184 oz/st (Fig. 30A). Gold in BT2 samples ranges from 0.001 oz/st to 5.66 oz/st with a mean Au concentration of 0.219 oz/st (Fig. 30B). Although the mean gold values for BT1 and BT2 are economic at today's gold prices ($\geq$ 0.10 oz/st), both breccia types have a wide range of Au grades from low to high.

Mineral Indicators

Native gold is exclusively located within pitted areas and along the rims of goethite crystals. Native gold is present in all goethite types indicating that the variable textures of goethite do not control the presence of gold. Increased goethite correlates with increased gold, making the presence and abundance of goethite an important gold indicator (Fig. 23). A complication is that while goethite can be identified under the microscope, in cannot, except in rare instances, be identified in hand sample.

Analytical work has shown a strong spatial correlation between Au-bearing goethite and quartz in both BT1 and BT2. The spatial association demonstrates that quartz precipitated as part of the same ore-stage event and that silicification correlates well with gold. However, the presence or absence of goethite in silicified rock is variable making quartz alone a poor indicator of gold concentration. Au grades in near identical samples (Fig. 24) vary due to the abundance or absence of Au-bearing goethite irrespective of quartz abundance.

Phengite is not spatially associated with Au-bearing goethite. Samples containing the mineral phengite have an average grade of 0.213 oz/st with a variance of 0.271 oz/st and gold grades that range from 0.001 oz/st to 5.9 oz/st (Fig. 31A). Furthermore, near identical phengite-rich samples (Fig. 25) vary in gold concentration due to the abundance or absence of Au-bearing goethite, demonstrating that no correlation exists between phengite abundance and gold grade.

Phengite crystallinity correlates poorly with gold (Fig. 31). Samples with excellent, good, and moderate crystallinity contain a wide range of gold values (Figs. 31B, 31C, 31D). Samples that exhibit poor phengite crystallinity have low gold concentrations 50% of the time (Fig. 31E); but such samples can also contain high-grade gold.

The carbonate minerals dolomite and calcite are the dominant minerals of the Bonanza King and Carrara formations. Dolomite is commonly present in both breccia types, whereas calcite is not present. Dolomite is never spatially associated with Au-bearing goethite crystals. Thus, dolomite is an indicator of sub-economic gold values.

The relationship between porosity and Au in BT1 is unlike its affiliation in BT2. In BT1 samples, abundant pore space correlates positively with high-grade Au (Fig. 26). This suggests that open space caused by decarbonatization was related to ore fluid influx, fluid-rock reaction, and Au mineralization in BT1. BT2 samples have abundant porosity, but have a wide range of Au grades (Fig. 30B). Some BT2 samples were altered, but not mineralized with economic concentrations of Au. Therefore, porosity and Au concentration correlate only in BT1.

CHAPTER 7
DISCUSSION

Formation of the 144 Zone Breccia

The proposed model for formation of the 144 Zone breccia differs from typical models for breccia formation. Breccias are defined as clastic rock composed of angular broken rock fragments or clasts larger than 2 mm that are held together by mineral cement or fine-grained matrix (Bates and Jackson, 1987; Blatt et al., 2006; Cas, et al., 2011). If the 144 Zone breccia is a true breccia, it should conform to all characteristics in the definition.

The shape and size of the clasts in the 144 Zone are quite variable. Angular to rounded clasts are commonly adjacent in any given sample. All clasts commonly range from 0.5 mm - 8 cm in diameter. However, at the microscopic scale, clasts have been identified as small as 100 - 300 um in diameter.

The matrix of both BT1 and BT2 are fine-grained. Individual matrix crystals range from 10 um - 100 um in diameter and cannot be individually distinguished in hand sample (Figs. 11, 13). The fine-grained matrix in the 144 Zone breccias is consistent with the definition of a breccia and is the only characteristic of the 144 Zone breccias that fully meets the criteria of a breccia.

The shape of the 144 Zone breccia does not conform to the dome and cone shapes that are commonly documented in breccia ore deposits (McCormick, et al., 1971). Furthermore, the overwhelming evidence supports the interpretation that the 144 Zone breccia formed by chemical replacement. Thus, the term pseudobreccia, defined as rock

that has the textures of a breccia, but which did not result from physical fracturing (Laznicka, 1988), is proposed for the 144 Zone.

High-Grade Dolomite and Calcite Samples

The low abundance or absence of dolomite and calcite generally correlates well with high gold value; however, Terraspec 4 analysis identified seventeen of 224 samples with economic grades (≥ 0.10 oz/st Au) as being dolomite- or calcite-rich, contradicting this relationship. Hand and optical petrography descriptions were reviewed to check the concentration of dolomite or calcite indicated by the spectral analysis and petrographic descriptions of these samples determined that quartz and phengite were more abundant than dolomite or calcite. The spectral data for these seventeen samples probably resulted from the spectral lens selectively collecting data from areas consisting primarily of dolomite or calcite, and not being representative of the entire sample.

Implications for Future Gold Exploration

Mineralization in the 144 Zone gold deposit is controlled by the contact of the lower Bonanza King Formation and the upper Carrara Formation. Furthermore, the breccia textures in the 144 Zone occur in the Bonanza King Formation and follow the Bonanza King - Carrara contact. This signifies that the base of the Bonanza King Formation is a promising target for future gold exploration.

Sub-economic Au prospects and economic concentrations of gold documented throughout the Bare Mountain range (Fig. 5) have two similarities: (1) all Au prospects in Bare Mountain are spatially associated with a quartz latite intrusion, and (2) quartz, sericite, and pyrite are commonly associated with Au. The similar mineralization styles and spatial association with quartz latite intrusions demonstrates a genetic relationship

between Au occurrences across the district. Furthermore, quartz latite swarms have been affected by potassium feldspar, sericitic, and argillic alteration that replaced sanidine and plagioclase (Castor and Weiss, 1992), indicating the genetic link between these quartz latite intrusions and Au-bearing fluids. This association further suggests that intrusive activity associated with the SWNVF (Fig. 3) is the most likely source of the Au-bearing fluids.

These findings indicate that Bare Mountain is a promising target for future exploration efforts. Mapping directed towards delineating the location of quartz latite intrusions and their potential intersections with the base of the Bonanza King Formation can provide future exploration targets for mineralization styles comparable to the 144 Zone.

Future work directed towards analyzing the quantitative elemental components for secondary phengite can assist in determining the source of components needed to form phengite. By comparing EPMA obtained chemistries of phengite within the dike and the 144 Zone to phengite within the Bonanza King Formation can define if an outside sources are needed to form phengite. If the chemistries match, then no outside source is needed. If they do not correlate well, this infers that an outside source is necessary to form phengite.

CHAPTER 8

CONCLUSIONS

Results from this study have demonstrated that Au in the 144 Zone pseudobreccia is located within pitted areas and along the rims of the mineral goethite. The presence of goethite correlates positively with Au and is the best mineral indicator for high concentrations of Au. Goethite replaced pyrite that likely precipitated with Au in open space, by sulfidation of the host rock, by replacing other minerals through ion diffusion or by fluid cooling, along fluid-rock reaction fronts.. Alternatively, gold-bearing fluids reacted with pre-ore stage diagenetic or detrital pyrites within the Bonanza King dolomite resulting in Au-bearing pyrites.

Gold and pyrite mineralization were coincident with silicification and replacement of dolomite in both BT1 and BT2. Goethite is always spatially associated with quartz, supporting the interpretation that gold, pyrite and quartz precipitated as part of the same ore-stage event. However, the concentration of goethite and gold in silicified rock ranges from abundant to absent making silicification a less reliable mineral indicator for gold than goethite.

BT1 formed from fluid-rock reaction that decarbonatized and silicified dolomite, transforming massive dolomite and phengitic dolomite into apparent clasts engulfed by quartz, minor phengite, pyrite and Au that resemble a breccia matrix. BT2 formed from extensive fluid-rock reaction that removed nearly all dolomite through decarbonatization. Precipitation of minor quartz and abundant phengite resulted in the formation of variable apparent quartz clasts in a phengite-rich matrix.

Textures from the microscopic to map scale demonstrate that the 144 Zone breccia formed through chemical replacement of the lowermost Bonanza King Formation. Solid micrometer inclusions of dolomite in quartz demonstrate silicification of dolomite in BT1 and BT2. Dolomite blocks that range from 1.5 meters – 9 meters across were observed in underground workings to be surrounded by BT1 and BT2, analogous to dolomite inclusions in quartz crystals at the microscopic scale. Initial stages of silicification and replacement are present in the upper part of the breccia, where dolomite is commonly crosscut by meter-scale veins of BT1.

Phengite is a poor indicator of gold and does not correlate with Au. Phengite was concentrated in BT1 by dissolution of dolomite, and formed in BT2 in response to alteration of feldspar in a quartz latite dike. Ionic diffusion of Al^{3+} and K^{+} that combined with Mg^{2+}, and Fe^{2+} that was liberated during dolomite dissolution, formed phengite.

Porosity is the only texture in the rock that correlates positively with Au in BT1. However, porosity does not correlate with Au in BT2, as all samples are porous. Phengite-rich rock formed from complete dissolution of dolomite and precipitation of phengite. The complete removal of dolomite and formation of BT2 is consistent with intense alteration along and near the margins of the quartz latite dike indicating that fluids likely rose along the margins of the quartz latite dike and moved laterally along the reactive Bonanza King – Carrara contact, where fluid-rock reaction formed BT1 and BT2 and precipitated Au. Mineralization in the 144 Zone gold deposit and breccia are controlled by the contact along the lower Bonanza King Formation and the Carrara Formation.

In addition, Au in other deposits near Bare Mountain exhibits alteration similar to the 144 Zone, and is spatially related to quartz latite intrusions associated with the SWNVF. These observations demonstrate a genetic relationship between Au in the district and the presence of quartz latite intrusions at Bare Mountain. The spatial and temporal relationships between Au and the Bonanza King-Carrara contact and the quartz latite dike demonstrate a key control for similar mineralization elsewhere in the district.

Table 1. Detection limits (D.L.) for the suite of elements quantified using JEOL-8900 Electron Probe Microanalyzer analysis.

Element	D.L. (wt%)
SeO_2	0.003
Ag	0.004
Au	0.013
As_2O_3	0.003
HgO	0.004
Tl_2O_3	0.026
SiO_2	0.003
PbO	0.006
Bi_2O_3	0.026
Al_2O_3	0.003
WO_3	0.016
CuO	0.008
ZnO	0.005
TeO_2	0.007
NiO	0.007
Sb_2O_3	0.005
CoO	0.007
SnO_2	0.005
TiO_2	0.011
MoO_3	0.006
Fe_2O_3	0.008
CaO	0.004
SO_2	0.003

Table modified from EMiL lab at UNLV (Ren, 2014).

Table 2. Whole rock geochemistry of unaltered and unmineralized drill core samples of Bonanza King and Carrara Formation.

Analysis	Weight	SiO2	Al2O3	Fe2O3	CaO	MgO	Na2O	K2O	MnO	TiO2	P2O5
Units	KG	wt%	wt%	wt%	wt%	wt%	wt%	wt%	wt%	wt%	wt%
MDL	0.01	0.01	0.01	0.01	0.01	0.01	0.01	0.01	0.01	0.01	0.01
Bonanza King DC02-21-680'	0.34	2.73	0.30	0.23	29.86	20.95	<0.01	0.11	0.02	0.03	<0.01
Carrara DC02-21-10	0.23	1.69	0.15	0.13	53.48	1.41	<0.01	0.06	<0.01	<0.01	<0.01

Analysis	Cr2O3	SO3	V2O5	Sr	Ba	Cu	Ni	Pb	Zn	Zr	LOI	SUM
Units	wt%	wt%	wt%	wt%	wt%	wt%	wt%	wt%	wt%	wt%	wt%	wt%
MDL	0.001	0.002	0.002	0.002	0.01	0.001	0.001	0.001	0.001	0.002	-5.11	0.01
Bonanza King DC02-21-680'	<0.001	0.311	0.002	0.005	<0.01	<0.001	<0.001	<0.001	<0.001	<0.002	45.93	100.45
Carrara DC02-21-10	<0.001	<0.002	<0.002	0.030	<0.01	<0.001	<0.001	<0.001	<0.001	<0.002	43.26	100.16

MDL = Minimum Detection Limit, wt% = weight percent, PPM = Parts Per Million, LOI = Loss on Ignition

Table 3. Trace element geochemistry of unaltered and unmineralized samples of Bonanza King and Carrara Formation.

Analysis	Mo	Cu	Pb	Zn	Ag	Ni	Co	Mn	Fe	As	U
Units	PPM	PPM	PPM	PPM	PPM	PPM	PPM	PPM	wt%	PPM	PPM
MDL	0.1	0.1	0.1	1	0.1	0.1	0.2	1	0.01	1	0.1
Bonanza King DC02-21-680'	0.2	0.4	7.8	5	0.1	0.9	0.3	127	0.17	2	0.1
Carrara DC02-21-10	<0.1	0.5	1.7	<1	<0.1	<0.1	<0.2	62	0.08	2	<0.1

Analysis	Au	Th	Sr	Cd	Sb	Bi	V	Ca	P	La	Cr
Units	PPM	PPM	PPM	PPM	PPM	PPM	PPM	wt%	wt%	PPM	PPM
MDL	0.1	0.1	1	0.1	0.1	0.1	1	0.01	0.001	0.1	1
Bonanza King DC02-21-680'	<0.1	0.4	58	<0.1	6.8	0.4	<1	19.64	0.002	2.5	5
Carrara DC02-21-10	<0.1	<0.1	301	<0.1	1.0	0.3	<1	37.93	0.003	0.8	4

Analysis	Mg	Ba	Ti	Al	Na	K	W	Zr	Ce	Sn	Y
Units	wt%	PPM	wt%	wt%	wt%	wt%	PPM	PPM	PPM	PPM	PPM
MDL	0.01	1	0.001	0.01	0.001	0.01	0.1	0.1	1	0.1	0.1
Bonanza King DC02-21-680'	11.93	9	0.005	0.16	0.023	0.11	<0.1	0.7	5	<0.1	3.2
Carrara DC02-21-10	0.86	7	0.002	0.08	0.006	0.05	<0.1	0.4	1	<0.1	0.6

Analysis	Nb	Ta	Be	Sc	Li	S	Rb	Hf	In	Re	Se
Units	PPM	PPM	PPM	PPM	PPM	wt%	PPM	PPM	PPM	PPM	PPM
MDL	0.1	0.1	1	1	0.1	0.1	0.1	0.1	0.05	0.005	1
Bonanza King DC02-21-680'	0.3	<0.1	<1	<1	2.4	<0.1	2.6	<0.1	<0.05	<0.005	<1
Carrara DC02-21-10	0.2	<0.1	<1	<1	1.0	<0.1	1.6	<0.1	<0.05	<0.005	<1

Analysis	Te	Tl
Units	PPM	PPM
MDL	0.5	0.5
DC02-21-680'-BKD	2.4	<0.5
DC02-21-10-CL	0.8	<0.5

MDL = Minimum Detection Limit, wt% = weight percent, PPM = Parts Per Million

Table 4. Classification of 144 Zone breccias. Physical and mineralogical characteristics of the two breccia types. Phen = phengite, qtz = quartz, phen dol = phengitic dolomite, goe = goethite, max = maximum, min = minimum, var = variance, S.D. = standard deviation.

	Physical Characteristics	Clast Composition	Matrix Composition	Clast Description	Other Characteristics	Au Grade
Breccia Type 1 **(BT1)**	Monolithic or heterolithic Matrix supported Crackle textures are rare	Phen dol > dol > qtz > goe	Qtz-rich matrix with lesser goe and phen Black to brown in color	phen dol - <1mm -8cm dol - <1mm -8cm qtz - <1mm - 5mm goe - <1mm - 4mm Clasts are rounded to angular	Fractures up to 5mm in width are common. Fractures commonly filled with white calcite	Max. = 1.869 oz/st Min. = 0.041 oz/st Mean = 0.184 oz/st Var = 0.092 oz/st S.D. = 0.303 oz/st
Breccia Type 2 **(BT2)**	Monolithic or heterolithic Matrix or clast supported	Qtz > dol > phen dol	Variable goe and phen Orange-red in color	qtz - 1mm - 6mm dol - 2mm - 1cm phen dol - 1mm - 2mm rounded to angular	Matrix is friable with varible porosity	Max = 5.66 oz/st Min. 0.001 oz/st Mean = 0.219 oz/st Var. = 0.354 oz/st S.D. = 0.595 oz/st

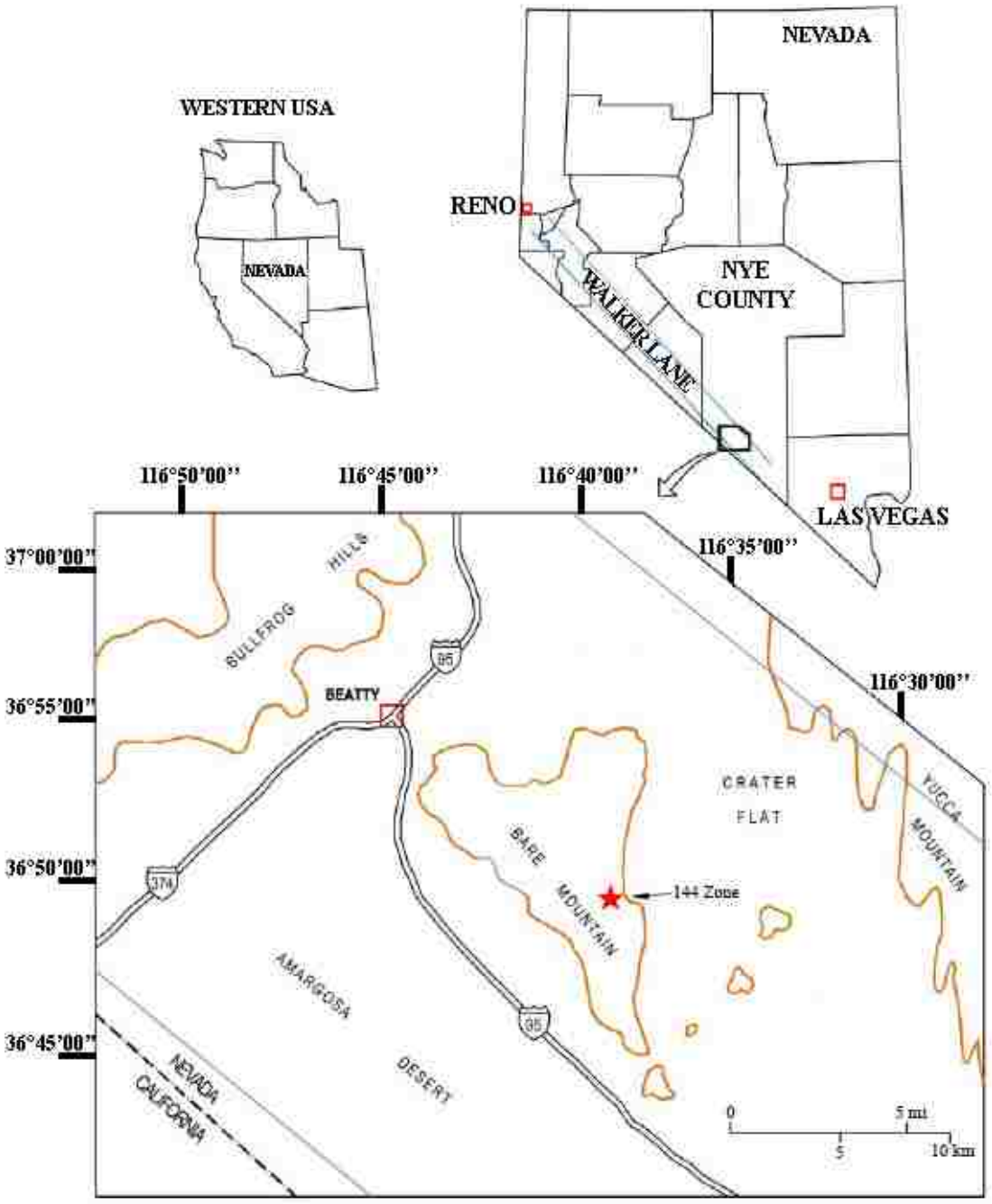

Figure 1. Regional setting of Nevada and Bare Mountain within the western United States. Location of the 144 Zone indicated by the red star (modified from Gillstrom, 2006).

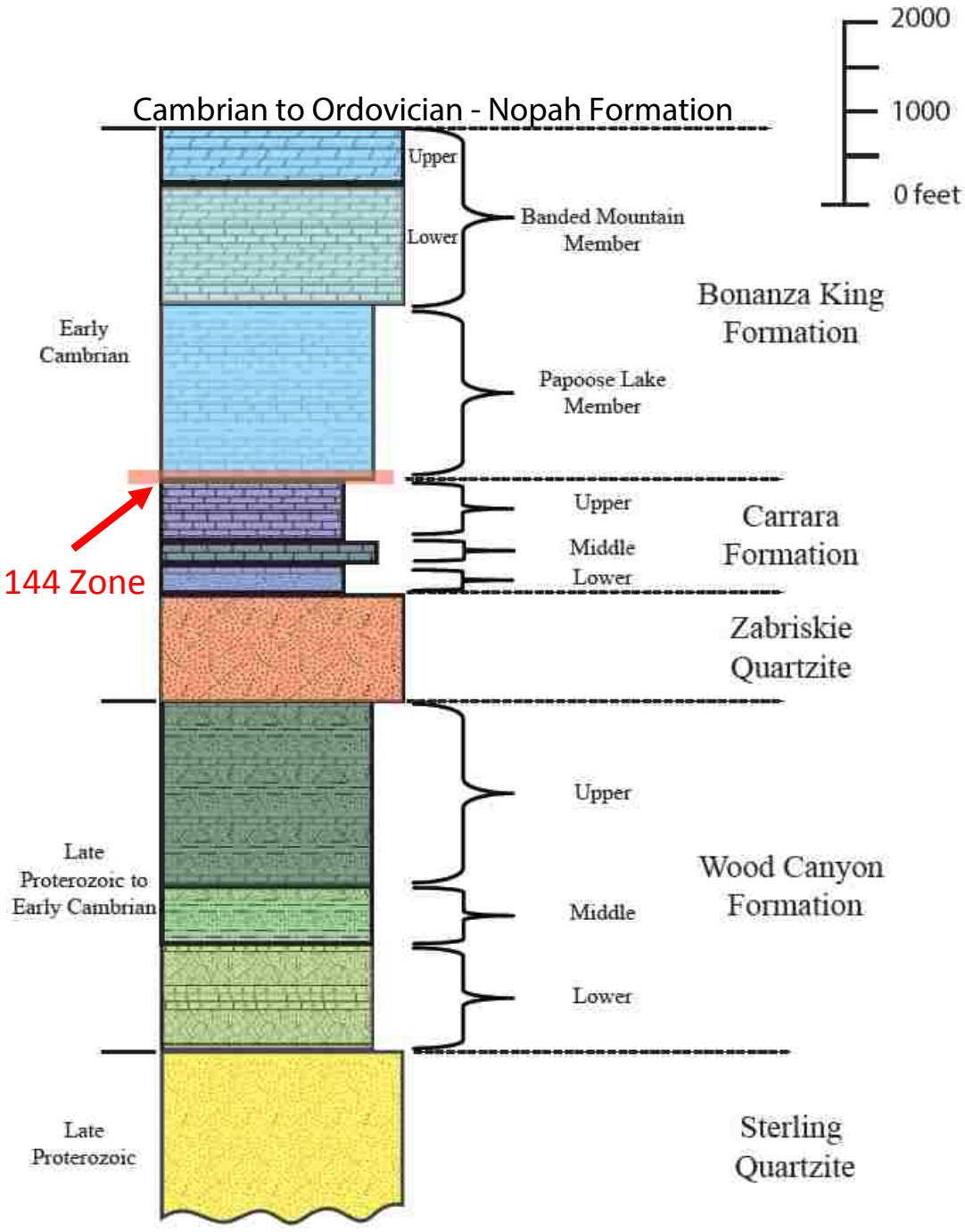

Figure 2**.** Stratigraphic column of the rocks associated with the 144 Zone, Bare Mountain, Nevada. Red box indicates the location of the 144 Zone mineralization (modified from Taylor, et. al., 2011).

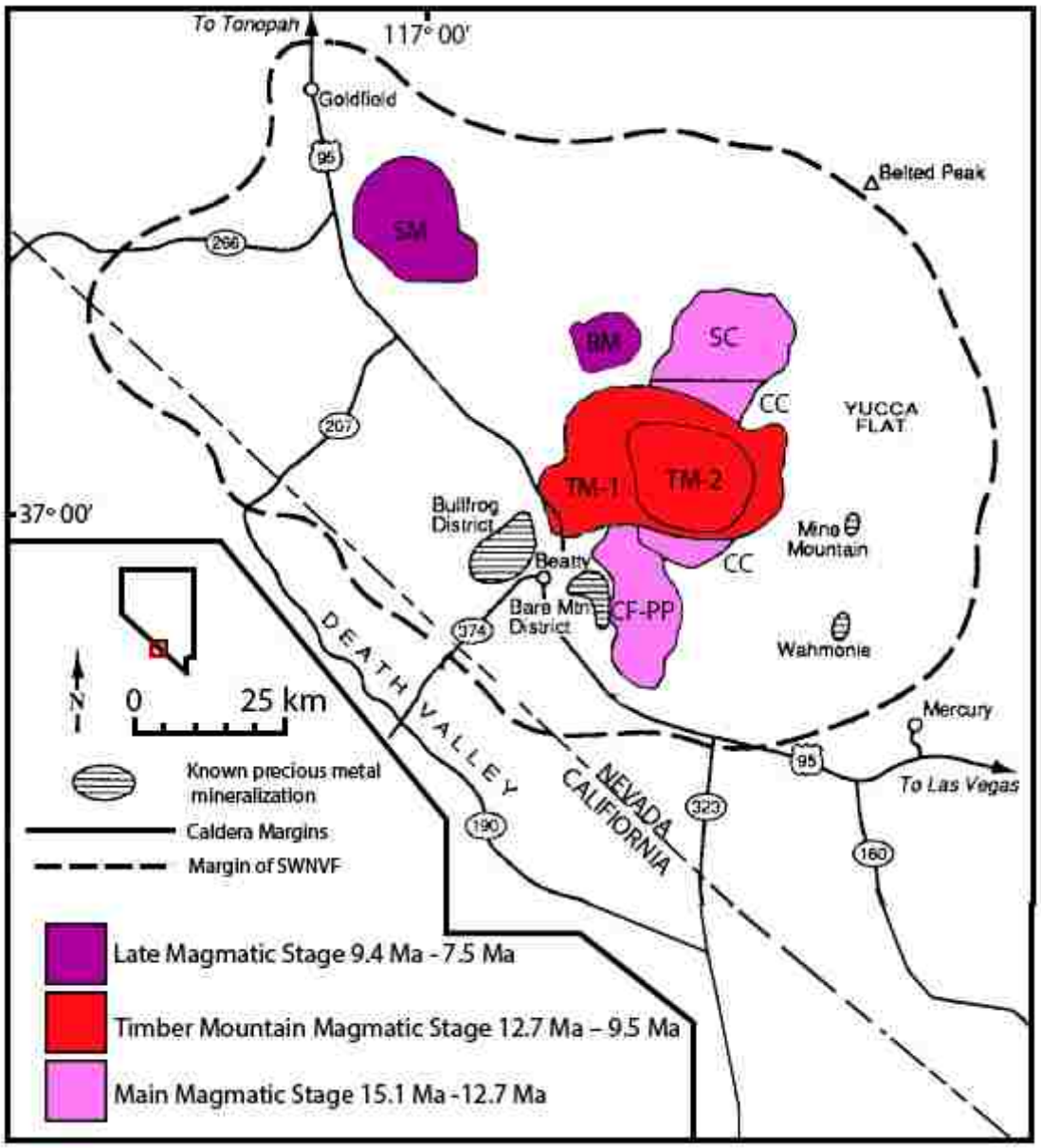

Figure 3. Map of the southwestern Nevada volcanic field (SWNVF) showing the location of magmatic sources and their timing of eruption (modified from Byers et al., 1989; Noble et al., 1991; and Castor and Weiss, 1992). *BM* **–** Black Mountain caldera, *CF-PP* – Inferred Crater Flat-Prospector Pass caldera complex, *CC* - Claim Canyon caldera, *SC* – Silent Canyon caldera, *SM* – Stonewall Mountain volcanic center, *TM-1* – Timber Mountain caldera complex I, *TM-2* – Timber Mountain caldera complex II. Heavy dashed line is the approximate limit of the SWNVF.

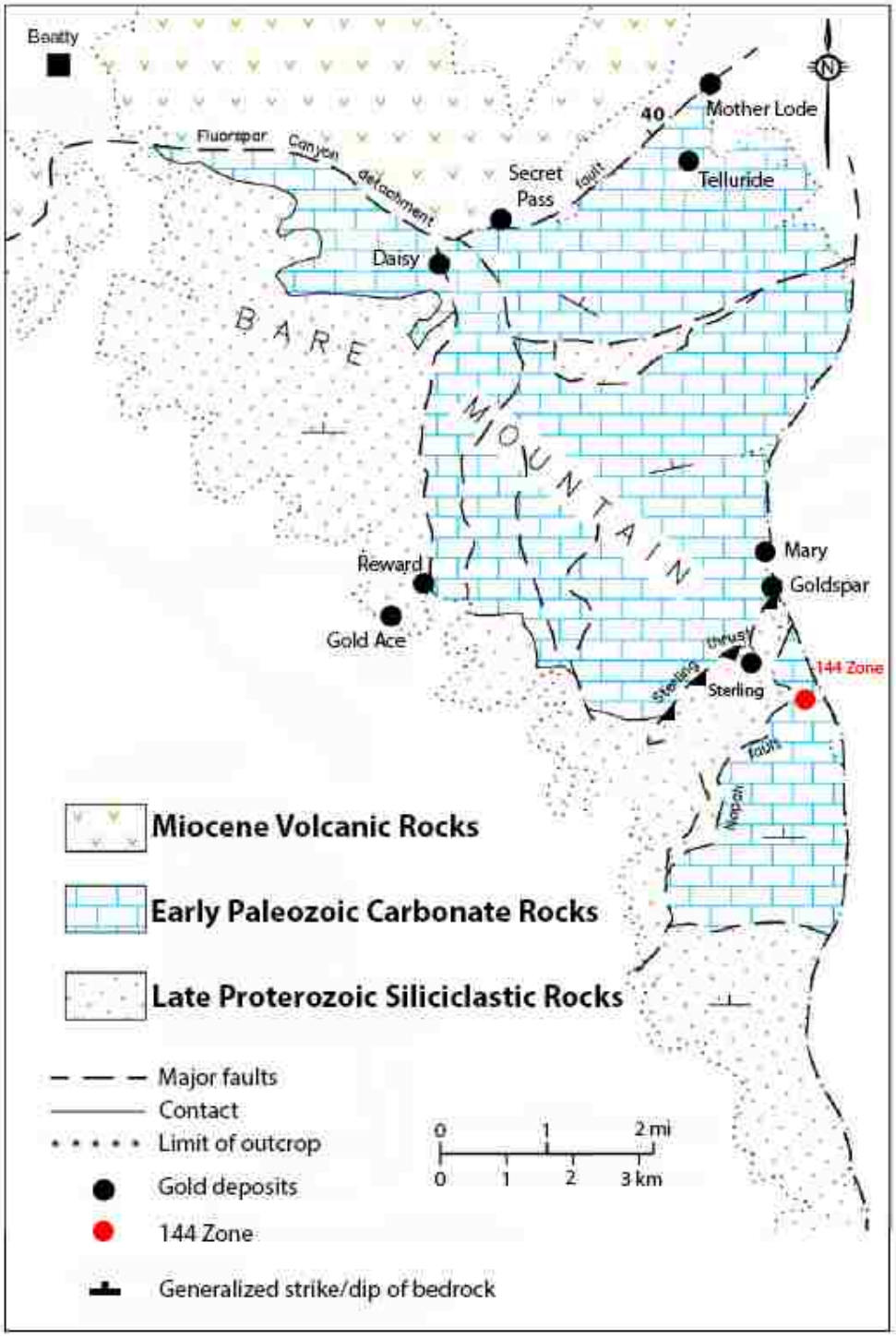

Figure 4. Geologic map of the Bare Mountain range, Nevada showing the simplified geology and location of gold deposits. Red dot indicates location of 144 Zone map figure (Modified from Gillstrom, 2006).

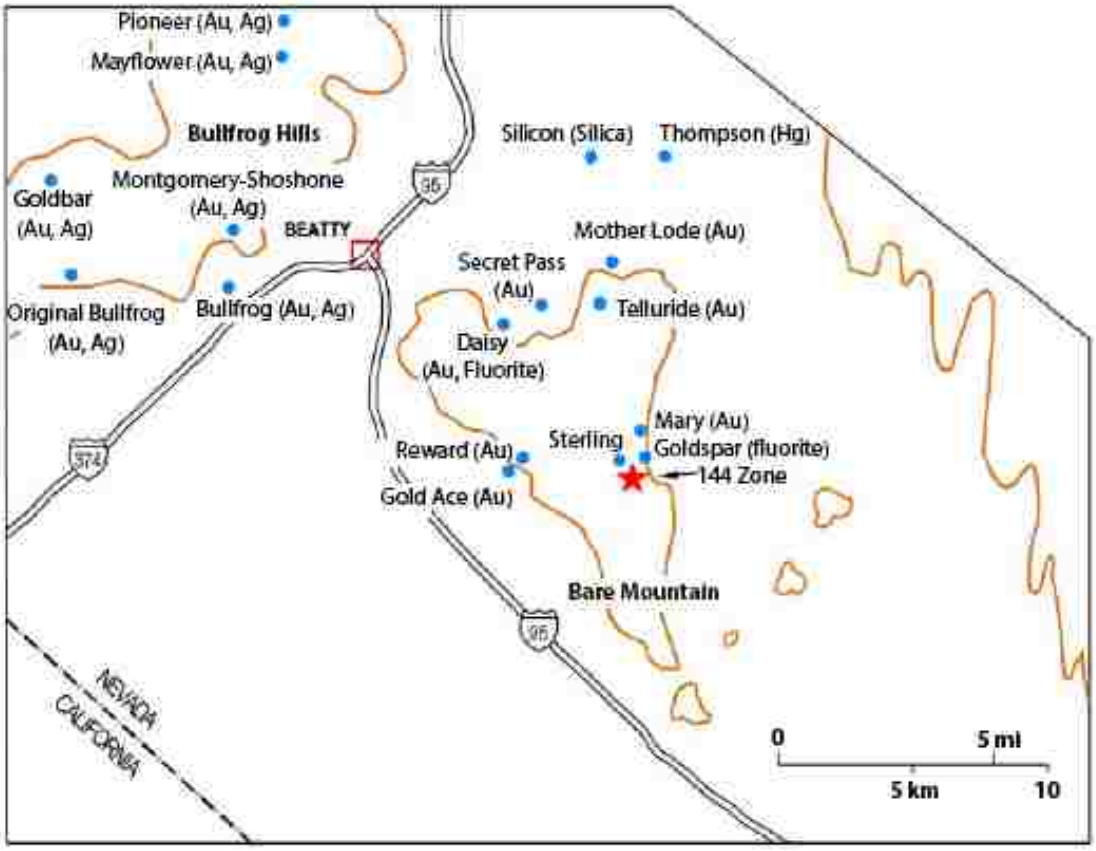

Figure 5. Historic and current mines (blue circles) within the Bare Mountain and Bullfrog Hills districts. Location of the 144 Zone indicated by the red star (modified from Gillstrom, 2006).

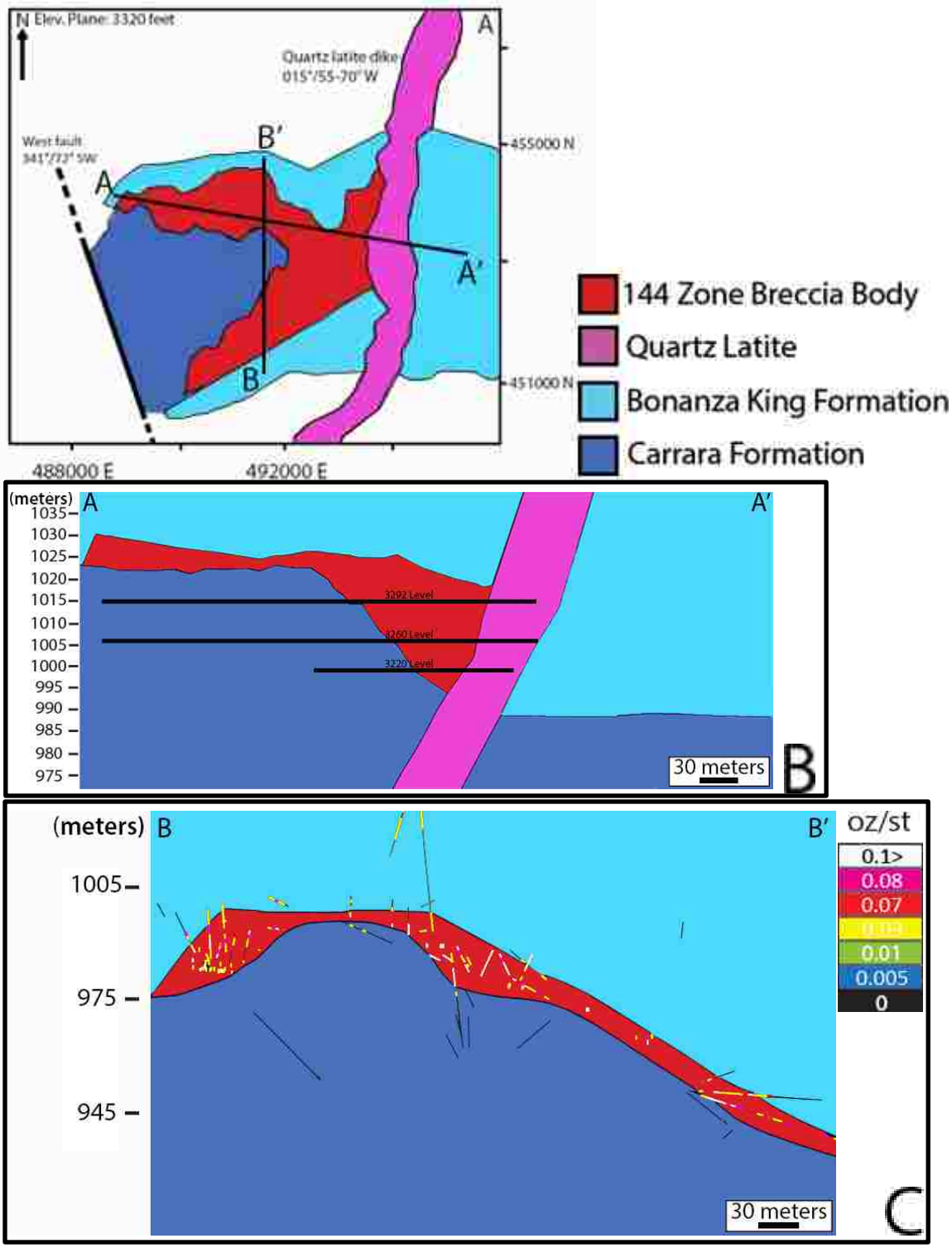

Figure 6. Map view and cross-sections of the 144 Zone. (A) Map view of the 144 Zone at an elevation plane of 3320 feet (Universal Transverse Mercator (UTM) grid for scale). (B) East-West (A-A') cross-section through the 144 Zone. Cross section displays location of 144 Zone along the Bonanza King-Carrara contact and its increased thickness proximal to a quartz latite dike. (C) South-North (B-B') cross-section of the 144 Zone looking west showing the 144 Zone breccia along the Bonanza King-Carrara contact. Breccia was constrained by drill holes, which are shown as lines in the figure. Key illustrates gold grade of drill core intervals in ounces/ton.

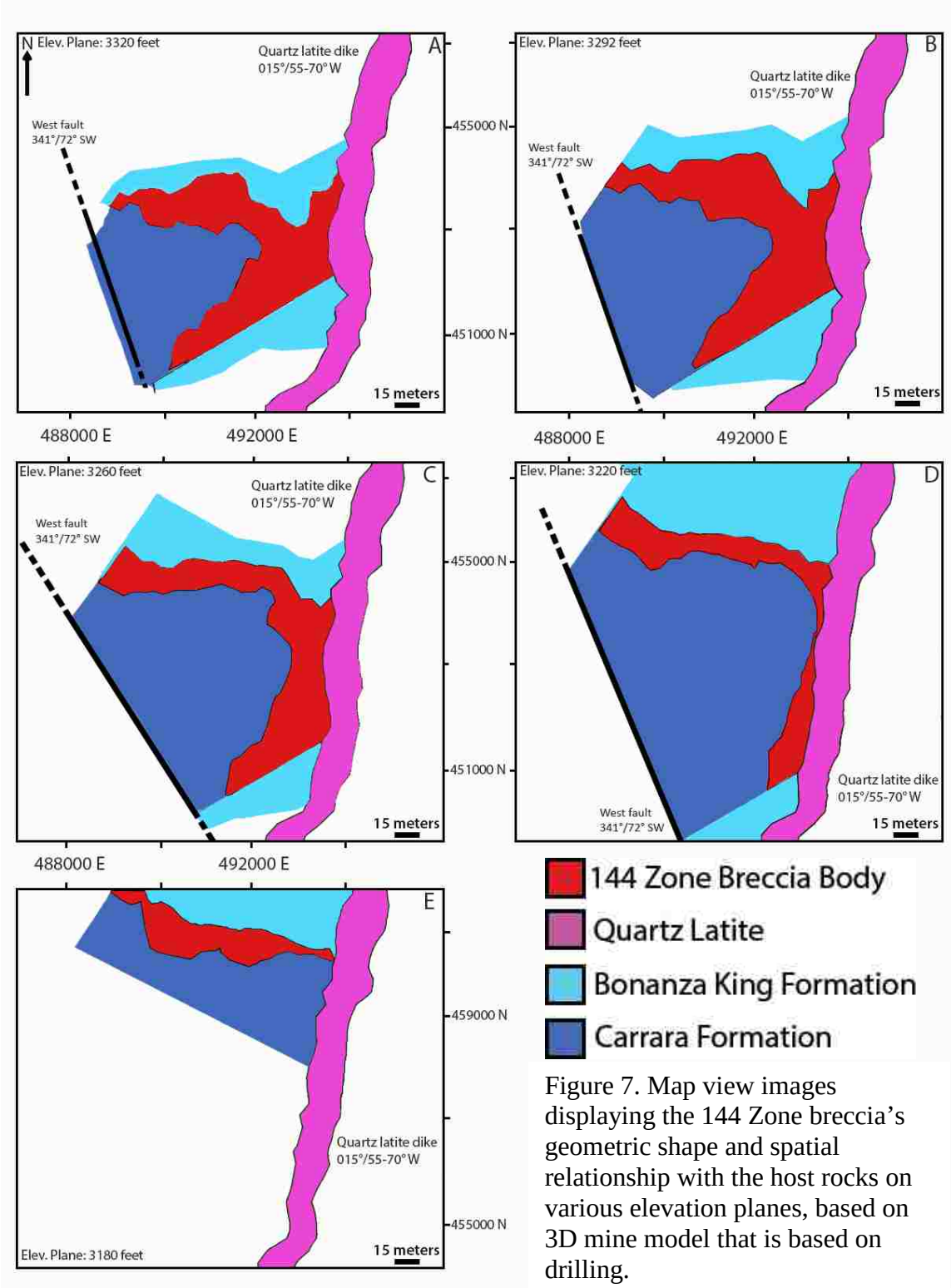

Figure 7. Map view images displaying the 144 Zone breccia's geometric shape and spatial relationship with the host rocks on various elevation planes, based on 3D mine model that is based on drilling.

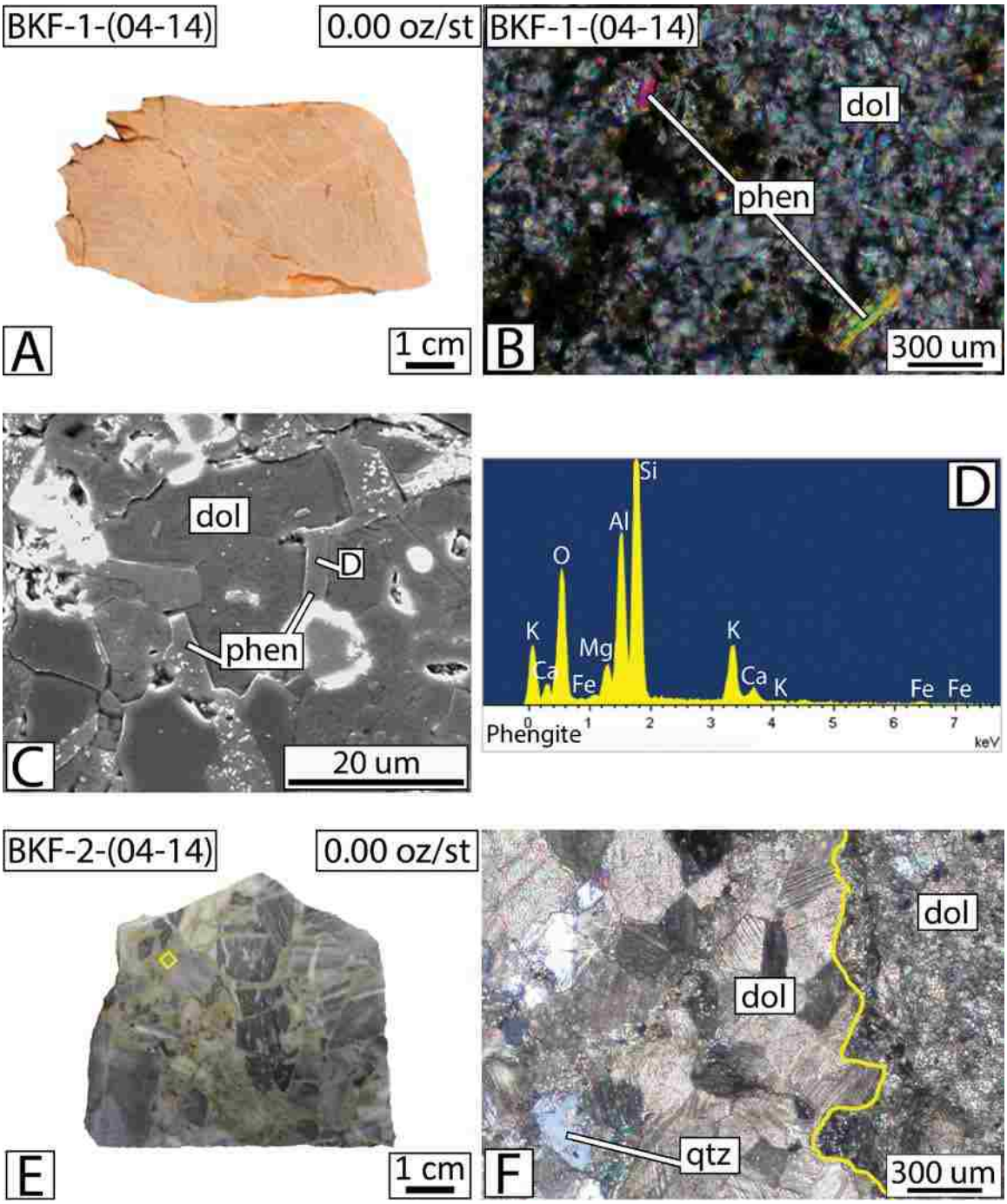

Figure 8. Unaltered and unmineralized Bonanza King Formation. Hand sample (A), XPTL photomicrograph (B), and BEI (C) of Bonanza King dolomite containing phengite. (D) SEM EDS analysis of phengite in C. Hand sample (E) and XPTL photomicrograph (F) of breccia textures exhibited in unaltered Bonanza King Formation. Yellow box in E is location of image F. Clasts (F, left) and matrix (F, right) are both composed of dolomite and lesser calcite. Yellow line in F represents contact between clast and matrix. Dol = dolomite, cc = calcite, qtz = quartz, phen = phengite, XPTL = crossed polarized transmitted light.

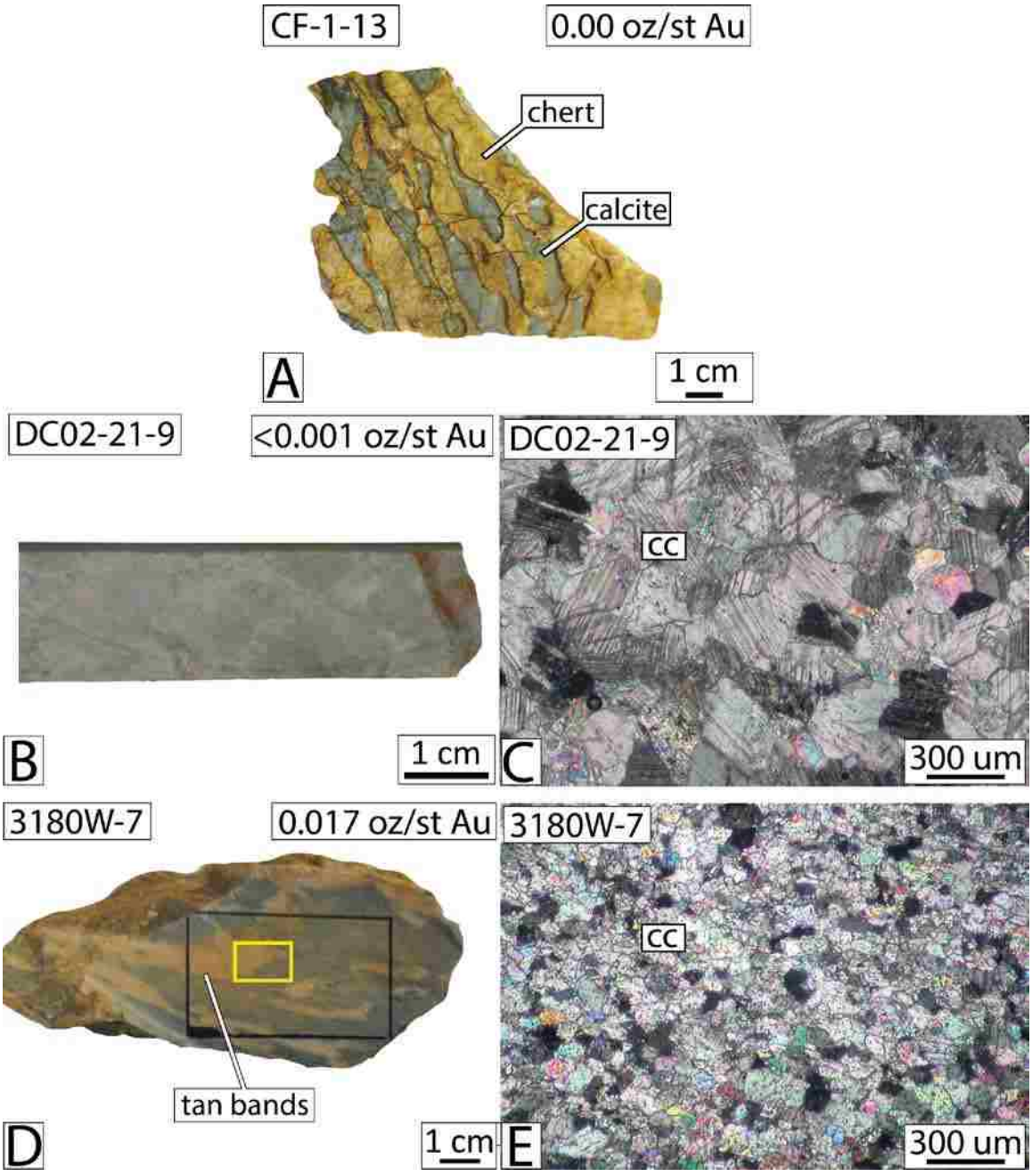

Figure 9. Unmineralized and low-grade Carrara Formation. (A) Hand sample of unaltered and unmineralized Carrara Formation limestone. (B) Drill core sample of unmineralized Carrara limestone and XPTL photomicrograph (C). (D) Low-grade Carrara limestone collected from the underground workings. Tan and grey bands are composed of calcite and cannot be distinguished at the microscopic scale (E). Cc = calcite, XPTL = crossed polarized transmitted light.

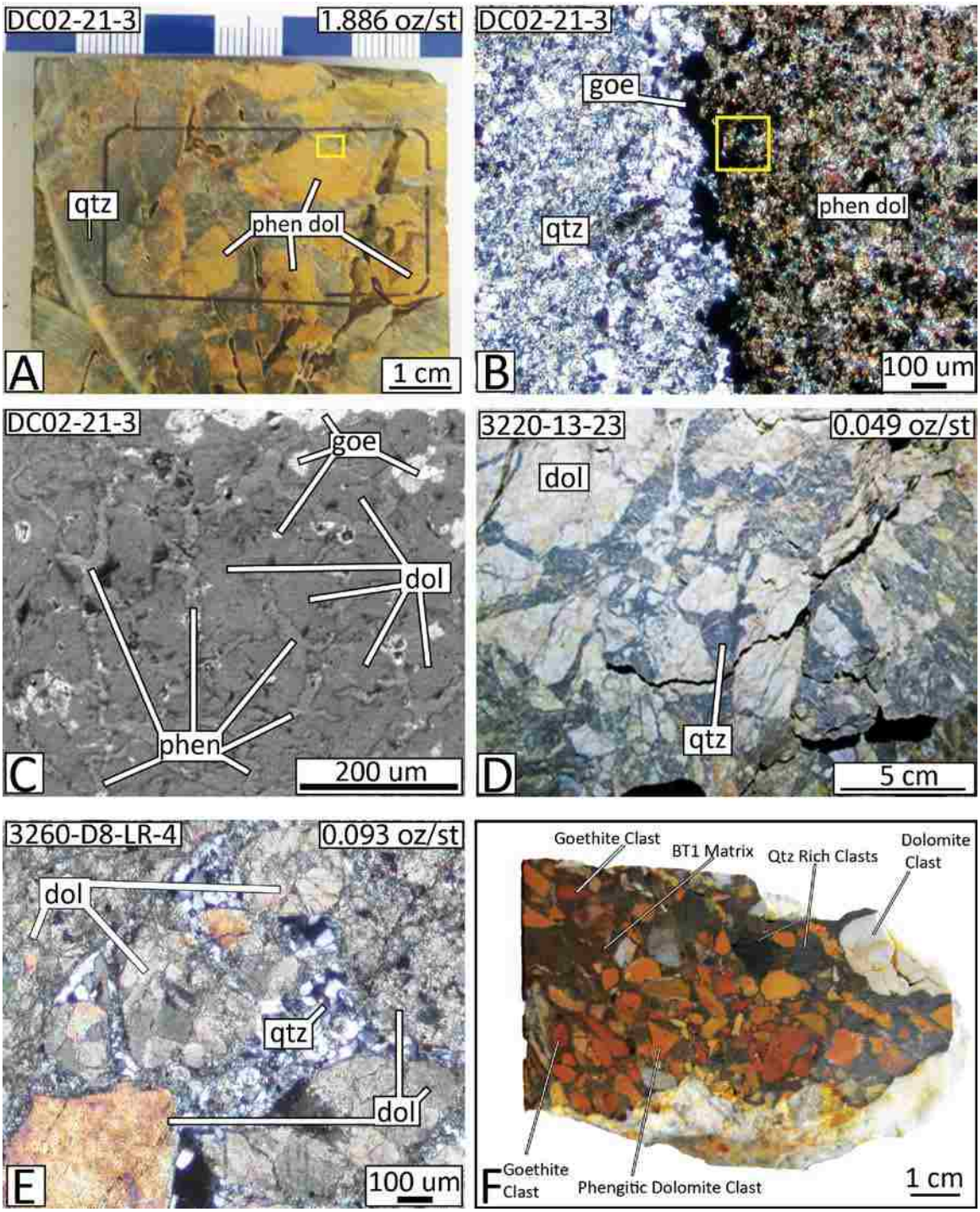

Figure 10. Photographs (A, D, F), XPTL (B, E), and BEI (C) displaying BT1 and the variety of clasts present in BT1. (A) Typical BT1 with tan phengitic dolomite clasts. (B) XPTL photomicrograph of a phengitic dolomite clast in contact with quartz matrix. Goethite is concentrated along clast-matrix contact. Yellow box in B shows location of image C. (C) BEI of phengitic dolomite clasts. (D) Underground rib photograph of BT1 monolithic breccia with dolomite clasts and quartz matrix. (E) Photomicrograph (XPTL) of BT1 breccia with dolomite clasts and quartz matrix. (F) Heterolithic BT1 displaying all clasts observed in BT1 breccias (0.029 oz/st). Qtz = quartz, goe = goethite, phen = phengite, dol = dolomite, phen dol = phengite and dolomite, XPTL = crossed polarized transmitted light.

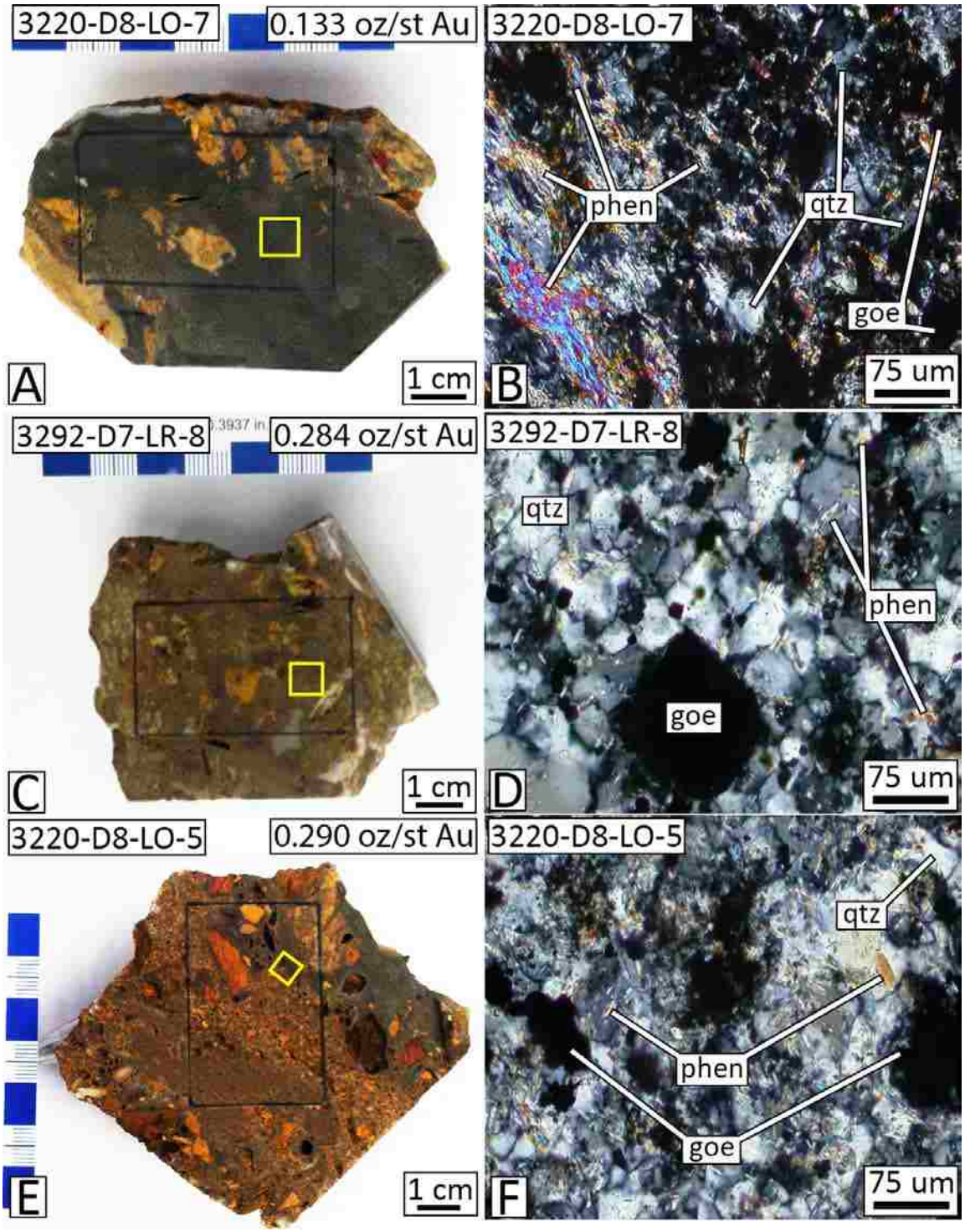

Figure 11. Breccia Type 1 matrix. Hand samples (A, C, E) of BT1 exhibiting black (A), brown (C) and black and brown (E) matrix. XPTL photomicrographs (B, D, F) show that regardless of color at the macroscopic level, the compositions of the matrices of BT1 samples are nearly identical. Qtz = quartz, goe = goethite, phen=phengite XPTL = crossed polarized transmitted light.

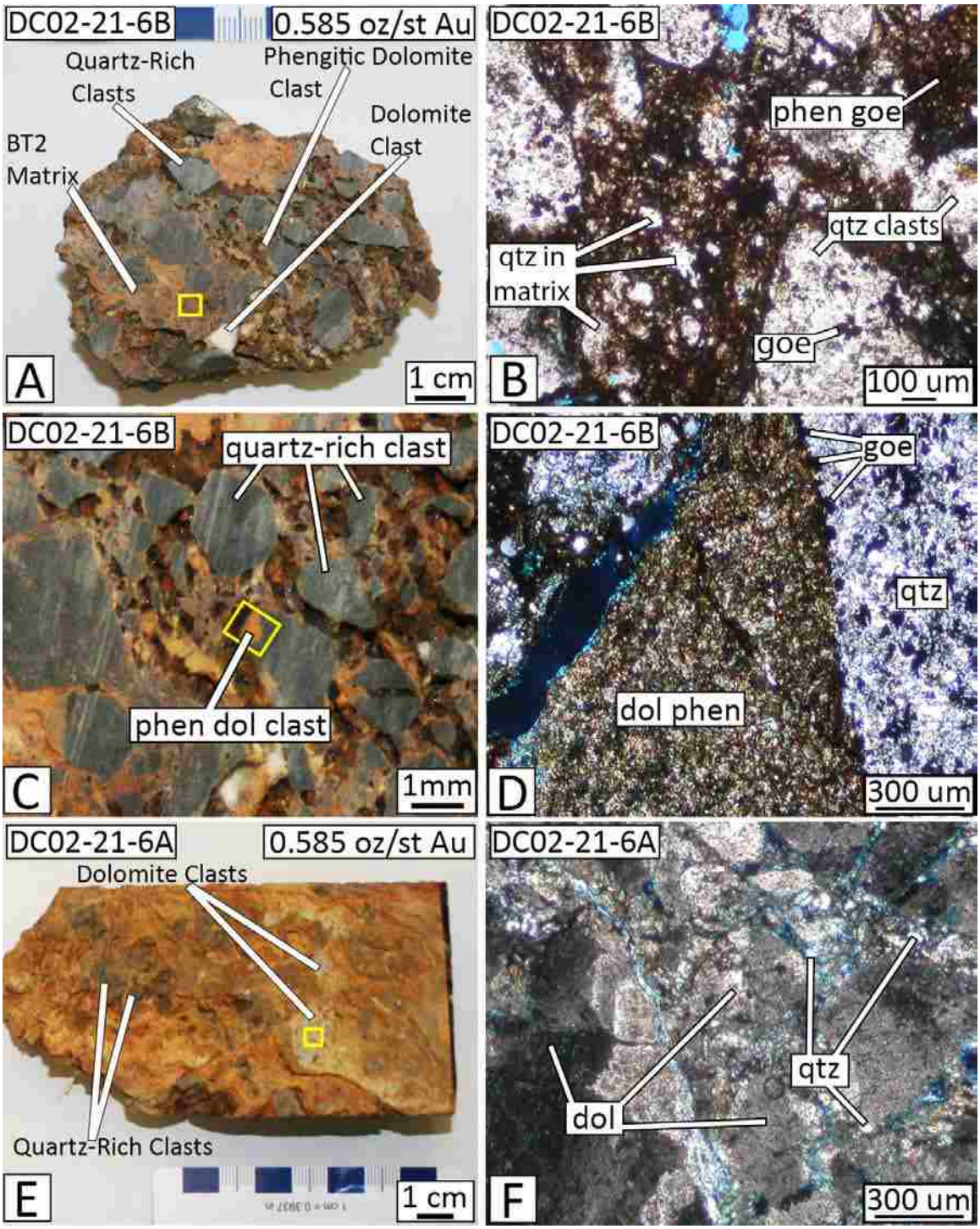

Figure 12. Breccia type 2 clasts. (A) BT2 hand sample with black, quartz-rich clasts and red-orange matrix. Yellow box in A shows location of B. (B) Photomicrograph of goethite-bearing quartz-rich clasts in a phengite-rich matrix with minor goethite and quartz (PPTL). (C) BT2 hand sample (A) with phengitic dolomite clast in a quartz-rich clast. Yellow box shows location of D. (D) Phengitic dolomite clast with goethite crystals along contact with quartz-rich clast (XPTL). (E) BT2 with dark quartz-rich clasts, light grey dolomite clasts, and yellow-orange matrix. Yellow box shows location of F. (F) Dolomite clasts with quartz veins (XPTL). Qtz = quartz, goe = goethite, phen = phengite, phen dol = phengite and dolomite, dol = dolomite, blue = epoxy, XPTL = crossed polarized transmitted light, PPTL = plain polarized transmitted light.

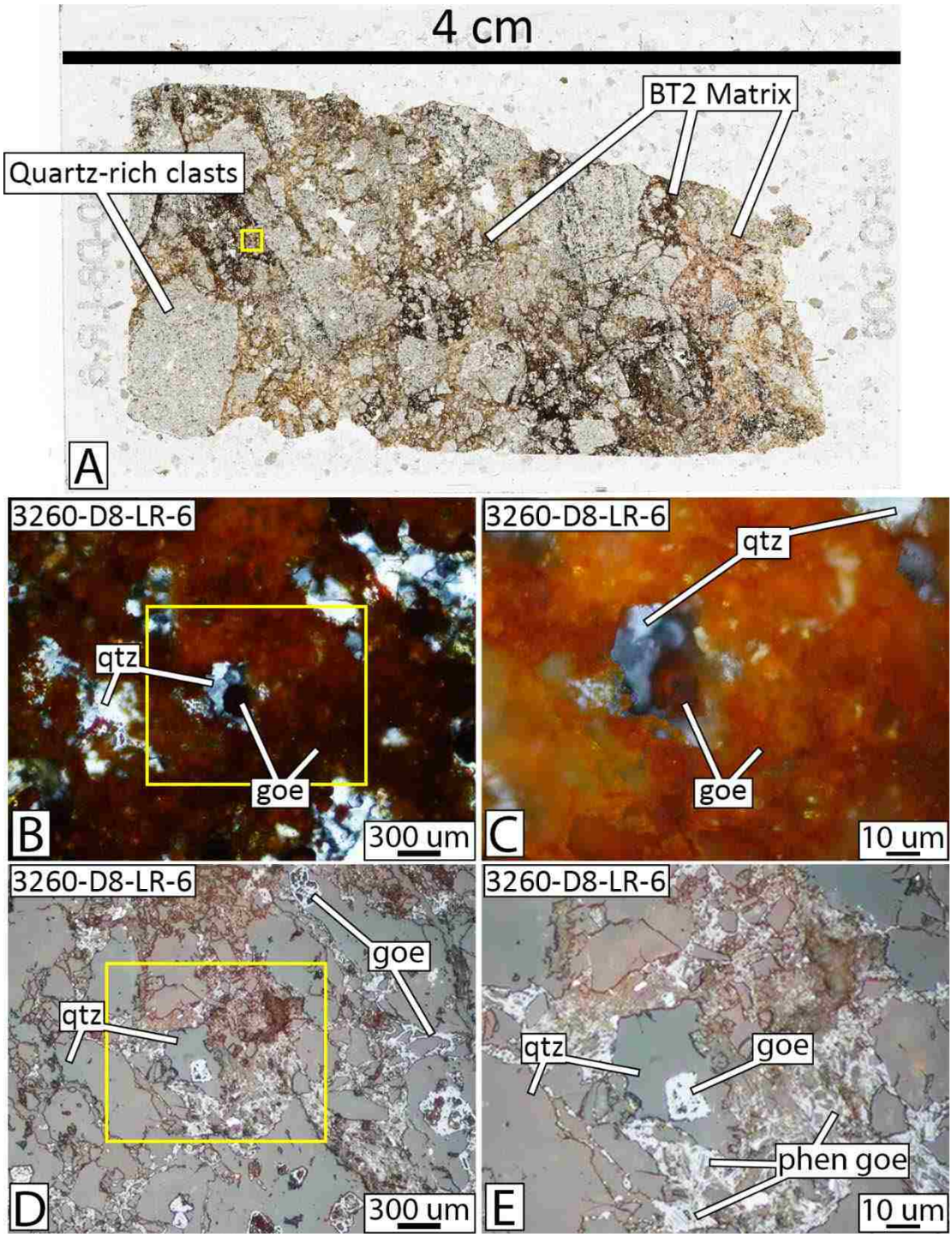

Figure 13. Polished section and photomicrographs showing the matrix of BT2 samples. (A) Polished section of BT2 showing clasts and matrix (red-orange) and the difficulty in determining the mineralogy of the matrix in hand sample. Yellow box in A shows location of B and D. (B, C) XPTL images of quartz clasts cemented by a phengite, goethite and minor quartz matrix. Yellow box in B shows location of C. Goethite staining makes it difficult to identify matrix minerals. (D, E) PPRL photomicrographs of B and C, respectively. Reflected light provides detail of matrix minerals not visible in transmitted light. Textural relationships between phengite, goethite and quartz crystals now visible Goethite is present in the matrix and quartz clasts. Qtz = quartz, goe = goethite, phen=phengite, XPTL = crossed polarized transmitted light, PPTL = plain polarized transmitted light.

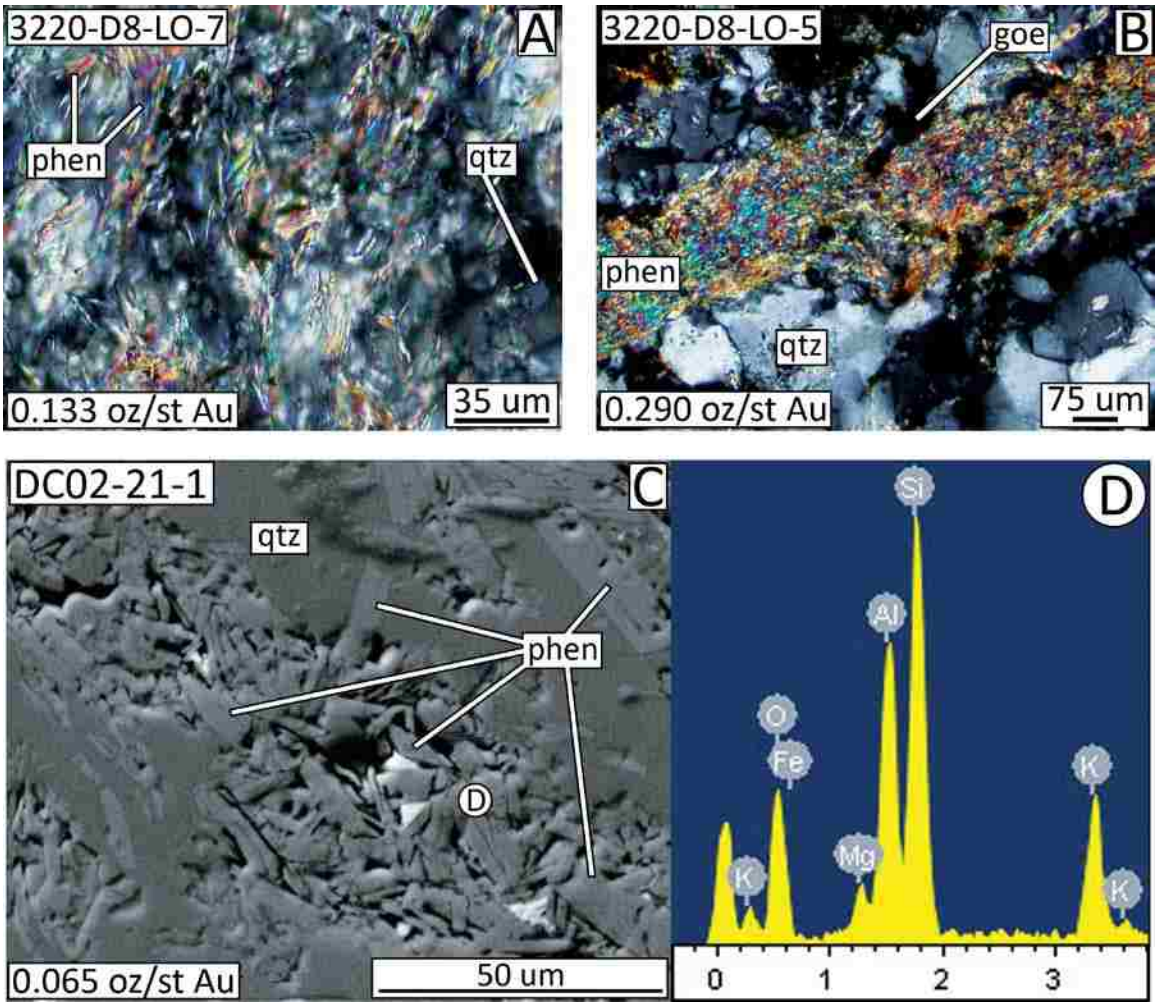

Figure 14. Photomicrographs and BEI displaying phengite. (A) Photomicrograph of bladed and sheaf phengite in quartz (XPTL). Bladed phengite ranges from 5 um – 40 um and occurs in both BT1 and BT2. (B) Photomicrograph of massive phengite, which is less common than individual bladed and sheaf textures and is located in between quartz crystals in BT1 (XPTL). (C) BEI of bladed and sheaf phengite surrounded by quartz within BT1 matrix. (D) EDS analysis results showing relative peaks for K, Al, Mg, SI, O and Fe confirming the presence of phengite. Phengite was also identified using TerraSpec 4 mineral analysis. Phen = phengite, qtz = quartz, goe = goethite, XPTL = crossed polarized transmitted light.

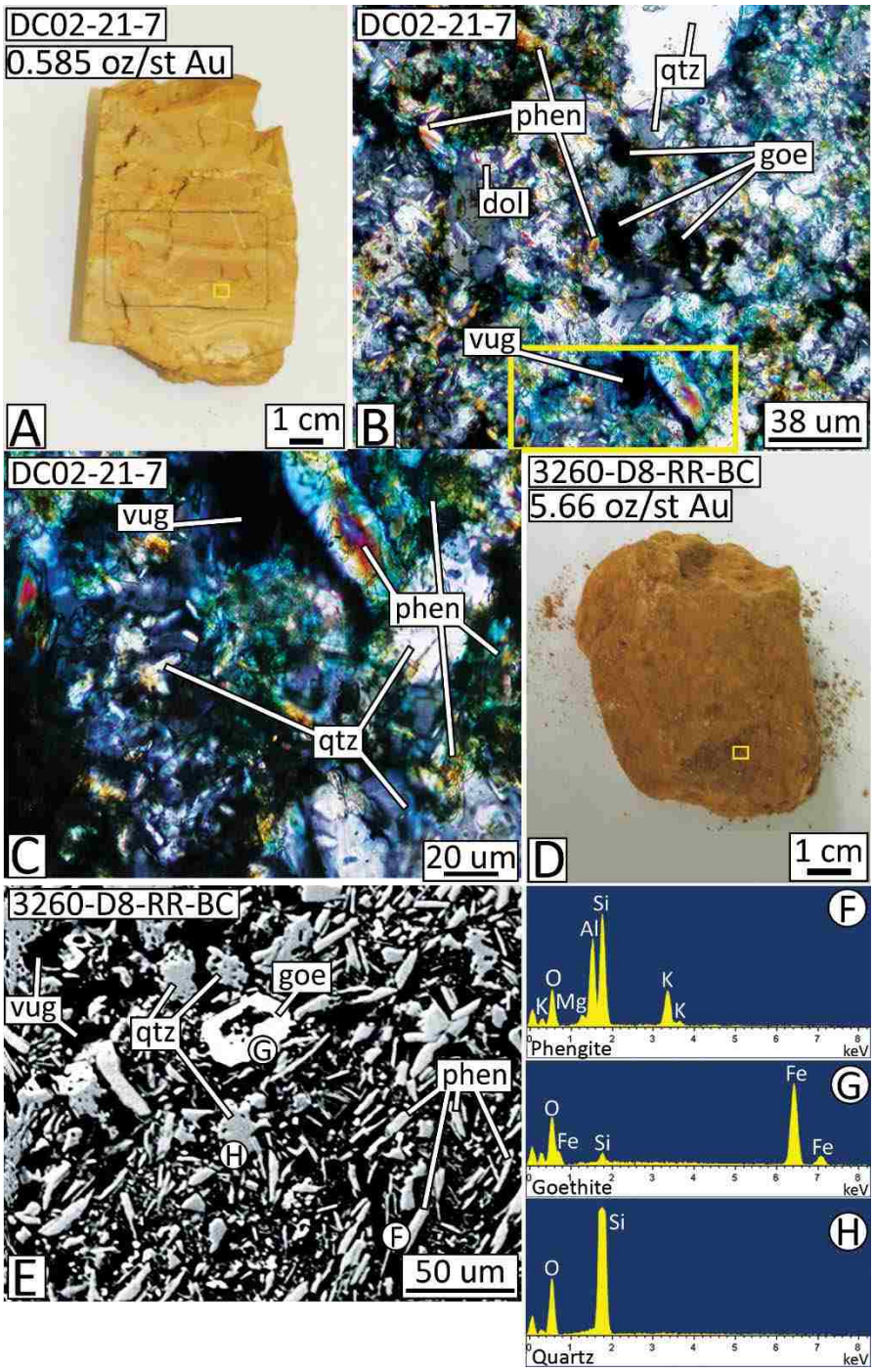

Figure 15: Hand samples (A, D), photomicrographs (B, C), and BEI displaying altered, phengite-rich samples. (A) Hand sample of phengite-rich altered rock. (B) Photomicrograph of A displaying phengite with lesser quartz and goethite (XPTL). Yellow box is location of image C. (C) Dominant phengite with lesser quartz, goethite and pore space (XPTL). (D) Hand sample of high-grade phengite-rich sample. (E) BEI of sample shown in D. Bladed and elongated crystals were confirmed as phengite with EDS analysis (F). Bright white near-cubic minerals are goethite (G) and grey anhedral crystals are quartz (H). Black represents open-space. Qtz = quartz, phen = phengite, goe = goethite, vug = open-space, dol = dolomite, XPTL = crossed polarized transmitted light.

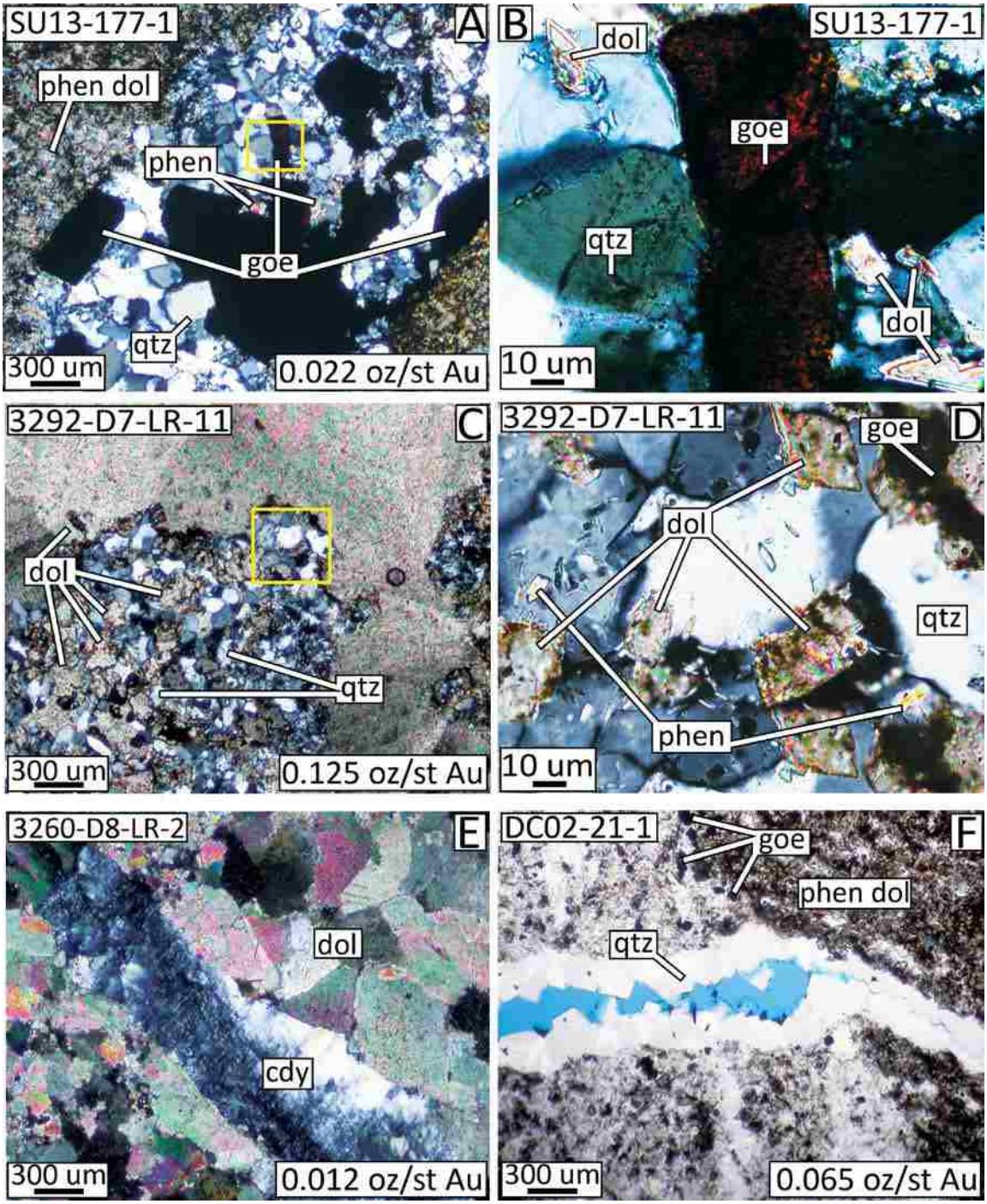

Figure 16. Photomicrographs displaying minerals and textures associated with silicification. (A) Anhedral quartz characteristic of silicification (XPTL). Quartz is commonly spatially associated with goethite and phengite. Yellow box is location of B. (B) Solid dolomite inclusions encapsulated in quartz (XPTL). (C) BT1 matrix and dolomite clast boundary (XPTL). Yellow box shows location of image D. (D) Solid dolomite inclusions encapsulated in quartz along the contact of a dolomite clast indicating progressive replacement of dolomite (XPTL). (E) Chalcedony within a dolomite-rich sample indicating open-space precipitation of chalcedony (XPTL). (F) Euhedral quartz crystals rimming a fracture (PPTL). Qtz = quartz, goe = goethite, phen=phengite, dol = dolomite, cdy = chalcedony, phen dol = phengite and dolomite, blue = epoxy, XPTL = crossed polarized transmitted light.

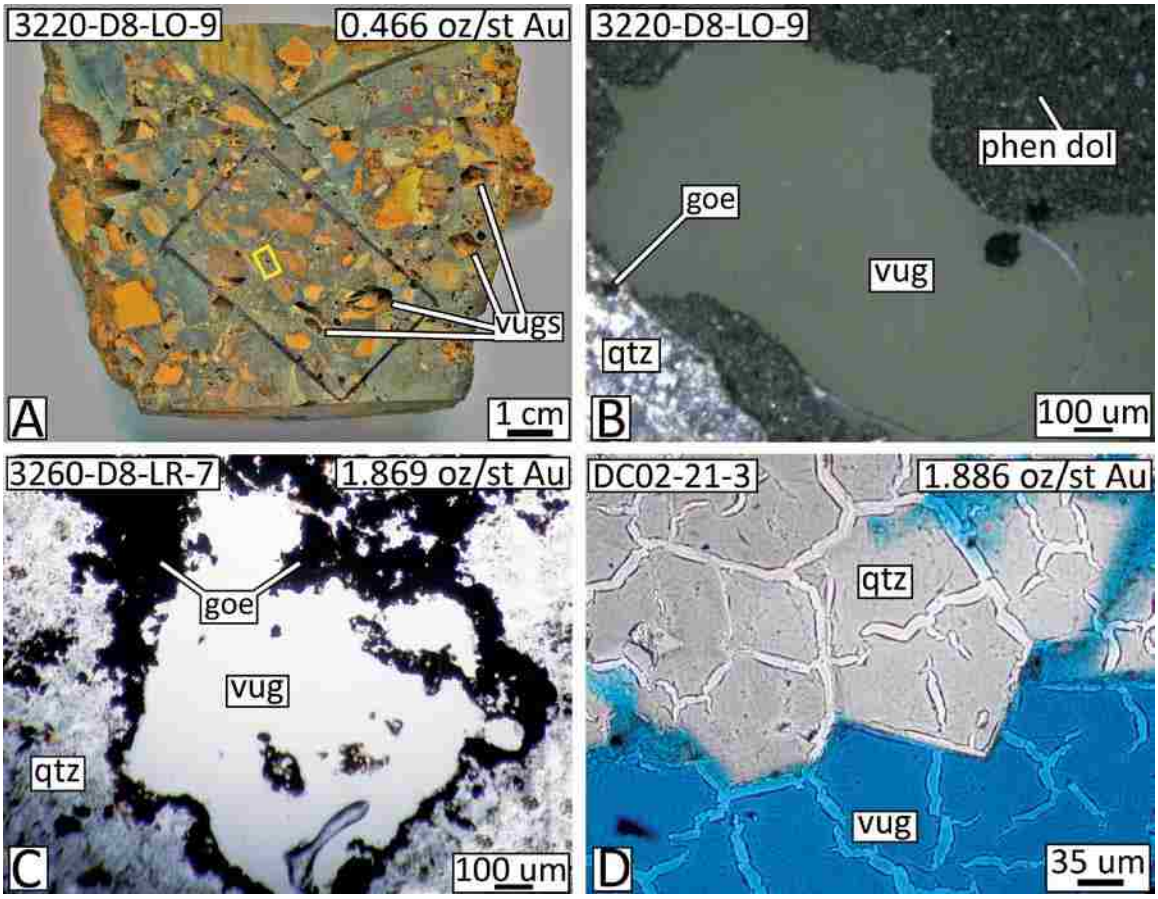

Figure 17. Vug formation. (A) BT1 with several rounded to angular vugs formed from decarbonatization. Yellow box is location of image B. (B) Photomicrograph of vug with remnant dolomite and minor phengite (PPRTL). (C) Photomicrograph of goethite (black) rimming a vug formed by decarbonatization (PPTL). (D) Photomicrograph of euhedral quartz rimming a vug (blue) (PPTL). Phen dol= phengite and dolomite, qtz = quartz, goe = goethite, blue epoxy = pore space, PPTL = plain polarized transmitted light, and PPRTL = Plain polarized reflective and transmitted light.

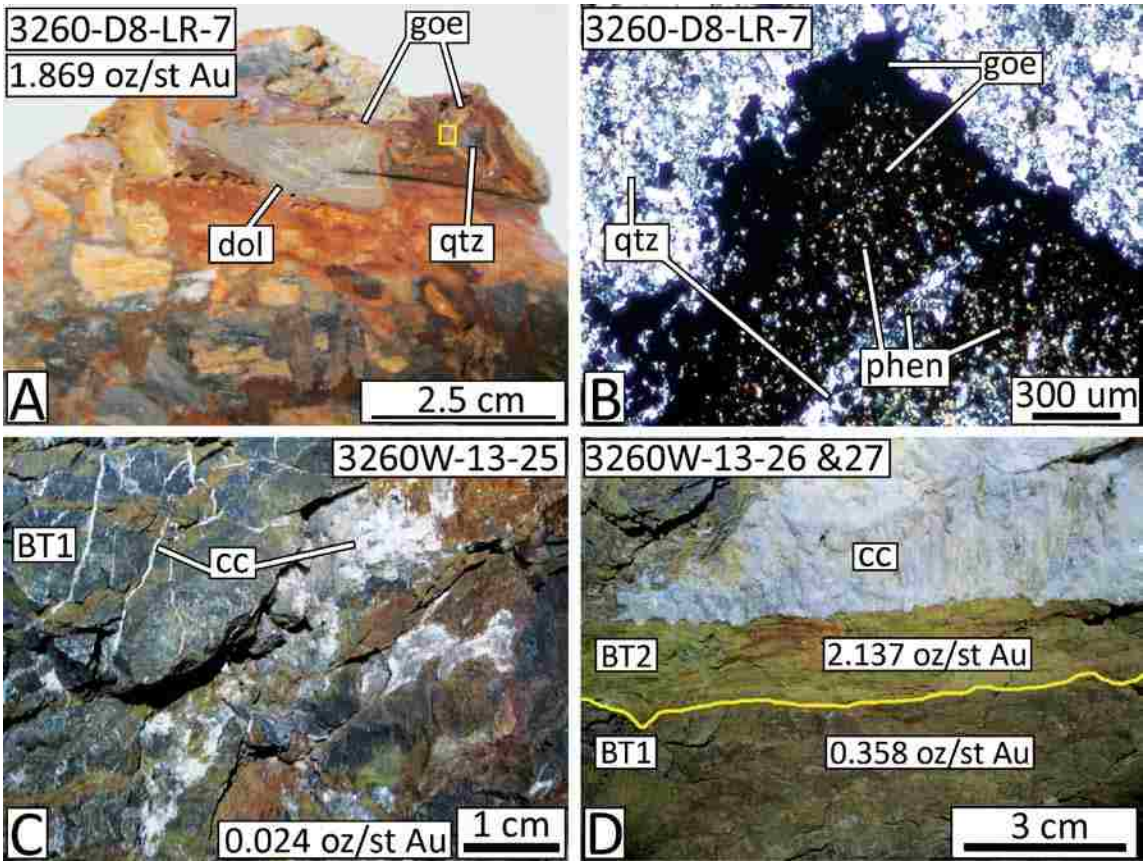

Figure 18. Post-ore oxidation and vein calcite. (A) BT1 with goethite (orange-red) rimming dolomite and quartz-rich clasts. This texture is rare in BT1. Yellow box is location of image B. (B) Quartz-rich clast with goethite rim. Clast is composed of minor phengite and goethite suggesting that this clast was once composed of dolomite and phengite (XPTL). (C) Photograph of underground rib with post-ore white calcite vein cross-cutting BT1. (D) Photograph of underground rib with calcite filling a cavity. Yellow line is contact between BT1 (below) and BT2 (above). Qtz = quartz, goe = goethite, phen=phengite, dol = dolomite, cc = calcite XPTL = crossed polarized transmitted light, BT1 = Breccia type 1, and BT2 = Breccia type 2.

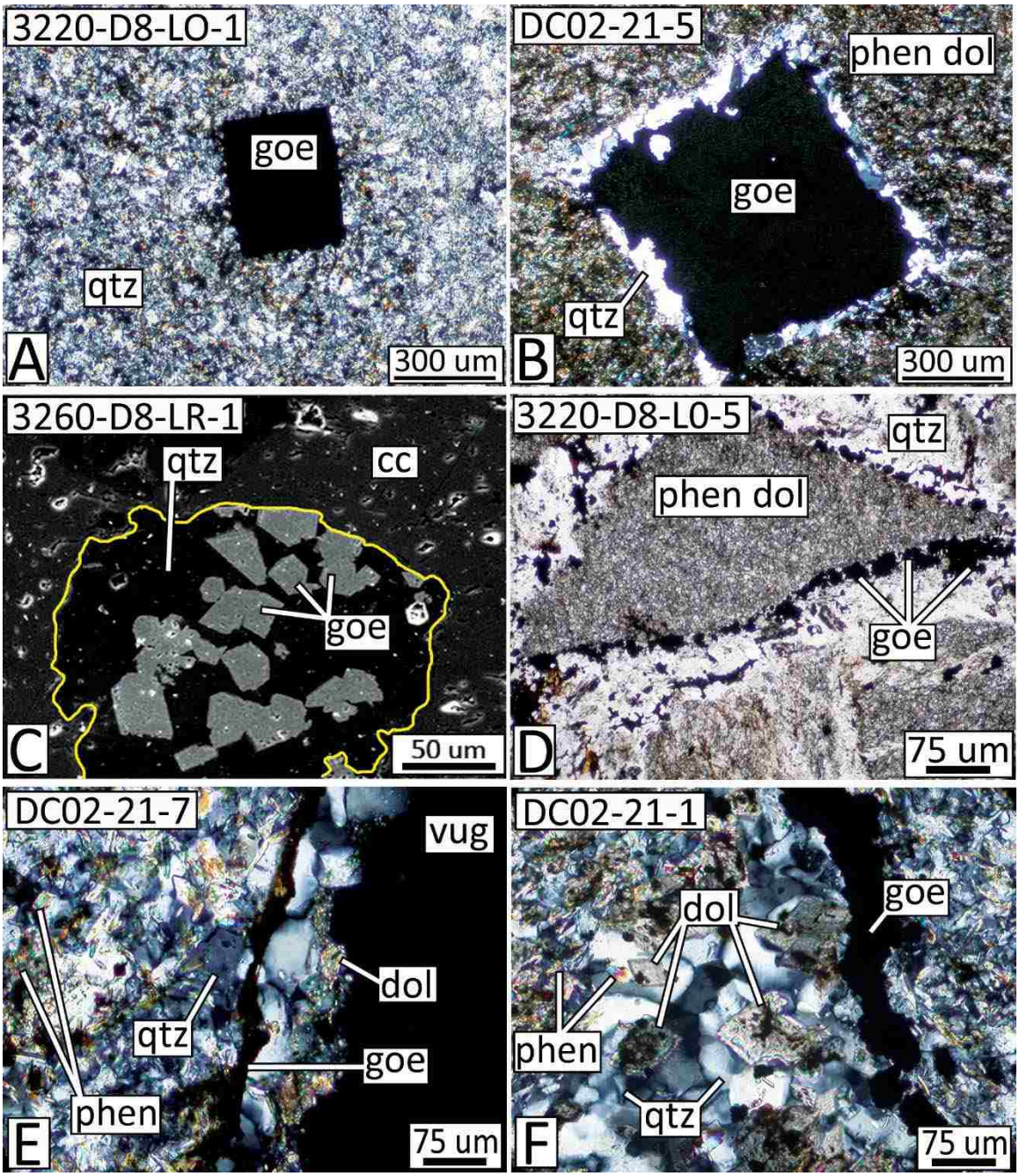

Figure 19. Goethite forms and textures. (A) Photomicrograph of type 1a goethite within BT1 matrix (XPTL). (B) Photomicrograph of type 1b goethite rimmed by quartz in a phengitic dolomite clast (XPTL). (C) BEI image of "clustered" type 1b goethite crystals within quartz in calcite. Yellow line is calcite-quartz boundary. (D) Photomicrograph of type 1b subhedral goethite crystals along the contact between BT1 matrix and a phengitic dolomite clast (PPTL). (E) Photomicrograph of Type 2 "vein-like" goethite near a vug and spatially associated with quartz (XPTL). (F) Photomicrograph of Type 2 anhedral goethite within BT1 matrix (XPTL). Phen dol = phengite and dolomite, goe = goethite, qtz = quartz, dol = dolomite, cc = calcite, vug = open-space, XPTL = crossed polarized transmitted light, and PPTL = plain polarized transmitted light.

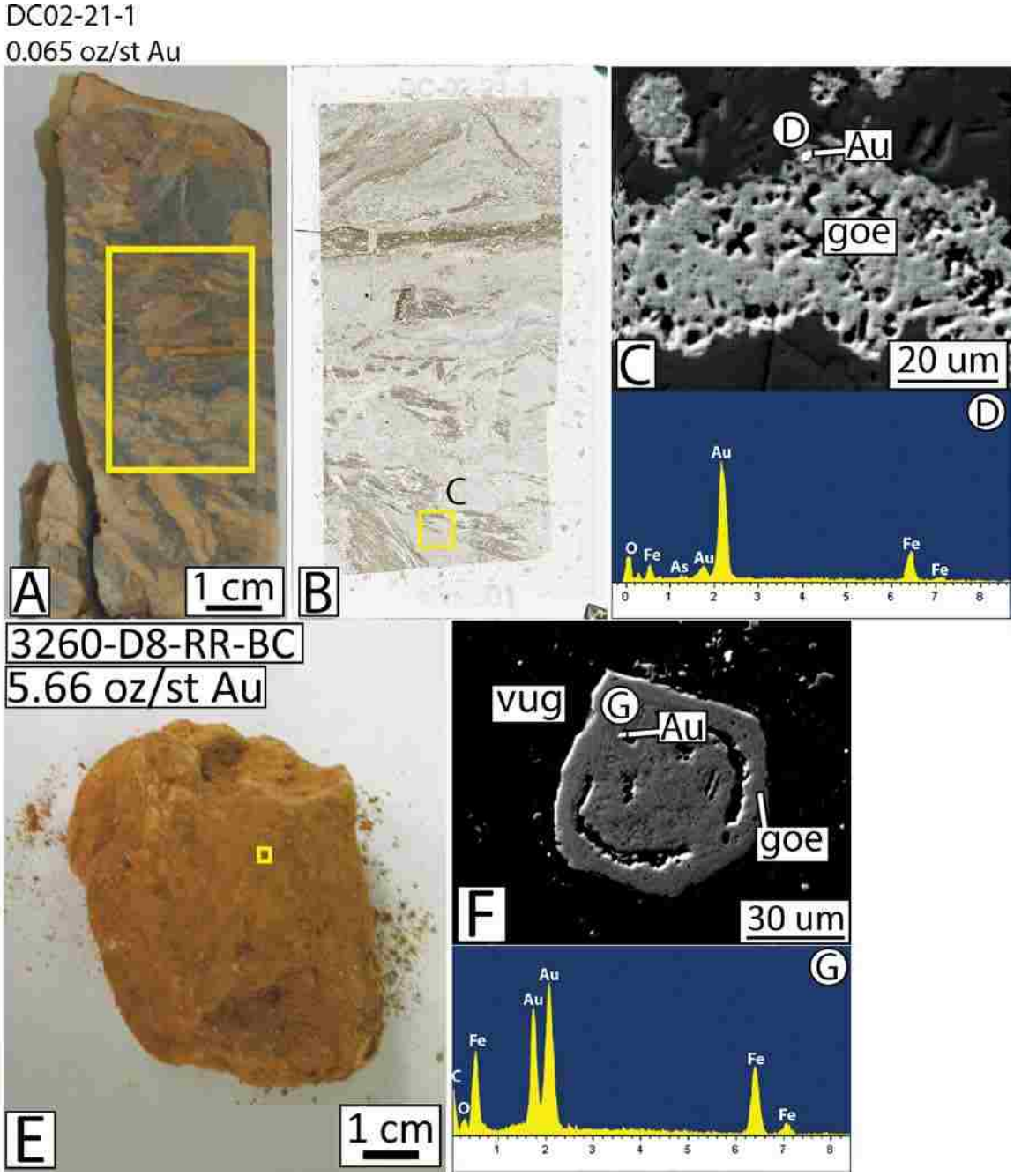

Figure 20. Hand samples, polished sections, and BEI images displaying the location of native gold in BT1 and BT2. (A) BT1 hand sample (box shows location of polished section B. (C) Type 2 Au-bearing goethite. Bright white area confirmed as native gold by EDS analysis (D). (E) Phengite-rich BT2 hand sample. Yellow box shows location of F. (F)Type 1b Au-bearing goethite. Bright white area confirmed as native gold by EDS analysis (G). Au = native gold, goe = goethite, and vug = pore space.

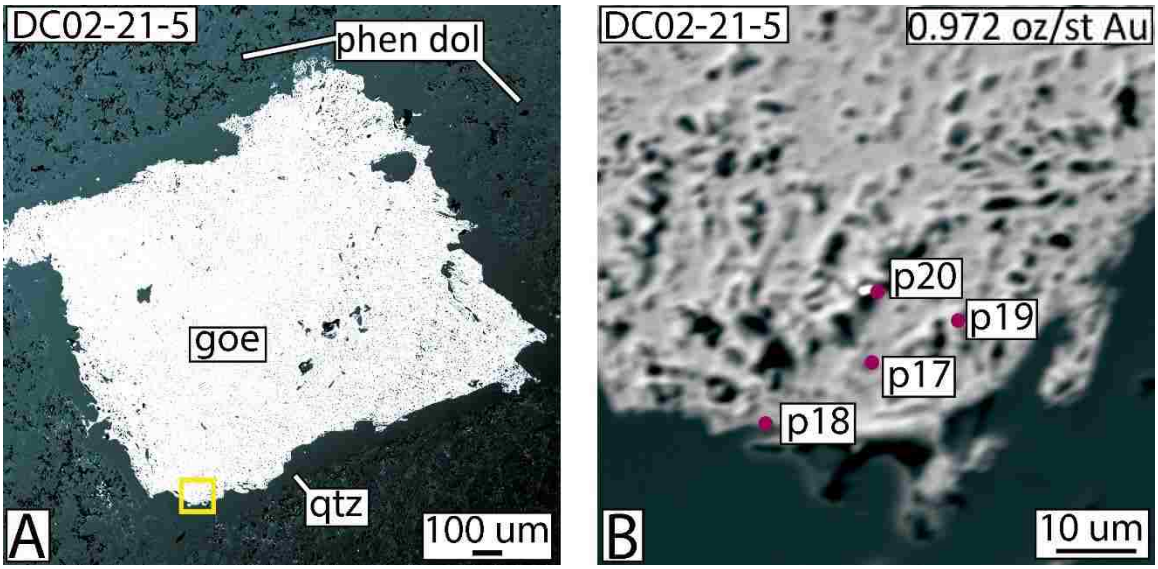

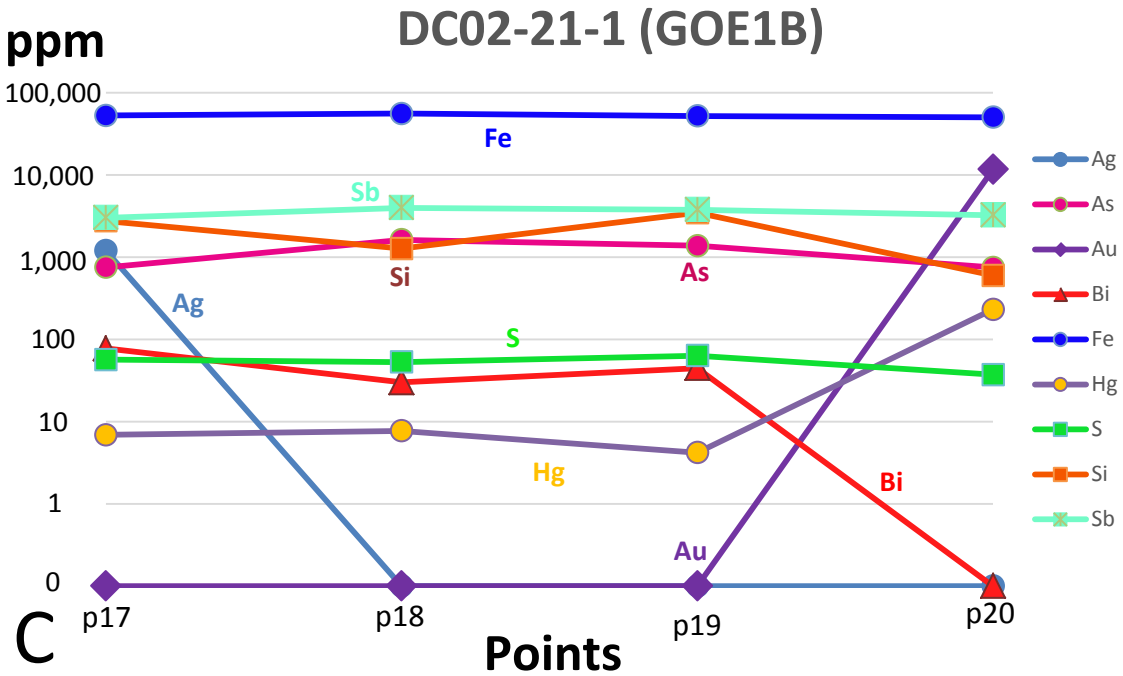

Figure 21. Gold location and analyses. (A) BEI of Type 1b Au-bearing goethite. Yellow box shows location of image B and four EPMA points. (C) Concentrations of gold and other elements in goethite. Image shows bright spot (p20) that contains Au with Sb, As, and Hg plus Fe, but not Ag or Bi. Goe = goethite, qtz = quartz, and phen dol = phengite and dolomite.

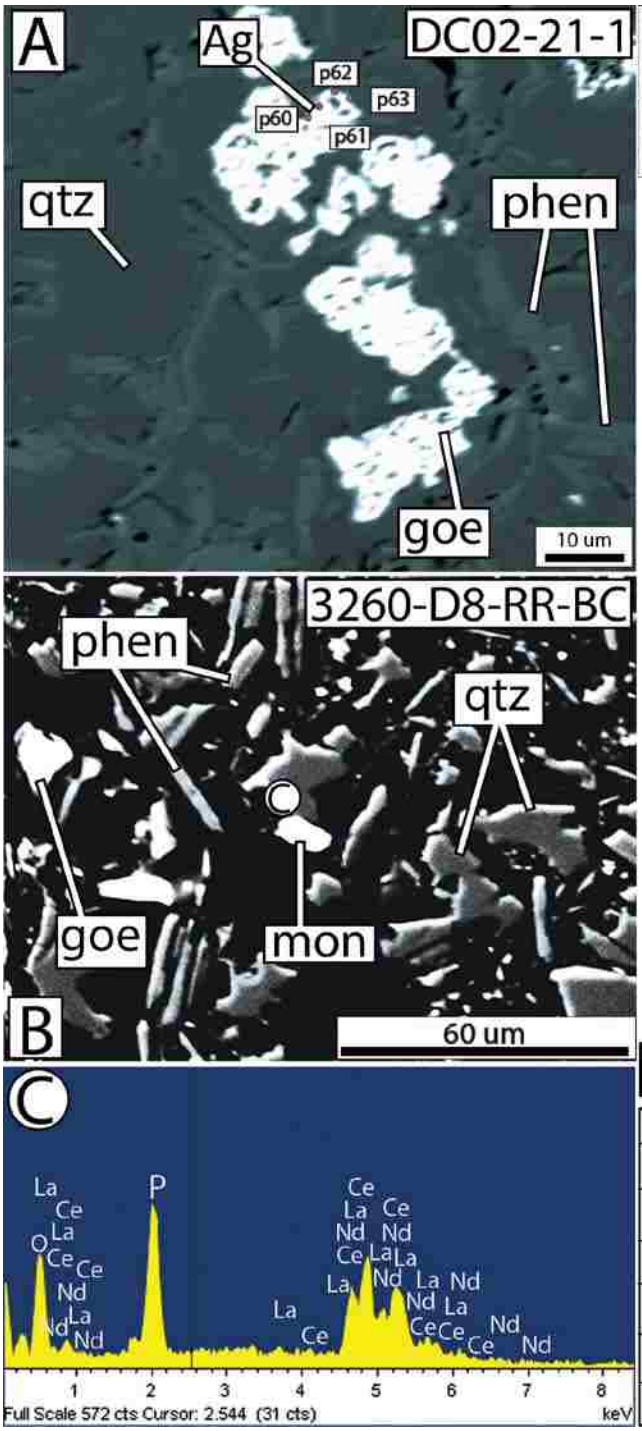

p60- Ag: 0.9 ppm Au: 0.0 ppm A
p61- Ag: 4,735 ppm Au: 5.8 ppm
p62- Ag: 2,689 ppm Au: 0.0 ppm
p63- Ag: 48.2 ppm Au: 0.0 ppm

Figure 22. Ag and REE-bearing monazite. (A) BEI of Type 1b, Ag-bearing goethite. Concentrations of Ag for each point (purple dots) are shown in the box to the right of the image. (B) BEI of a phengite-rich BT2 sample with REE-rich monazite (bright white). Black areas are pore space. (C) EDS analysis of monazite. Results show relative peaks for Ce, La and Nd confirming the presence of REEs. (D) Table with semi-quantitative analyses of each element. Qtz = quartz, phen = phengite, goe = goethite, mon = monazite, P = Phosphorous, Ce = Cesium, La = Lanthanum, Nd = Neodymium

D

Element	Weight %	Atomic %
P	13.89	17.19
La	21.04	5.81
Ce	31.61	8.65
Nd	5.55	1.48
O	27.91	66.88
Total	100.00	100.01

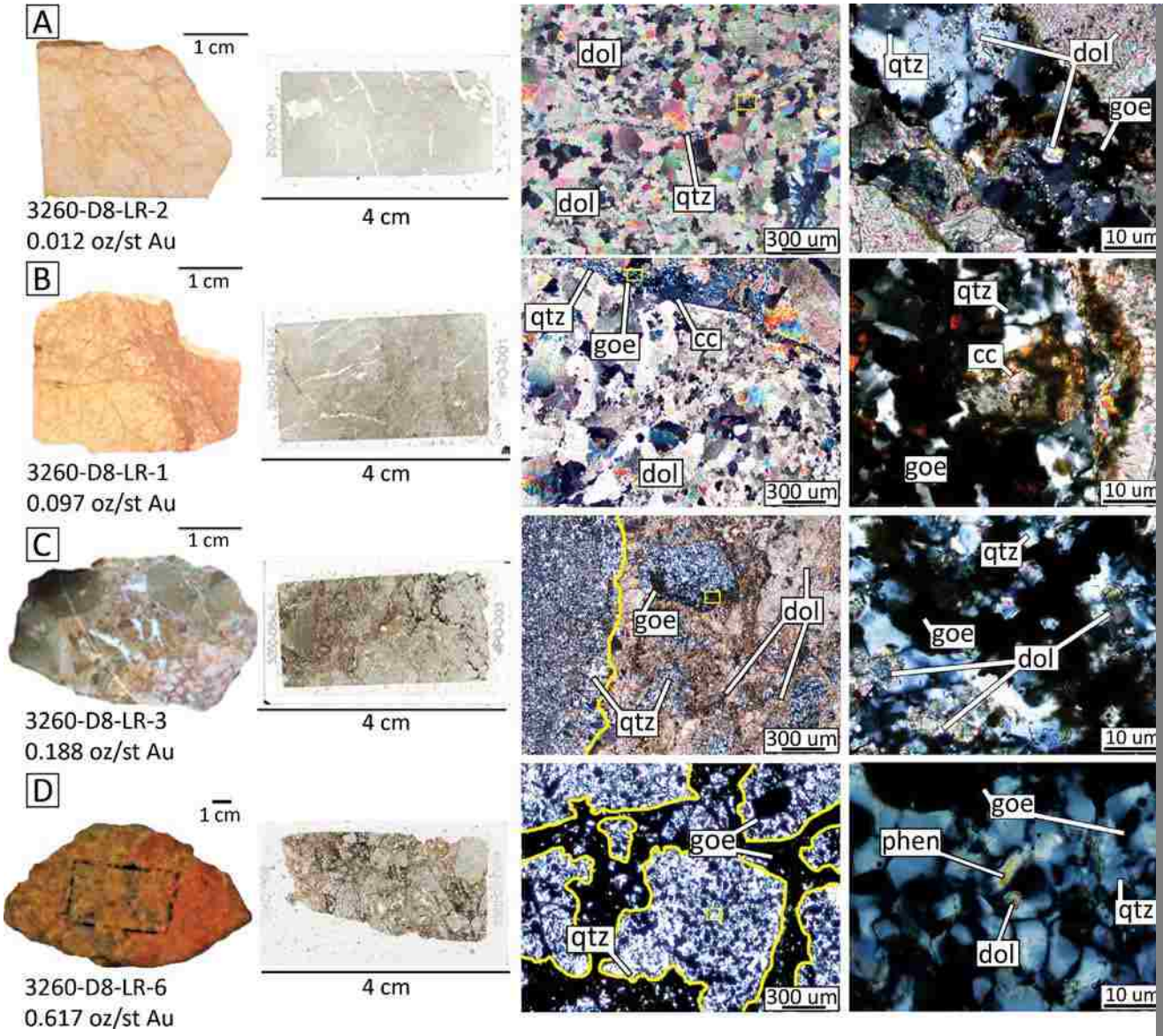

Figure 23. Hand Samples (left), polished sections (center) and photomicrographs under crossed polarized, transmitted light showing typical mineral composition of each sample(right), and under transmitted light displaying evidence of replacement (far right) of four samples from an approximately 2 meter transect sampled on the 3260' level. Increase in Au concentration correlates with increasing goethite, quartz and fracture intensity. (A) Dolomite-rich sample with trace quartz and goethite in a 20 um wide vein. Parallel vein walls and dolomite inclusions indicate open-space precipitation of quartz. (B) Noticeable increase in quartz and goethite. Vein walls in photomicrograph are irregular. (C) Significant increase in Au, goethite, and quartz and noticeable decrease in dolomite. Dolomite replacement by quartz isolating dolomite into "apparent" clasts. (D) Sample is composed entirely of phengite, quartz and goethite. Dolomite has been replaced. Dol = dolomite, cc = calcite, qtz = quartz, goe = goethite.

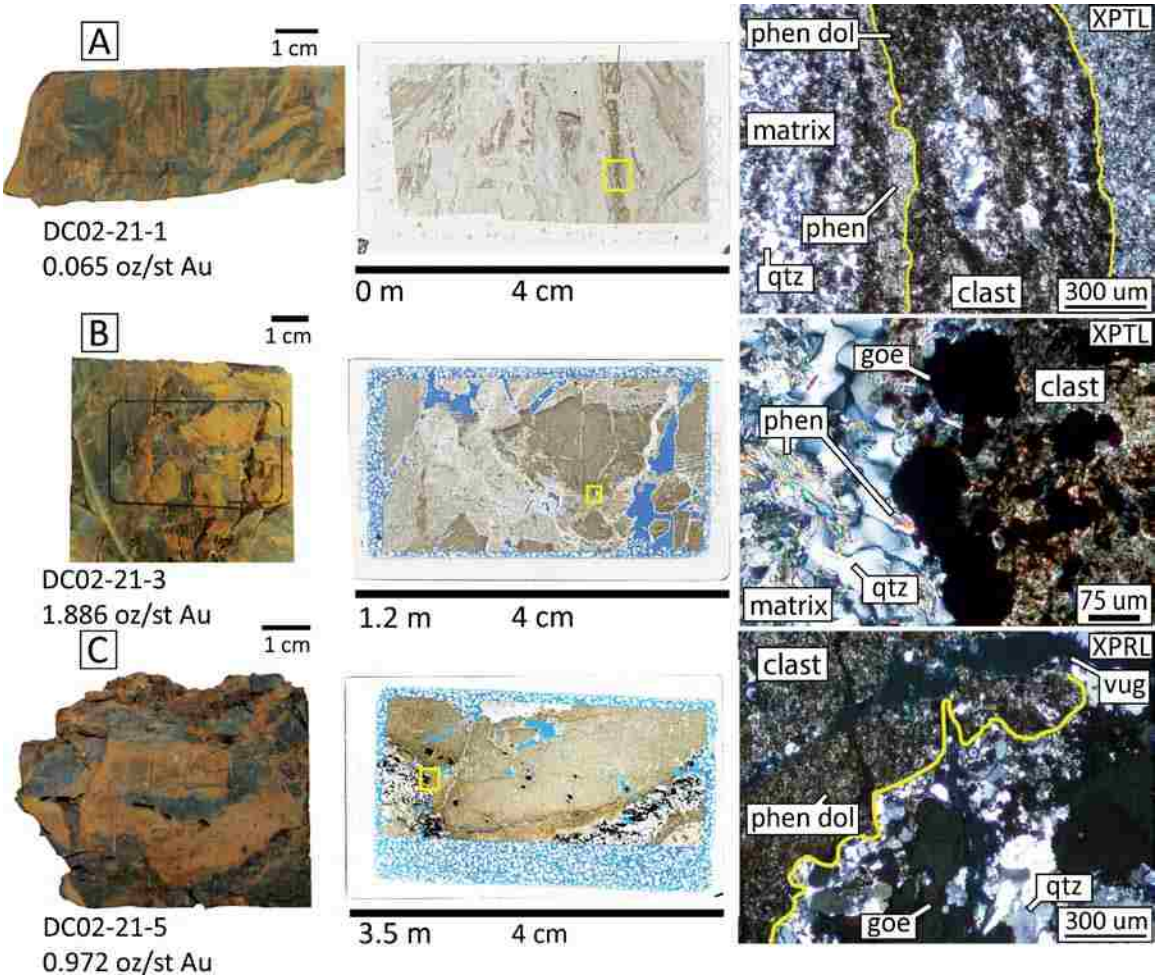

Figure 24. BT1 samples (left), polished sections (center) and photomicrographs (right) that exhibit little variation in mineralogy or hand sample texture though Au increases with increasing goethite and porosity over 3.5 meters. Au occurs exclusively in goethite and all goethite is associated with quartz. Qtz = quartz, phen = phengite, phen dol = phengitic dolomite, goe = goethite, blue = epoxy, vug = pore space XPRL = crossed polarized reflected light, XPTL = crossed polarized transmitted light.

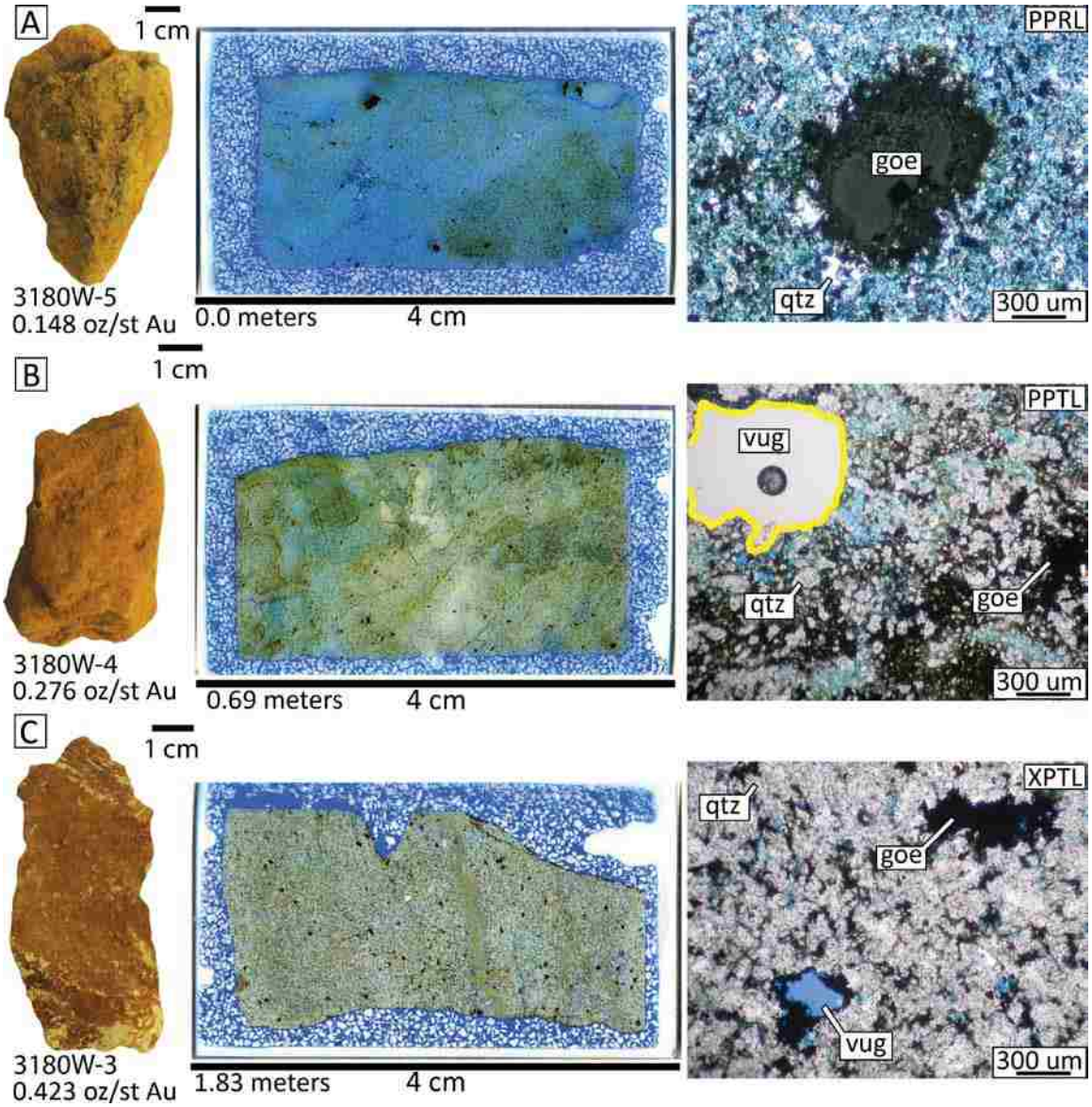

Figure 25. BT2 Samples (left), polished sections (center) and photomicrographs (right) of a three sample 2.5 meter transect across highly altered, phengite-rich samples that vary little in hand sample mineralogy, though Au increases significantly. The increase in Au is associated with an increase in goethite which is illustrated in polished section and in photomicrographs. Samples B and C exhibit a greater abundance of goethite in open space than sample A. Yellow lines outline vugs. Qtz = quartz, goe = goethite, phen = phengite, vug/blue = pore space, XPTL = crossed polarized transmitted light, PPRL = plain polarized reflective light, PPTL = plain polarized transmitted light.

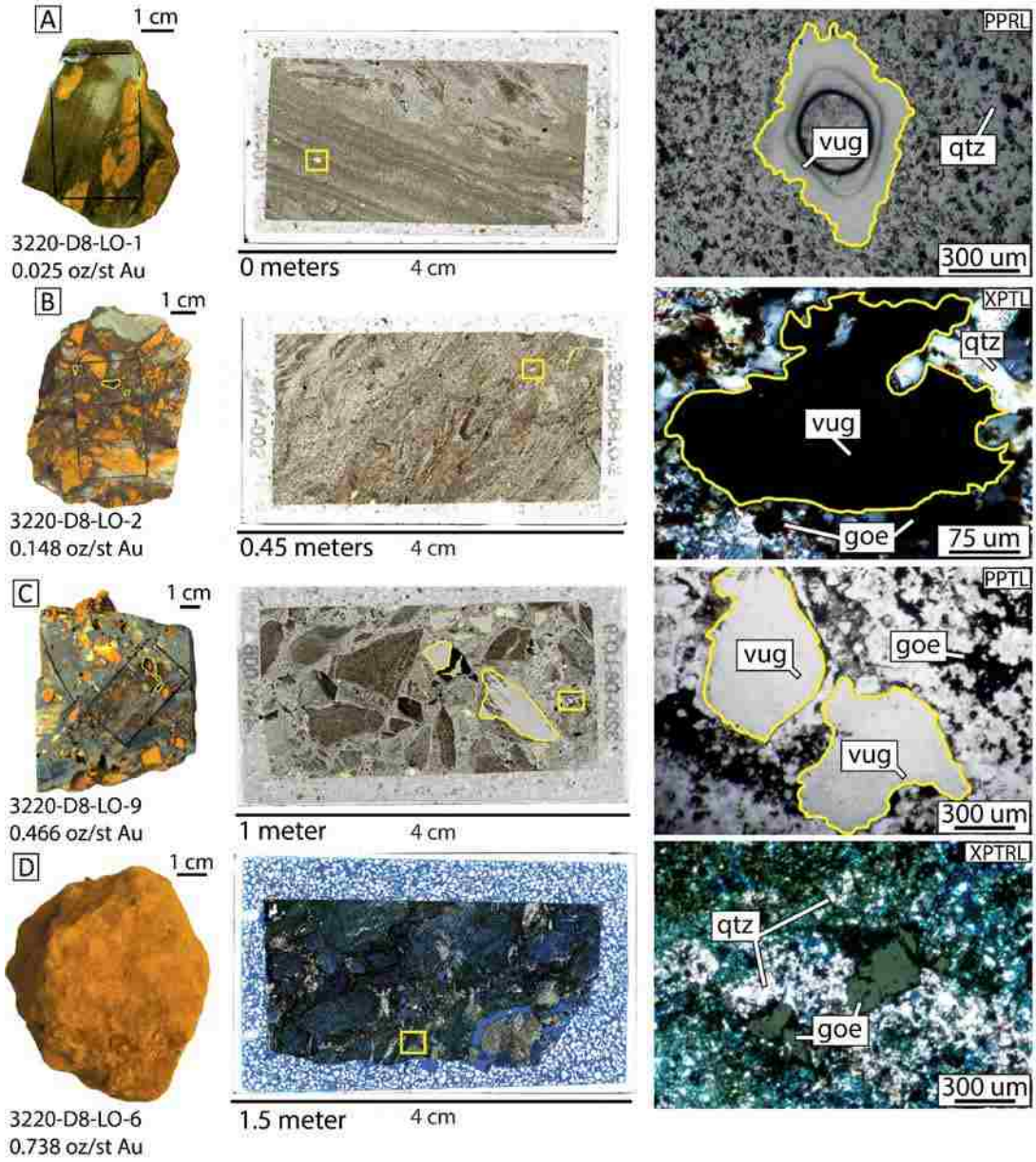

Figure 26. Hand Samples (left), polished sections (center) and photomicrographs (right) of a transect exhibiting an increase in gold that correlates with an increase in porosity and goethite over 1.5 meters. (A) BT1. The abundance of vugs and goethite are low. Vugs reach 600 um in diameter. (B) BT1. An increase in vugs is apparent in both hand sample and polished section. Vugs range up to 5 mm in diameter. (C) BT1. Vugs increase in abundance and size. Vugs are ≤1 cm and are associated with or rimmed by goethite. (D) A phengite-rich sample of BT2 exhibits a significant increase in Au, pore space, and goethite compared to A, B, and C. In polished section, low relief black to brown material is phengite- and goethite-dominant matrix with trace quartz cementing the quartz-rich clasts that appear grey in polished section. Qtz = quartz, phen = phengite, goe = goethite, blue = pore space, XPTRL = crossed polarized transmitted and reflected light. PPTL = plain polarized transmitted light, XPTL = crossed polarized transmitted light, PPRL = plain polarized reflected light.

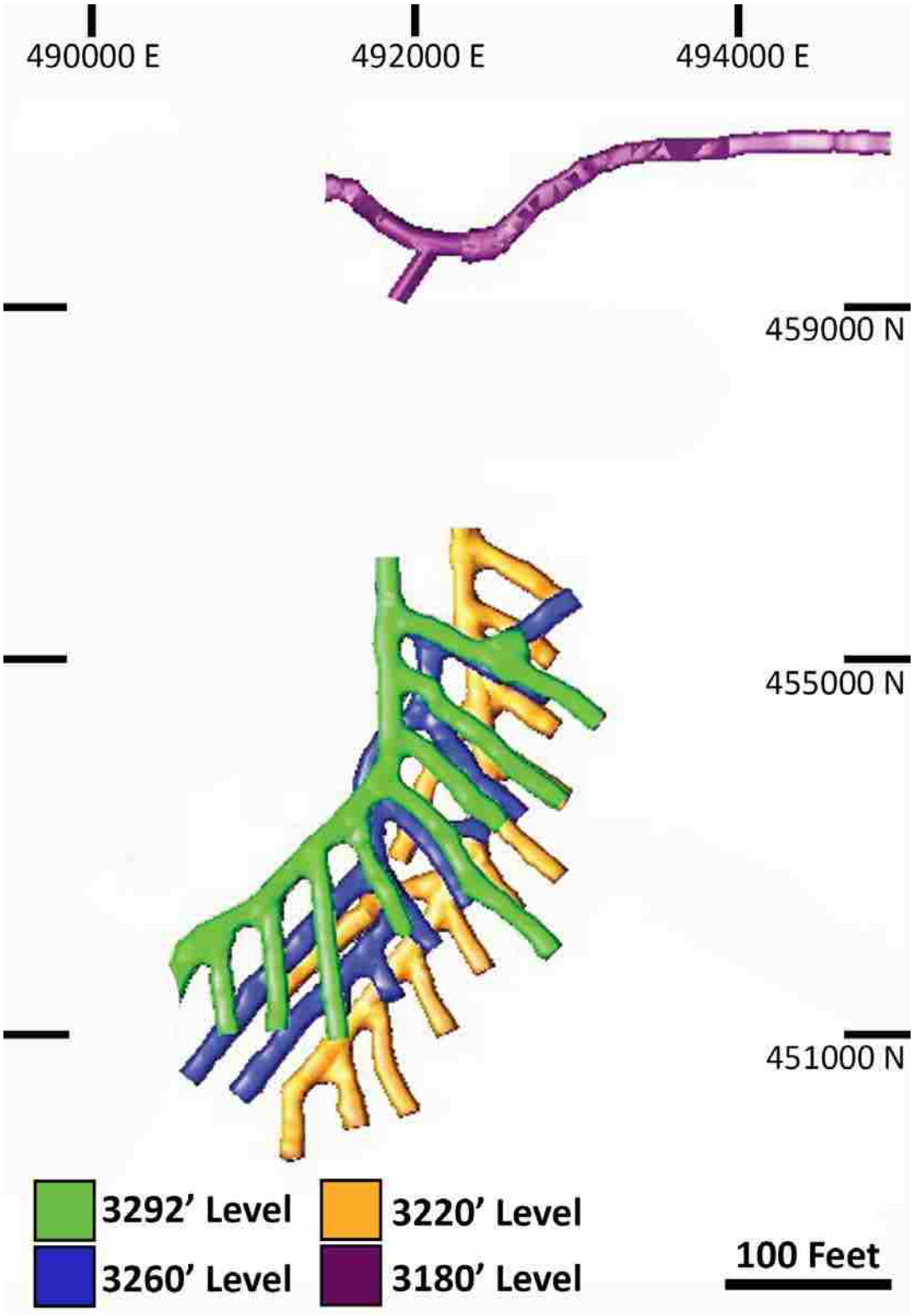

Figure 27. Map view of the underground workings of the 144 Zone depicting relative locations of the different levels and drifts.

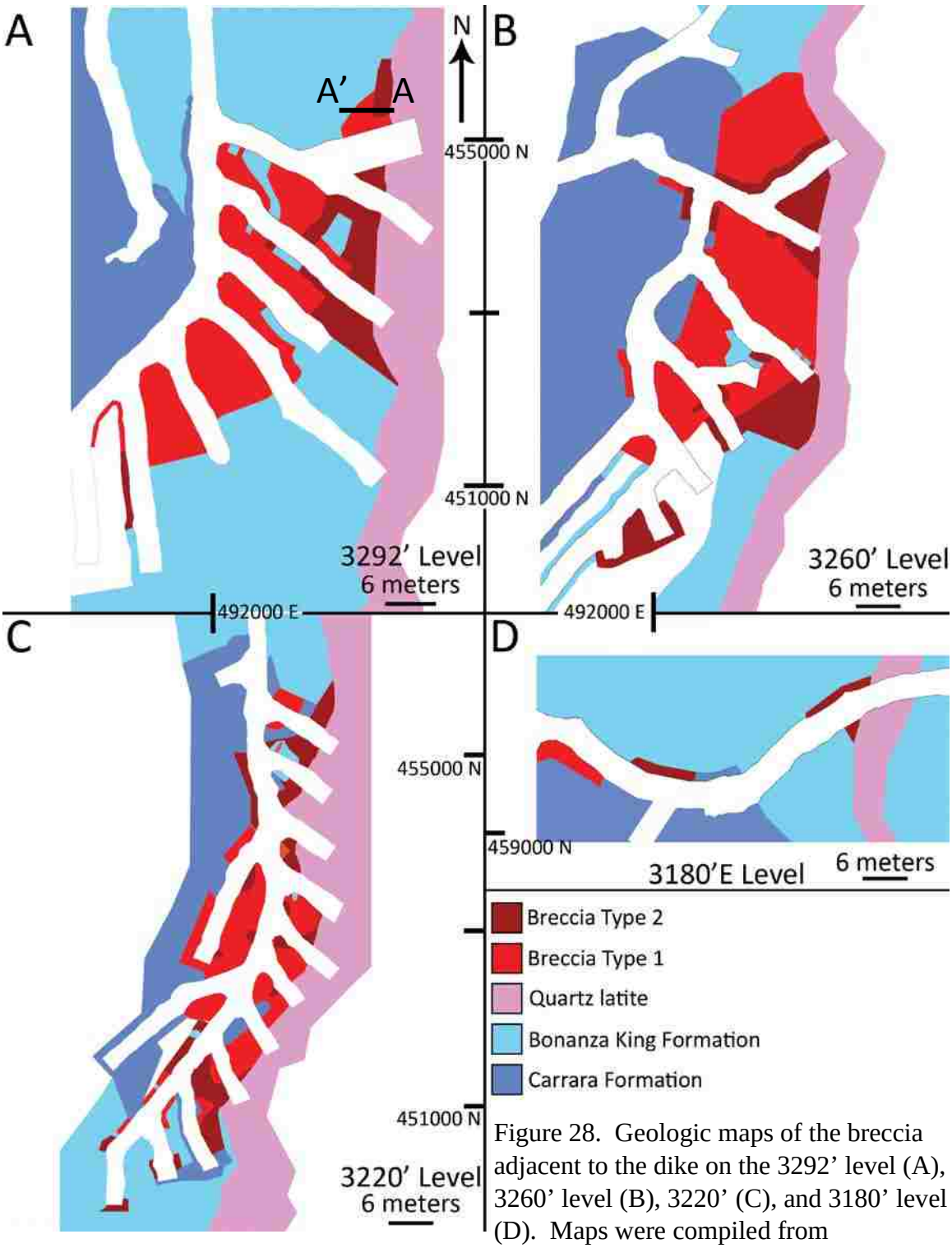

Figure 28. Geologic maps of the breccia adjacent to the dike on the 3292' level (A), 3260' level (B), 3220' (C), and 3180' level (D). Maps were compiled from underground rib mapping and drill core intersections. Universal Transverse Mercator (UTM) northing coordinates for scale.

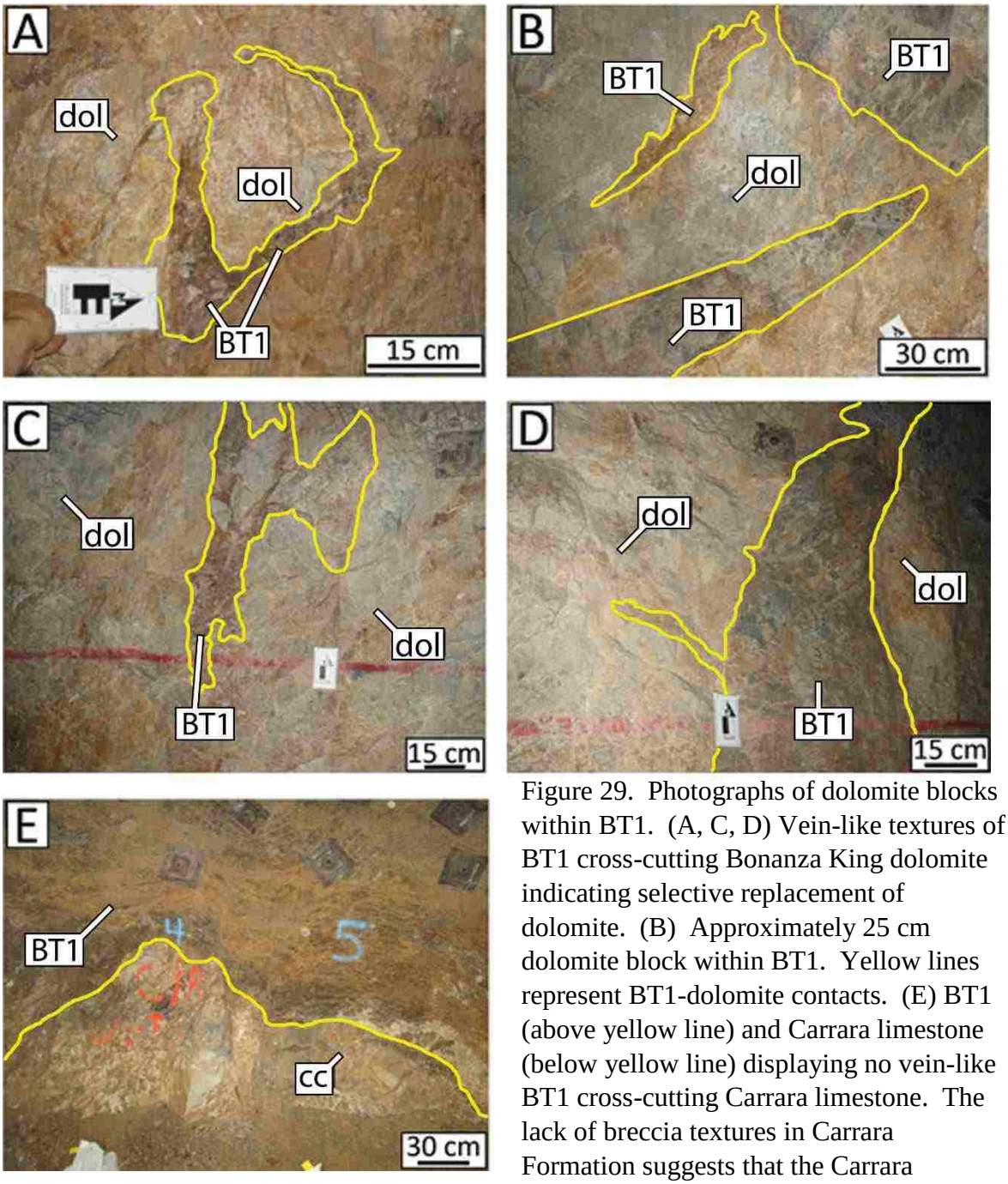

Figure 29. Photographs of dolomite blocks within BT1. (A, C, D) Vein-like textures of BT1 cross-cutting Bonanza King dolomite indicating selective replacement of dolomite. (B) Approximately 25 cm dolomite block within BT1. Yellow lines represent BT1-dolomite contacts. (E) BT1 (above yellow line) and Carrara limestone (below yellow line) displaying no vein-like BT1 cross-cutting Carrara limestone. The lack of breccia textures in Carrara Formation suggests that the Carrara limestone was not a part of breccia formation.

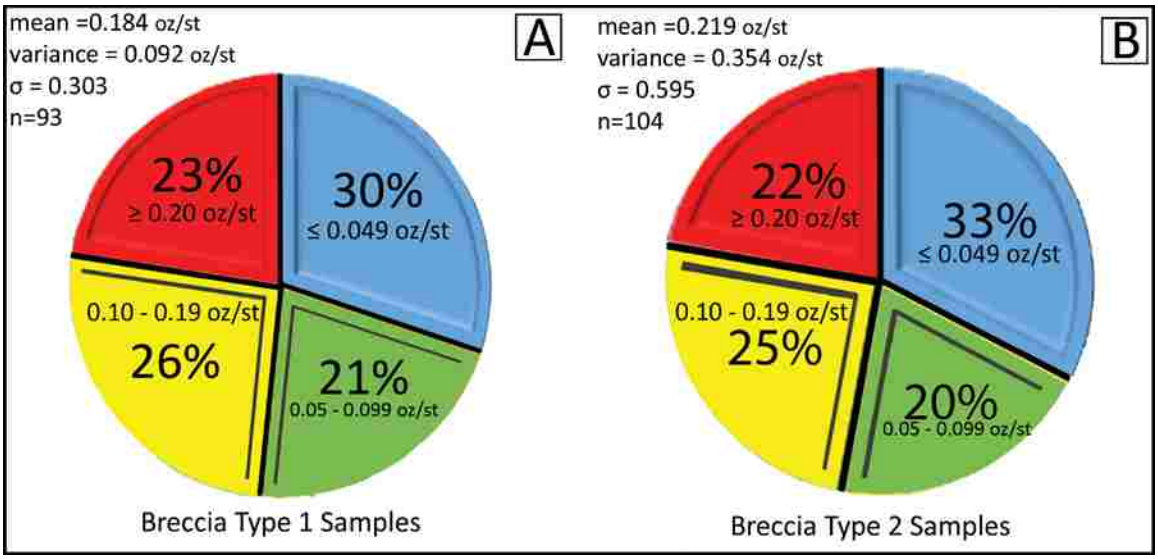

Figure 30. Pie graphs displaying the large range of gold values in BT1 (A) and BT2 (B) samples. Neither breccia type is exclusively associated with high- or low-grade Au

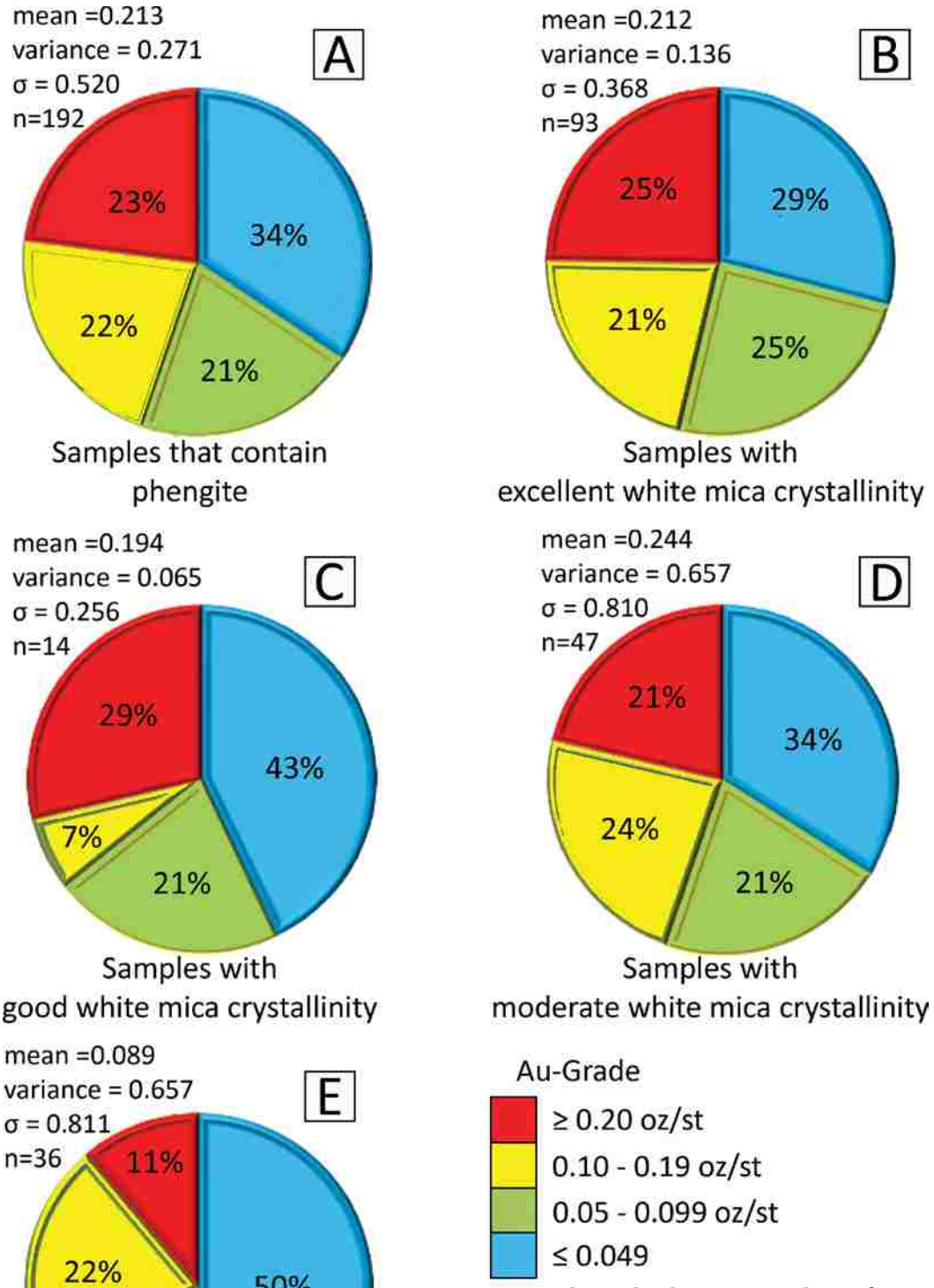

Figure 31. Pie charts displaying Au values of samples where phengite is present (A) and the correlations between Au and phengite crystallinity (B, C, D, E). Samples with phengite have a large range of gold values. Samples with a poor phengite crystallinity have sub-economic concentrations half the time. Excellent, good, and moderate crystallinity samples have no correlation demonstrating a large range of Au values.

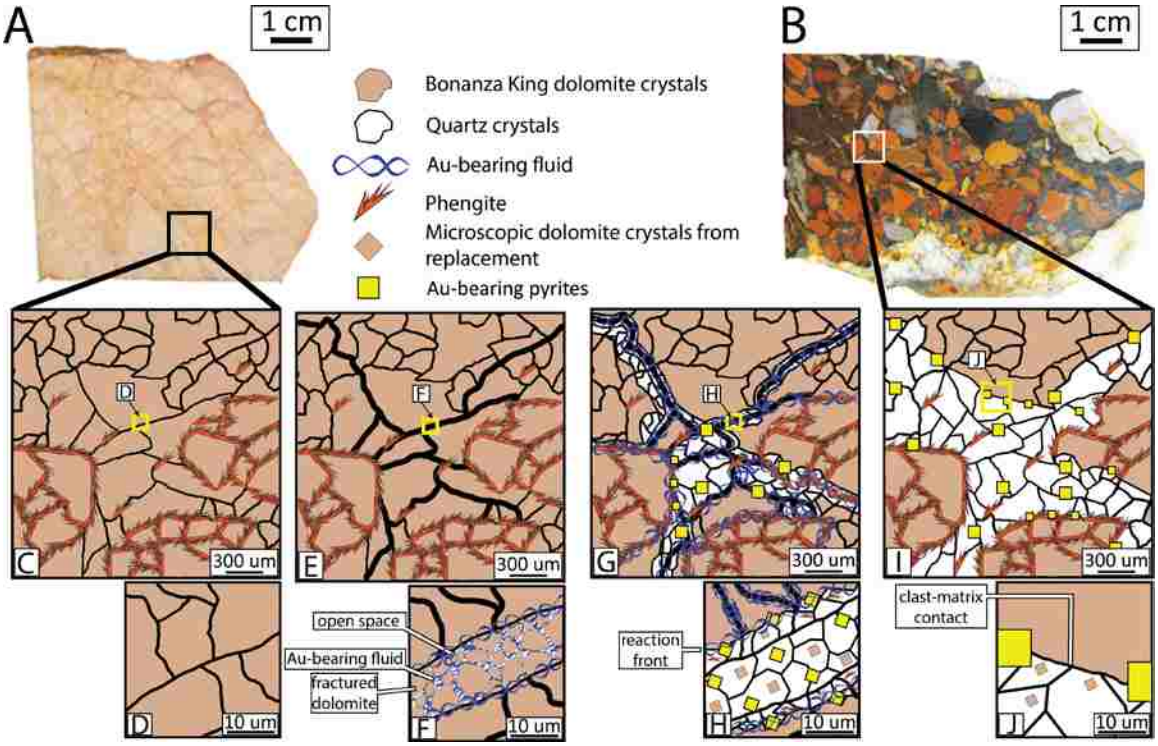

Figure 32. Hand sample images and schematic diagram illustrating formation of BT1. (A) Bonanza King dolomite. (B) Heterolithic BT1. (C, D) Bonanza King host rock composed of dolomite and minor phengite. (E, F) Bonanza King dolomite is fractured permitting Au-bearing fluid flow. Fractures contain fragments of dolomite. Hydrothermal fluids initially penetrate remaining open space in fractures. (G) Hydrothermal fluids penetrate along fractures and crystal boundaries between dolomite and phengite crystals in the dolomite. Hydrothermal fluids decarbonize and replace dolomite with. (H) Within fractures, quartz precipitates in open space and replaces fragments of dolomite. Au-bearing pyrites also precipitate as dolomite is removed. (I) Continued dolomite removal transforms dolomite into an apparent breccia with phengitic dolomite and dolomite clasts. Concurrently, quartz, minor phengite, pyrite and Au form the BT1 matrix. (J) Along clast-matrix boundaries, microscopic inclusions of dolomite are common and document chemical replacement as the mechanism responsible for BT1 formation.

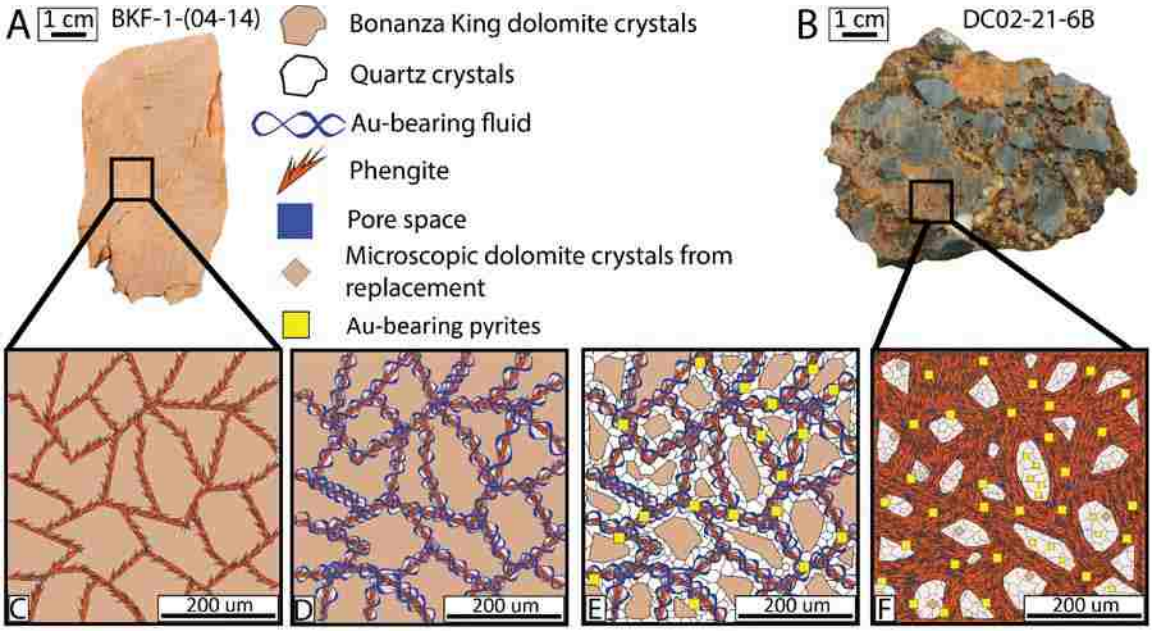

Figure 33: Hand sample images and schematic diagram illustrating formation of BT2. (A) Bonanza King dolomite. (B) Heterolithic BT2. (C) Bonanza King rock comprised of dolomite and phengite. (D) Hydrothermal fluids invade Bonanza King dolomite along phengite and dolomite crystal boundaries. (E) Fluid-rock reactions remove carbonate, replace dolomite with quartz, and precipitate Au-bearing pyrite and secondary phengite related to alteration of the quartz latite dike, effectively increasing the abundance of phengite, quartz and Au-bearing pyrites. (F) Complete removal of dolomite by quartz replacement and decarbonatization results in quartz clasts in a matrix of phengite, Au-bearing pyrite, and minor quartz. Abundant phengite is a product of ore fluids altering the quartz latite dike. Ions of phengite were then transported to pore space by ion diffusion where they were then consumed to precipitate phengite or phengite crystals were physically moved by the ore fluid after altering dike minerals.

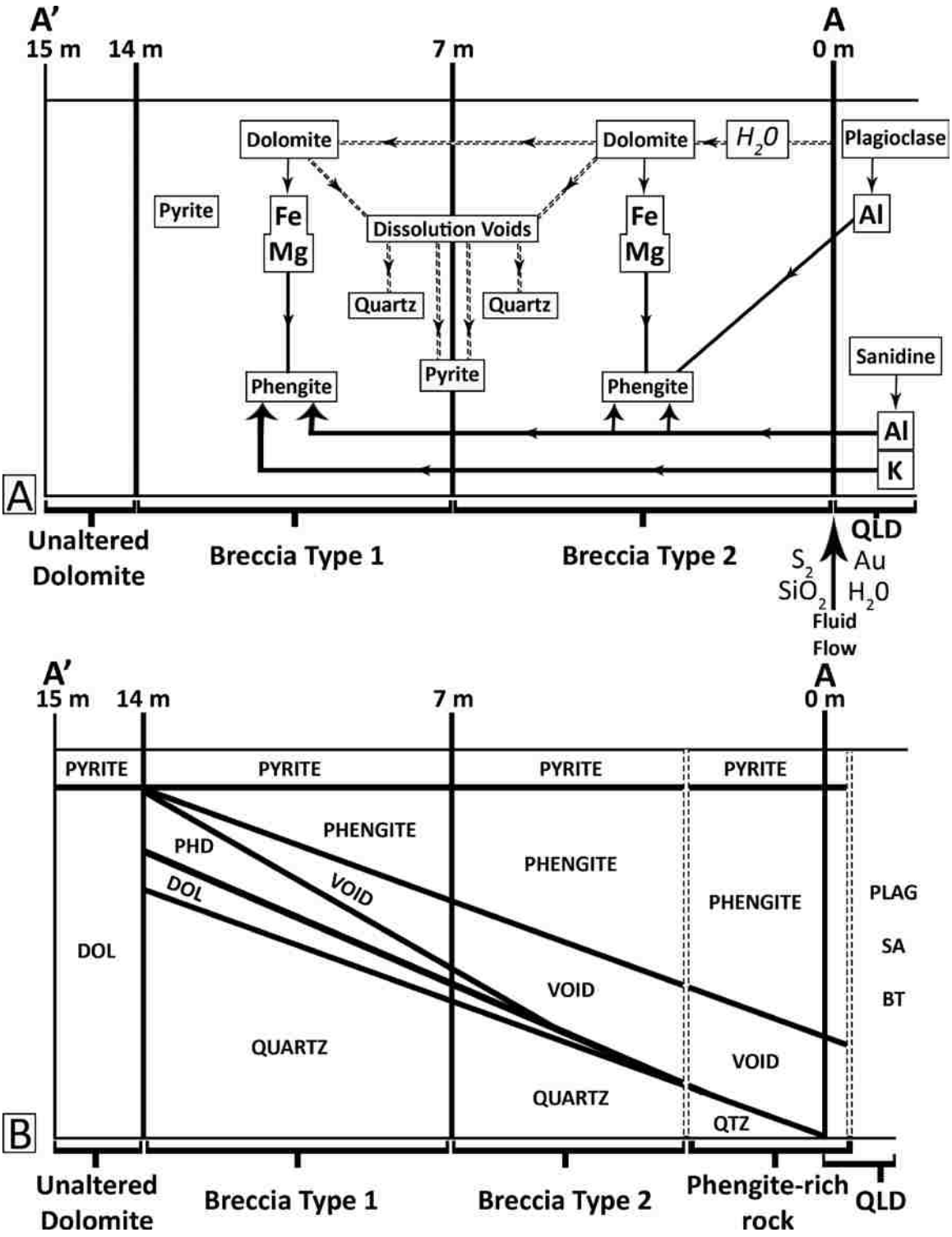

Figure 34. Model for (A) the chemical transfer of elemental components during alteration of the quartz latite dike that led to secondary phengite precipitation and (B) the relative abundance of minerals in each rock type along the A-A' transect in Fig. 28A. Al and K ions released during alteration of sanidine and plagioclase in the dike, were transported via ionic diffusion and reacted with the fluid to precipitate phengite. Phengite decreases away from the dike as quartz and dolomite increase. (A). Void = Pore space, qtz = quartz, dol = dolomite, sa = sanidine, phd = phengitic dolomite, plag = plagioclase, sa = sanidine, bt = biotite and QLD = quartz latite dike

APPENDIX A

SAMPLES LIST

The 244 samples collected for this study are listed here and include samples from the underground workings of the 144 Zone, two drill holes and from outcrop samples. This appendix provides each sample footage or location and Au assay (oz/st). Additionally, an X identifies samples from which polished sections were made and analytical techniques performed on the sample.

Sample Identification Key

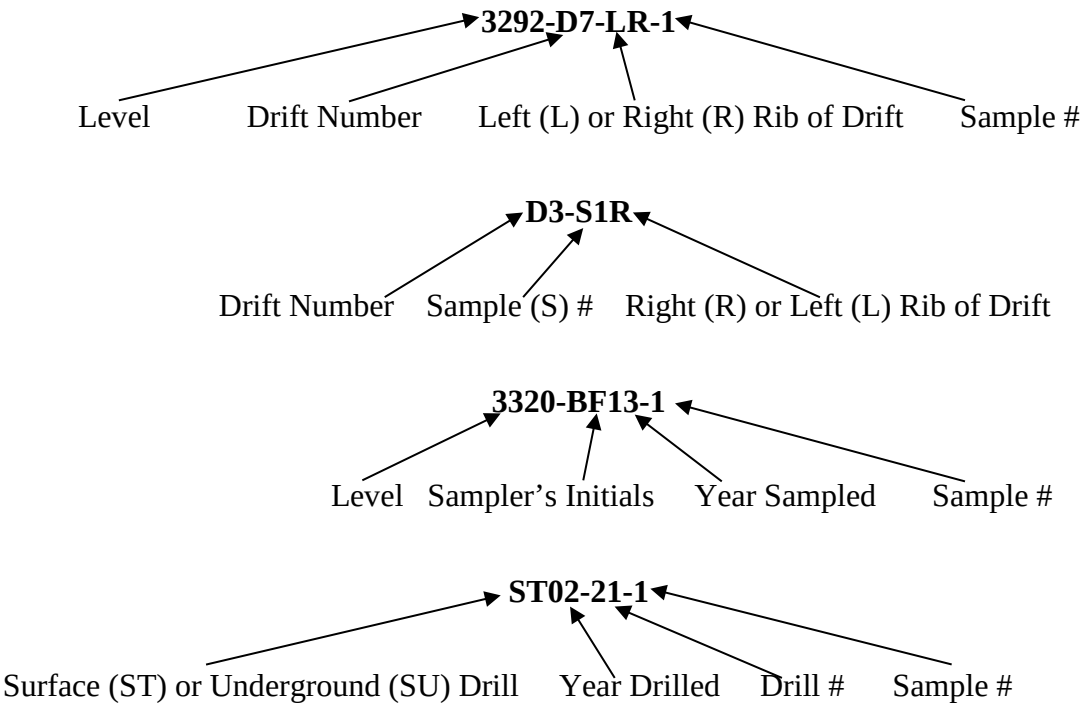

Level or Zone ID	Sample ID	Au (oz/st)	Thin Section	EPMA	SEM	TerraSpec
3320' Level	3320-BF-1	0.205				x
	3320-BF-2	0.092				x
	3320-BF-3	0.019				x
	3320-BF-4	0.108				x
	3320-BF-5	0.067				x
	3320-BF-6	0.078				x
3292' Level	D3-S1R	0.015				x
	D3-S2R	0.012				x
	D3-S3R	0.029				x
	D3-S4R	0.035				x
	D3-5R	0.01				x
	D3-S6R	0.042				x
	D3-S7R	0.239				x
	D3-S9R	0.228				x
	D3-S10R	0.074				x
	D3-S11R	0.046				x
	D3-S14R	0.002				x
	D4-S1R	0.372				x
	D4-S2R	0.374				x
	D4-S3R	0.016				x
	D4-S4R	0.211				x
	3292-D7-LR-1	0.346				
	3292-D7-LR-2	0.172				
	3292-D7-LR-3	0.451				
	3292-D7-LR-4	0.313				
	3292-D7-LR-5	0.372				
	3292-D7-LR-6	0.16				x
	3292-D7-LR-7	0.315				
	3292-D7-LR-8	0.284	x			x
	3292-D7-LR-9	0.216	x			x
	3292-D7-LR-10	0.16				x
	3292-D7-LR-11	0.125	x			x
3292'W Level	3292W-BF1	0.002				x
	3292W-BF2	0.085				x
	3292W-BF3	0.034				x
	3292W-BF4	0.088				x
3285' Level	3285-BF-1	0.092				x
	3285-BF-2	0.181				x
	3285-BF-3	0.04				x
	3285-BF-4	0.026				x

Level or Zone ID	Sample ID	Au (oz/st)	Thin Section	EPMA	SEM	TerraSpec
	3285-BF-5	0.026				x
	3285-BF-6	0.001				x
	3285-BF-7	0.044				x
	3285-BF-8	0.133				x
3275'	3275-BF-1	0.145				x
Level	3275-BF-2	0.096				x
	3275-BF-3	0.047				x
	3275-BF-4	0.051				x
	3275-BF-5	0.062				x
	3275-BF-6	0.099				x
	3275-BF-7	0.093				x
	3275-BF-8	0.102				x
	3275-BF-9	0.04				x
	3275-BF-10	0.009				x
	3275-BF-11	0.098				x
	3275-BF-12	0.032				x
3260'	D9-S1R	0.257				x
Level	D9-S2R	0.738				x
	D9-S3R	0.924				x
	D9-S4R	0.234				x
	D9-S5R	0.057				x
	D9-S6R	0.053				x
	D9-S7R	0.006				x
	D9-S8R	0.006				x
	D9-S9R	0.16				x
	D8-S1L	0.308				x
	D9-S11R	0.695				x
	D9-S12R	0.102				x
	D9-S13R	0.141				x
	D8-S2L	0.065				x
	D8-S4L	0.065				x
	D8-S5L	0.027				x
	D8-S6L	0.11				x
	D8-S7L	0.168				x
	D8-S8L	0.17				x
	D8-S9L	0.23				x
	D8-S10R	0.034				x
	D8-Bacon Clay	5.659	x		x	x
	3260-D8-LR-1	0.097	x		x	x
	3260-D8-LR-2	0.012	x		x	x
	3260-D8-LR-3	0.188	x		x	x

Level or Zone ID	Sample ID	Au (oz/st)	Thin Section	EPMA	SEM	TerraSpec
	3260-D8-LR-4	0.093	x			x
	3260-D8-LR-5	0.036	x			x
	3260-D8-LR-6	0.617	x			x
	3260-D8-LR-7	1.869	x			x
	3260-D8-LR-8	0.104	x			x
	3260-BF-1	0.509				x
	3260-BF-2	0.247				x
	3260-BF-3	0.026				x
	3260-BF-4	0.138				x
	3260-BF-5	0.013				x
	3260-BF-6	0.037				x
	3260-BF-7	0.097				x
	3260-BF-8	0.088				x
3260'W Level	3260W-BF-1	0.055				x
	3260W-BF-2	0.032				x
	3260W-BF-3	0.041				x
	3260W-BF-4	0.021				x
	3260W-BF-5	0.049				x
	3260W-BF-6	0.034				x
	3260W-BF-7	0.014				x
	3260W-BF-8	0.035				x
	3260W-BF-9	0.088				x
	3260W-BF-10	0.004				x
	3260W-BF-11	0.098				x
	3260W-BF-12	0.098				x
	3260W-BF-13	0.115				x
	3260W-BF-14	0.312				x
	3260W-BF-15	0.052				x
	3260W-BF-16	0.001				x
	3260W-BF-17	0.077				x
	3260W-BF-18	0.2				x
	3260W-BF-19	0.041				x
	3260W-BF-20	0.031				x
	3260W-BF-21	0.037				x
	3260W-BF-22	0.044				x
	3260W-BF-23	0.13				x
	3260W-BF-24	0.136				x
	3260W-BF-25	0.024				x
	326W-BF-26	2.137				x
	3260W-BF-27	0.358				x

Level or Zone ID	Sample ID	Au (oz/st)	Thin Section	EPMA	SEM	TerraSpec
	3260W-BF-28	0.009				x
	3260W-BF-30	0.117				x
	3260W-BF-31	0.158				x
	3260W-LR-1	0.091				x
	3260W-LR-2	0.052				x
	3260W-LR-3	0.046				x
	3260W-LR-4	0.118				x
	3260W-LR-5	0.14				x
	3260W-LR-6	0.047				x
	3260W-LR-7	0.122				x
3220'	3220-D8-LO-1	0.028	x			
Level	3220-D8-LO-2	0.11	x			
	3220-D8-LO-3	0.306				
	3220-D8-LO-4	0.183				
	3220-D8-LO-5	0.29	x			
	3220-D8-LO-6	0.738	x			x
	3220-D8-LO-7	0.133	x			x
	3220-D8-LO-8	0.334				x
	3220-D8-LO-9	0.466	x			x
	3220-D8-LO-10	0.148	x			x
	3220-D8-LO-11	0.176				x
	3220-BF13-1	0.007				
	3220-BF13-2	0.032				
	3220-BF13-3	0.05				
	3220-BF-4	0.299				
	3220-BF-5	0.026				
	3220-BF-6	0.001				x
	3220-BF-7	0.212				x
	3220-BF-8	0.138				x
	3220-BF-9	0.106				x
	3220-BF-10	0.019				x
	3220-BF-7b	0.157				x
	3220-BF-8b	0.459				x
	3220-BF13-11	0.019				x
	3220-BF13-12	0.039				x
	3220-BF13-13	0.014				x
	3220-BF13-14	0.058				x
	3220-BF13-15	0.005				x
	3220-BF13-16	0.021				x
	3220-BF13-17	0.015				x
	3220-BF13-18	0.047				x

Level or Zone ID	Sample ID	Au (oz/st)	Thin Section	EPMA	SEM	TerraSpec
	3220-BF13-19	0.031				x
	3220-BF13-20	0.002				x
	3220-BF13-21	0.085				x
	3220-BF13-22	0.009				x
	3220-BF13-23	0.049				x
	3220-BF13-24	0.171				x
	3220-BF13-25	0.118				x
	3220-BF13-26	0.064				x
	3220-BF13-27	0.161				x
	3220-BF13-28	0.07				x
	3220-BF13-29	0.204				x
	3220-BF13-30	0.089				x
	3220-BF13-31	0.062				x
	3220-BF13-32	0.141				x
	3220-BF13-33	0.011				x
	3220-BF13-34	0.793				x
	3220-BF13-35	0.052				x
	3220-BF13-36	0.097				x
	3220-BF13-37	0.038				x
	3220-BF13-38	0.079				x
	3220-BF13-39	0.236				x
	3220-BF13-40	0.845				x
	3220-BF13-41	0.072				x
	3220-BF13-42	0.003				x
	3220-BF13-43	0.01				x
	3220-BF13-44	0.167				x
	3220-BF13-45	0.552				x
	3220-BF13-46	0.173				x
	3220-BF13-47	0.051				x
	3220-BF13-48	0.07				x
	3220-BF13-49	0.034				x
	3220-BF13-50	0.073				x
	3220-BF13-51	0.253				x
	3220-BF13-52	0.003				x
3180' W Level	3180-W-1	0.437				x
	3180-W-2	0.38				x
	3180-W-3	0.423	x			x
	3180-W-4	0.276	x			x
	3180-W-5	0.148	x			x
	3180-W-6	0.171				x

Level or Zone ID	Sample ID	Au (oz/st)	Thin Section	EPMA	SEM	TerraSpec
	3180 W-7	0.017	x			x
	3180 W-8	0.227				x
	3180 W-9	0.015				x
	3180 W-10	0.394				x
	3180W-BF-1	0.108				x
	3180W-BF-2	0.105				x
	3180W-BF-3	0.072				x
	3180W-BF-4	0.006				x
	3180W-BF-5	0.157				x
	3180W-BF-6	0.033				x
	3180W-BF-7	0.134				x
	3180W-BF-8	0.004				x
	3180W-BF-9	0.11				x
	3180W-BF-10	0.128				x
	3180W-BF-11	0.016				x
	3180W-BF-12	0.047				x
	3180W-BF-13	0.073				x
3180' E Level	3180E-BF-1	0.11				x
	3180E-BF-2	0.112				x
	3180E-BF-3	0.007				x
	3180E-BF-4	0.006				x
	3180E-BF-5	0.004				x
	3180E-BF-6	0				x
	3180E-BF-7	0.003				x
	3180E-BF-8	0.005				x
Outcrop Samples	BKF-1	N/a	x		x	x
	BKF-2-BRX	N/a	x		x	x

Drill Core	footage (feet)	Sample ID	Au (oz/st)	Thin Section	EPMA	SEM	TerraSpec
Hole ID	718’3” –719’	DC02-21-1	0.065	X	X	X	X
ST02-21	721'-722'3"	DC02-21-2	0.223	X			X
	723'-723'11"	DC02-21-3	1.866	X	X	X	X
	727'-729'	DC02-21-4	1.967				
	729'4"-729'5"	DC02-21-5	0.972	X	X	X	X
	734'4"-734'9"	DC02-21-6A	0.585	X			X
	734'4"-734'9"	DC02-21-6B	0.585	X			X
	736'8"-737'	DC02-21-7	0.585	X			X
	739'-740'	DC02-21-8	0.464	X			X
	740'-741'	DC02-21-9	0.002	X		X	X
	713'5"-714'	DC02-21-10	0.177	X		X	X
	702'-706'	DC02-21-11	0.068	X			X
SU13-177	105.8’ – 106.4’	SU13-177-1	0.02	X			
	106.4’ – 106.6’	SU13-177-2	0.02	X			
	106.6’ – 106.9’	SU13-177-3	0.02	X			

APPENDIX B

SAMPLE DESCRIPTIONS

Hand samples collected for this project were described prior to analytical work. Hand sample descriptions focused on identifying physical and visible indicators for gold and improving rock type classification during underground drift mapping.

3220-BF-6	Competent rock, appears to be altered and fractured dolomite. High red and orange oxidation, minor white calcification present, clay alteration on sample.
3220-BF-7	Heterolithic breccia with black hard quartz matrix. Clasts are red and black, red clasts are rounded to subrounded, and have plastic texture and fine. Black clasts are fine, brittle, and angular. Matrix is somewhat oxidized. minor amount of vugs 1mm in diameter, minor white calcite.
3220-BF-8	Clay rock, soft, friable, highly oxidized, orange and red in color. Pieces of breccia within clay.
3220-BF-9	Clay rock with black fragments, orange, minor yellow and red.
3220-BF-10	Clay rock, very soft, friable orange and red color.
3220-BF-7b	Clay rock, soft. Highly oxidized, with minor orange and red colors. Minor pieces of silicification in sample
3220-BF-8b	Monolithic breccia within clay matrix heterolithic breccia, matrix is hard, brown-red in color. Clasts are angular to subrounded fine to medium grained. Minor red oxidation on clasts, orange clasts present.
3220-BF13-11	Heterolithic breccia with a clay matrix, friable, oxidized. Clasts are black (silicified) and tan angular to subangular and fine to medium grained.
3220-BF13-12	Monolithic breccia with clay matrix with white unaltered dolostone clasts. Oxidation and clay alteration in matrix. White calcite is present
3220-BF13-13	Monolithic breccia, silicified matrix, tan clasts and minor white calcite present. Clasts are rounded to subangular. Fine to coarse grained.
3220-BF13-14	Monolithic breccia with white unaltered dolomite clasts and a brown silicified matrix. Clasts are fine to coarse, subangular - subrounded. Minor oxidation.
3220-BF13-15	Monolithic breccia with clay matrix and unaltered white clasts. Matrix is oxidized and all clasts are fine grained subrounded.
3220-BF13-16	Heterolithic breccia. Minor clay matrix, framework supported. No silicification, soft. Clasts are black and tan

	in color and are angular to rounded and fine to medium grained.
3220-BF13-17	Heterolithic breccia. Strong oxidation. Hard silicified matrix, minor amount of tan clasts can be identified. Minor white calcite.
3220-BF13-18	Monolithic breccia with tan clasts and black matrix. Clasts are fine-medium grained, rounded to subrounded. Minor oxidation only on clast, not on matrix (possible oxides?). Strongly silicified matrix, with minor white calcite in veins.
3220-BF13-19	Heterolithic breccia with a black matrix and black, white, and tan clasts. Black matrix is silicified and is being fractured. Fractures are filled in with clay minerals (minor). Clasts are subangular. Rounded and medium grained. Some elongated tan clasts. Minor white calcite.
3220-BF13-20	Heterolithic breccia with high amounts of clay as matrix. Soft yellow clay. Clasts are unaltered White dolostone and black clasts.
3220-BF13-21	Heterolithic breccia with a clay matrix and black, white, and tan clasts. Friable, orange with minor red color. Clasts are fine, subrounded, dominated by black clasts.
3220-BF13-22	Heterolithic breccia with a black matrix (hard, silicified). Tan and black clasts. Minor oxidation, no clay. Clasts are fine to medium, rounded. Minor white calcite
3220-BF13-23	Monolithic breccia with black matrix and very large dolomite clasts. Matrix is silicified. Extremely low amount of oxidation on matrix. Clasts are mostly large, 20 cm long, dolomite clasts. Angular - subrounded. A very minor amount of tan and red clasts. (Red clasts are fine to medium grained. White calcite veins present.
3220-BF13-24	Similar to 3220-BF13-23 except for a higher degree of calcite and more clay alteration. No large dolostone clasts present.
3220-BF13-25	Heterolithic breccia with silicified matrix with tan, white and black clasts. Minor orange oxidation in matrix. Clasts are dominantly tan in color, oxidized, fine to coarse, rounded. Minor white unaltered dolomite clasts angular, fine –medium grained. Minor amount of vugs and minor white calcite.

3220-BF13-26	Heterolithic breccia with brown silicified matrix and black, tan, white, and red clasts. Matrix is hard, silicified, and has minor clay alteration (orange). Clasts are subangular to subrounded and fine to medium grained. Vugs present, minor white calcite.
3220-BF13-27	Heterolithic breccia. Extremely similar to 3220-BF13-26, but the matrix is more oxidized and there is a noticeable increase in clay alteration.
3220-BF13-28	Heterolithic breccia with a black matrix and black, tan, and white clasts. Silicified matrix. Minor clay alteration and oxidation on matrix (red-orange). White calcite in veins breaking up matrix. Clasts are fine-medium grained, angular-subangular. Unusually hard dolomite clasts (thought to be quartz replacing dolomite)
3220-BF13-29	Heterolithic breccia that has been highly clay altered. Orange, yellow, and red in color. Sampled near dike. Breaks in hand.
3220-BF13-30	Monolithic breccia with a black matrix and tan clasts. Matrix is silicified. Few clasts, mostly tan. Rounded and medium grained. White calcite present
3220-BF13-31	Heterolithic breccia with a silicified matrix with black, and tan clasts. Highly oxidized matrix. Clasts are fine, angular –subrounded. Minor to no clay.
3220-BF13-32	Highly clay altered rock, breaks within hand. Sample taken next to dike contact.
3220-BF13-33	Extremely clay altered rock, friable, yellow with minor red in color.
3220-BF13-34	Heterolithic breccia with high clay alteration. Minor white clasts in yellow soft matrix. Clasts are fine-medium grained, subrounded.
3220-BF13-35	Heterolithic breccia with a clay matrix and black and tan clasts. Matrix is red/orange in color. Clasts are fine and angular.

3220-BF13-36	Heterolithic breccia with black and white clasts. Highly silicified matrix, minor oxidation on matrix. Clasts are fine and angular. High white calcite.
3220-BF13-37	Heterolithic breccia with a black, silicified matrix. Clasts are black and red in color, very minor amount of clasts. Fine grained and subrounded.
3220-BF13-38	Clay altered rock. High clay content. Friable. Taken near contact with dike
3220-BF13-39	Banded black and soft limestone. Tan bands. White calcite and oxidation present.
3220-BF13-40	Very similar to 3220-BF13-39 but there is no banding.
3220-BF13-41	Heterolithic breccia with a black silicified and an orange, clay matrix. Black clasts found within clay matrix and tan clasts in the hard black matrix. Clasts fine – medium grained and angular – rounded.
3220-BF13-42	Heterolithic breccia with black, tan, and white clasts in a black silicified matrix. Matrix is partially oxidized (not much). Clasts range from medium to coarse grained and are subangular to subrounded. Minor amount of vugs.
3220-BF13-43	Highly clay altered rock. Soft. Minor, fine, black clasts.
3220-BF13-44	Heterolithic breccia with a brown matrix and tan and black clasts. Matrix is silicified, with minor oxidation. Minor white calcite. Clasts are mainly tan in color (oxidized) medium – coarse grained, plastic, subangular – rounded. Black clasts are in the minority, fine and angular. Minor vugs
3220-BF13-45	High clay alteration. Friable.
3220-BF13-46	Heterolithic breccia with a clay matrix with black and tan clasts within a black silicified matrix. Breccia within breccia. Black silicified matrix contains tan clasts that are medium grained and subrounded. Black matrix is contains a clay matrix. Clasts in the clay matrix is fine to coarse grained, subangular to subrounded, minor white calcite in clay matrix.
3220-BF13-47	Heterolithic breccia with an orange clay altered matrix with black, white, tan, and red clasts. Clast supported. Matrix is soft. Clasts are fine to coarse grained, angular –subrounded. White calcite present

3220-BF13-48	Heterolithic breccia with an orange clay matrix. Same as 3220-BF13-47. No white calcite.
3220-BF13-49	Highly clay altered rock. Deep orange color. Friable.
3220-BF13-50	Heterolithic breccia with a clay matrix and tan and black clasts. Black clasts are fine, subangular. Tan clasts are medium grained, subrounded.
3220-BF13-51	Highly clay altered rock. Breaks in hand. Red/orange color. Taken near dike contact.
3220-BF13-52	Heterolithic breccia with a clay matrix and black and tan clasts. Oxidation on matrix. Black clasts are coarse, grained and angular (silicified). Tan clasts are rounded and medium grained.
3260-BF-1	Black limestone, with minor tan bands. Bedding is present, clay in bedding.
3260-BF-2	Heterolithic breccia with a clay matrix and very large white clasts and minor tan and black clasts. Clasts are subrounded to subangular. Up to 5 cm in size. White calcite present, matrix supported.
3260-BF-3	Heterolithic breccia with a black matrix with tan, black and white clasts. Matrix is silicified, oxidized in some areas. Clasts are medium – coarse grained, angular – subangular. White calcite present.
3260-BF-4	Highly clay altered rock, soft, breaks in hands.
3260-BF-5	Heterolithic breccia with a clay matrix (orange-red) with black and tan clasts. Black clasts are fine, angular and appear to be silicified. Tan clasts are located in black clast and in clay matrix. Tan clasts are fine to medium grained.
3260-BF-6	Monolithic breccia with a black matrix and tan clasts. Matrix is silicified, matrix supported breccia. Clasts are fine to medium grained, rounded to subrounded. White calcite is present.
3260-BF-7	Heterolithic breccia with a clay matrix and black, tan, and white clasts. Matrix is friable and orange in color. Framework supported breccia. Clasts are fine to medium grained and angular.
3260-BF-8	Heterolithic breccia with a brown/black matrix with tan, red, and white clasts. Matrix is silicified. Clasts are fine to coarse, rounded to angular. Large white calcite veins.

3260-BF-9	Tan clasts surrounded by white calcite. White calcite is acting as a matrix. Clasts are subrounded to subangular and medium grained.
3260-BF-10	Heterolithic breccia with a black matrix. Matrix is silicified. Clasts are tan and black. White calcite present in fractures within matrix. Clasts are fine to med grained, rounded to subangular and elongated.
3260-BF-11	Highly fractured limestone. Clay alteration is present in bedding planes. Oxidation is minor.
3260-BF-12	Heterolithic breccia sample with two matrix compositions. One is silicifed and black, the other is orange and clay altered. Tan clasts are located within black matrix exclusively. Orange matrix appears to have cross-cut the silicifed matrix.
3260-BF-13	Monolithic breccia with a black matrix and tan clasts. Matrix is hard and silicified. Clasts are tan, with oxidation, rounded to subrounded and medium to coarse grained. Higher than usual abundance of white calcite, minor vugs.
3260-BF-14	Heterolithic breccia with an orange matrix and black, tan, and grey clasts. Matrix is soft, oxidized and composed of clay. Black clasts are fine to medium grained and angular. Tan clasts are rounded to subrounded and medium grained. Rare tan clasts in silicified matrix.
3260-BF-15	Highly clay altered rock, soft, orange-red in color.
3260-BF-16	Limestone. Oxidized. White calcite present, bedded. Located below breccia. Sharp contact.
3260-BF-17	Heterolithic breccia with an orange and black matrix, very similar to 3260-BF-14. Exception is that this breccia is clast supported.
3260-BF-18	Heterolithic breccia with a blackish/brown matrix with tan, grey, red, and black clasts. Matrix supported and clast supported. Matrix is silicified and slightly oxidized. Tan clasts are fine to coarse grained and rounded to angular.
3260-BF-19	Highly clay altered rock. Friable and oxidized.
3260-BF-20	Heterolithic breccia with a hard, silicifed, black to minor red matrix and tan, grey and red clasts. Clasts are not very abundant. Tan clasts dominate. Fine to medium grained and subrounded.

3260-BF-21	Monolithic breccia with a yellow-orange clay and oxidized matrix and unaltered dolostone clasts. Matrix slightly crumbles in hand. Clast supported. Clasts are dolomite medium to very coarse. Subangular to angular. Minor red to orange oxidation on dolomite clasts.
3260-BF-22	Heterolithic breccia with a reddish-brown matrix with tan and grey clasts. Matrix has minor clay alteration and visible red oxidation. Tan Clasts are rounded and fine grained. Grey clasts are dolomite and are less abundant. Clasts are angular and subrounded.
3260-BF-23	Heterolithic breccia with a brownish matrix and tan and white clasts. Matrix is silicified and has visible (red) oxidation. Clast supported, all clasts seem to be subangular to angular and fine to coarse grained. Minor rounded to subrounded clasts. White calcite is present.
3260-BF-24	Highly clay altered rock, very soft. Yellow and minor red color.
3260-BF-25	Black, soft limestone with red oxidation. Bedding present.
3260-BF-26	Highly clay rich rock. Orange-red in color. Minor fragments of silicifed rock and dolomite present.
3260-BF-27	Heterolithic breccia with a red/orange clay matrix with mainly black clasts and a few dolomite clasts. Sample was taken directly below 3260-BF26. Clasts are subrounded to subangular and are fine to medium grained.
3260-BF-28	Black limestone with oxidation and clay minerals located within bedding planes.
3260-BF-30	Heterolithic breccia with an orange matrix with black, white and tan clasts. Matrix is oxidized and clay altered. Black clasts are dominant and contain what appear to be tan clasts. White and tan clasts can also be seen in oxidized clay matrix. All clasts range from subrounded to subangular and are medium grained.
3260-BF-31	Highly clay altered rock, very soft. Yellow and minor red color.
3285-BF-1	Highly clay altered rock orange in color. Friable.
3285-BF-2	Monolithic breccia with a black matrix and tan clasts. Matrix is hard, silicified, and contains fractures filled with white calcite. Vugs present. Tan clasts are medium to coarse grained and subrounded to rounded. Some clasts have visible oxidation (red).

3285-BF-3	Clay-rich rock, very soft. Red in color with minor white bands that are not calcite.
3285-BF-4	Heterolithic breccia with an orange-red matrix and black, white, and tan clasts. Matrix is composed of clay. White and tan clasts are found in orange matrix and black clasts rounded to subrounded, fine – medium grained. Black clasts are subrounded – subangular and medium grain.
3285-BF-5	Bedded Limestone. Grey in color, noticeable bedding, and minor white calcite present. Clay minerals in bedding.
3285-BF-6	Clay altered rock. Red, white, and orange color. Friable.
3285-BF-7	Heterolithic breccia with an orange-yellow matrix and grey, black and tan clasts. Matrix is composed of clay. Tan clasts are fine to coarse grained and subangular to rounded. Grey and black clasts are rounded – subangular. Fine to coarse grained. Minor white calcite present.
3285-BF-8	Heterolithic breccia similar to 3285-BF-7 but grey clasts are absent.
3292W-BF1	Fractured Limestone with minor oxidation. Minor clay minerals (yellow-orange color). Bedding can still be distinguished.
3292W-BF2	Heterolithic breccia with a clay (orange) matrix and black clasts. Matrix is friable. Black clasts are minor, and are fine to coarse grained.
3292W-BF3	Heterolithic breccia with an orange matrix and white and black clasts. Matrix is highly clay altered. Clasts are angular to subangular and coarse grained.
3292W-BF4	Heterolithic breccia with an orange matrix and black and white clasts. Matrix is composed of clay minerals, is oxidized, and is friable. Black clasts are dominant, silicified. White clasts are dolomite. Clasts are fine to coarse grained and subangular to subrounded.
3180E-BF-1	Heterolithic breccia with a brownish/black silicifed matrix and white, tan, and black clasts. Matrix is slightly oxidized. Minor white calcite located in fractures within matrix. Clasts are dominantly white dolomite and tan with minor oxidation. All clasts are subrounded, fine to medium grained.

3180E-BF-2	Heterolithic breccia with an orange clay-rich matrix and black clasts. Matrix is soft. Black clasts are fine grained, rounded – subangular and silicified.
3180E-BF-3	Monolithic breccia with an orange matrix and white clasts. Matrix is somewhat soft and dominated by clay. Clasts are white, fine to coarse grained and subrounded to subangular.
3180E-BF-4	Highly clay altered rock (pale yellow in color) and soft.
3180E-BF-5	Limestone with tan bands. Bedding is present. Reacted readily to HCl.
3180E-BF-6	Bedded Limestone. Bedding is present, oxidation (red) present.
3180E-BF-7	Heterolithic breccia with an orange clay matrix and black clasts. Black clasts majority are silicifed, angular – subrounded and medium grained with rare coarse grained clasts
3180E-BF-8	Heterolithic breccia with a red-orange matrix and black and tan clasts. Matrix is soft and composed of clay. Clasts are mainly all black, and appear silicified. Black clasts are medium to fine grained, angular to subangular. Rare tan clasts are fine to medium grained, and subrounded. They are found in the black clasts.
3180W-BF-1	Clay rich rock, soft (yellow in color).
3180W-BF-2	Limestone with what appears to be very minor silicification. Bedding is not apparent. Minor oxidation.
3180W-BF-3	Highly clay altered rock (orange in color) and soft.
3180W-BF-4	Monolithic breccia with an orange, clay matrix and silicifed black clasts. Clast supported. Clasts are coarse to very coarse grained with minor medium grained clasts. All clasts are angular. Clasts are in the same orientation.
3180W-BF-5	Highly clay altered rock (orange in color).
3180W-BF-6	Heterolithic breccia with a brown matrix and tan and grey clasts. Matrix is silicified. Matrix supported breccia. Clasts are very minor, subangular to subrounded and fine grained. White calcite is abundant.

3180W-BF-7	Heterolithic breccia with an orange-yellow, clay matrix and black and tan clasts. Black clasts are fine, minor, and angular. Tan clasts are minor, fine to medium grained, rounded to subrounded, and are elongated.
3180W-BF-8	Heterolithic breccia with a black matrix and black and tan clasts. Matrix is silicified, and has minor amounts of oxidation (red in color). Tan clasts are dominant, fine to coarse grained, and are subangular to rounded. Black clasts are medium to coarse grained, and angular.
3180W-BF-9	Heterolithic breccia with an orange matrix and black, tan, and white clasts. Matrix is minor in abundance and composed of clay. Black clasts within orange matrix are fine grained, angular and are high in abundance. Tan clasts are fine grained and are rounded to subrounded. White calcite is present.
3180W-BF-10	Heterolithic breccia with an orange matrix and black, white and tan clasts. Matrix is highly clay altered, Black clasts are medium to coarse grained, angular to subangular and contain rare medium grained tan clasts which are rounded to subrounded. White clasts are minor, but are very coarse grained. Dolomite clasts are located within the clay matrix.
3180W-BF-11	Highly clay altered rock with minor amounts of black clasts. Clasts are fine to medium grained and contain white calcite.
3180W-BF-12	Heterolithic breccia with a yellow-orange matrix and black and white clasts. Matrix is soft, clay altered, and soft. Clasts are affine to medium grained. And angular to subrounded. Larger clasts appear to be rounded.
3180W-BF-13	Highly clay altered rock, yellow-orange in color.
3275-BF-1	Heterolithic breccia with a dark orange matrix and black, white, and tan clasts. Matrix is clay altered with a powdery feel. Black clasts are dominant, are angular and fine – medium grained. White calcite is present as veins in black clasts. Orange/tan clasts are minor and angular to subangular. White clasts are dolomite. They are angular and fine to medium grained.
3275-BF-2	Heterolithic breccia with an orange clay matrix with black and minor white clasts. Minor amount of vugs. Black clast are fine-medium grained and subangular to angular. White clasts are dolomite. They are fine grained, subrounded to subangular.

3275-BF-3	Heterolithic breccia with a brown matrix with black and white clasts. Matrix is silicified with minor vugs and white calcite in fractures. Black clasts are angular and medium to fine grained. White clasts are minor, fine grained, and angular.
3275-BF-4	Heterolithic breccia with an orange matrix with black and white clasts. Matrix is composed of clay minerals, soft, has minor vugs. Black clasts are the dominant clasts. They are fine to coarse grained and are subrounded to subangular. White clasts are minor, fine grained, rounded –subangular.
3275-BF-5	Heterolithic breccia with a brown, silicified matrix with tan, white and black clasts. Matrix has minor vugs and white calcite. Black, white, and brown clasts range from rounded to angular and are mostly fine to medium grained.
3275-BF-6	Heterolithic breccia with an orange matrix with tan, black, and white clasts. Matrix is clay altered with minor white calcite. Clasts are angular to subrounded. Rare tan clasts in black clasts.
3275-BF-7	Highly clay altered rock. Orange-yellow in color.
3275-BF-8	Heterolithic breccia with a brown matrix with black, tan and white clasts. Matrix is silicified, Black and tan clasts are medium to coarse grained subangular to subrounded. White clasts are dolomite.
3275-BF-9	Highly clay altered rock. Soft and orange in color.
3275-BF-10	Slightly fractured limestone. Minor oxidation and brown carbonate mineral present (ankerite?)
3275-BF-11	Heterolithic breccia with an orange matrix and black clasts. Matrix is clay. All clasts are fine grained and range from subrounded to subangular. Clasts are rounded to subrounded.
3275-BF-12	Heterolithic breccia with a black matrix and tan, black, and white clasts. Matrix is silicified with minor oxidation and, minor white calcite. Black clasts are medium grained and subrounded. Tan clasts are the dominant clast type, fine to coarse grained, rounded - subrounded. White clasts are minor, fine grained and subrounded.

3220-D8-LO-1	Monolithic breccia with a black, silicified matrix and tan clasts. Matrix has very few to no vugs. Vugs are < 1mm in diameter. White calcite veins present. No oxidation on matrix, minor clay alteration. Tan clasts are not abundant (3-5%), medium to coarse grained (.5 – 1.5 cm in length), sub-angular to sub-rounded. Powdered clasts react to HCl. Matrix supported
3220-D8-LO-2	Monolithic breccia with a brown, silicified matrix and tan clasts. Matrix has minor oxidation. Few vugs, up to .5 mm in length. Clasts are low in abundance (5-15%), medium to coarse grained (.5 cm – 1 cm in length, and subrounded to subangular. Matrix Supported.
3220-D8-LO-3	Monolithic breccia with a black and brown silicified matrix and tan clasts. Clasts are coarse grained, (.5 cm – 2 cm) angular – subrounded. Matrix has minor red oxidation. Vugs are present, up to 1.5 cm in diameter, somewhat circular.
3220-D8-LO-4	Monolithic breccia with a brown and black silicified with tan clasts. Clasts are very fine grained and have visible oxidation.
3220-D8-LO-5	Monolithic breccia with a black to brown, silicified matrix with tan clasts. Clasts are angular to subangular and fine to medium grained. Some clasts have vugs. Minor white calcite on matrix. High abundance of vugs (15-20%) 1 – 7.5 mm in size.
3220-D8-LO-6	Highly clay altered sample, dark orange in color, very soft and friable.
3220-D8-LO-7	Monolithic breccia with a black silicified matrix and tan clasts. Clasts are soft, and low in abundance. Some clasts possess vugs. Clasts are subrounded mostly with few subangular clasts. Matrix supported. No visible oxidation on matrix.
3220-D8-LO-8	Monolithic breccia with a black, slightly brown, silicifed matrix. Matrix supported. Minor vugs in matrix, few mm in diameter. 25% clasts. Clasts are medium to coarse grained up to 5 cm in length and subangular.
3220-D8-LO-9	Heterolithic breccia with a black, silicified matrix and tan and white clasts. Matrix has minor white calcite a high concentration of vugs that are up to 1 cm in length (15-20%). Clast supported. Tan clasts are dominant, fine to coarse grained up to 2.5 cm in length and angular. White clasts are dolomite and minor.

3220-D8-LO-10	Monolithic breccia with a black silicifed matrix and tan clasts. Matrix has a small abundance of vugs and white calcite. Vugs are very small and rounded. White calcite in veins. Clasts are high in abundance, medium to coarse grained up to 5 cm in length, subangular to subrounded. Rare vugs in clasts. One dolomite clast found in sample, dolomite in composition.
3220-D8-LO-11	Monolithic breccia with an orange clay matrix and black clasts. Clasts are fine to medium grained.
3320-BF-1	Heterolithic breccia with an orange matrix and black and white clasts. Matrix consists of secondary clay minerals and oxidized. Black clasts are silicifed and are the dominant clast type. They are fine grained and angular. White clasts are dolomite and minor, fine grained and subangular.
3320-BF-2	Heterolithic breccia with a black matrix with tan, grey and red clasts. Matrix is fractured and occasionally contain white calcite. Tan clasts are the dominant clast type. They are fine to coarse grained and rounded to subrounded. Grey clasts are dolomite and minor. They are subangular to subrounded. Red oxidation is either a clast or oxide minerals.
3320-BF-3	Heterolithic breccia with a minor clay (yellow-orange) matrix with black and tan clasts. Clay matrix is soft and is located in between silicified black clasts. Black clasts are coarse grained, angular to subangular. White calcite present in silicified clasts. Tan clasts are located within black clasts. They are medium grained and subrounded to rounded.
3320-BF-4	Heterolithic breccia with an orange clay matrix black, grey and tan clasts. Black clasts are silicified and are fine to medium grained and rounded. White dolomite clasts are minor, angular and medium grained. Tan clasts are medium to fine grained and rounded. White calcite present in breccia.
3320-BF-5	Monolithic breccia with a black matrix and tan clasts. Matrix is silicified. Matrix supported breccia. Clasts are tan, rounded to subrounded, fine to coarse grained. Minor white calite in veins. Taken adjacent to a 3 foot wide calcite vein.
3320-BF-6	Heterolithic breccia with a black matrix and white and tan clasts. Matrix have red oxides. Matrix supported breccia. Clasts are fine to medium grained, mostly medium grained. Clasts are rounded to subangular. Tan clasts are dominant. White clasts are dolomite. White calcite is located in vugs. Vugs present.

3292-D3-S1R	Monolithic breccia with a black, silicified matrix and tan clasts. Clasts are medium grained and subrounded to subangular. Matrix supported. Minor white calcite.
3292-D3-S2R	Highly clay altered rock. Orange in color. Soft.
3292-D3-S3R	Heterolithic breccia with a black, silicified matrix and tan and white clasts. Matrix supported. Clasts are dominantly tan. White clasts are dolomite. Clasts are subrounded to subangular. White calcite and red oxidation present in matrix.
3292-D3-S4R	Monolithic breccia with an orange, clay altered matrix and black clasts. Matrix is soft. Matrix supported. Black clasts are silicified, minor and fine grained.
3292-D3-5R	Heterolithic breccia with a clay, dark red matrix with black and white clasts. Matrix is soft and friable. Clasts are dominantly black, silicified clasts. Minor white, dolomite clasts. All clasts are fine grained rounded to subrounded.
3292-D3-S6R	Monolithic breccia with a black silicified matrix and tan clasts. Matrix supported. Clasts are elongated and rounded, medium to coarse grained.
3292-D3-S7R	Monolithic breccia with a yellow-orange matrix and coarse white, dolomite clasts. Clast supported. Clasts are subangular to subrounded.
3292-D3-S9R	Highly clay altered rock. Dark orange in color. Minor white calcite veins.
3292-D3-S10R	Monolithic breccia with a black silicified matrix and tan clasts. Minor white calcite veins. Tan clasts are very coarse, up to 8 cm in diameter, 10 um in diameter is rare. Matrix supported.
3292-D3-S11R	Monolithic breccia with an orange-red matrix and coarse grained black clasts. Clasts are silicified. And up to 4 cm in diameter. Clast supported. Matrix is minor.
3292-D3-S14R	Breccia with a silicifed matrix. Clasts are tan and minor. White calcite present in veins.
3292-D4-S1R	Sample taken from dolomite rock that has minor silicification. Silicified rock is surrounding dolomite rock on the rib.
3292-D4-S2R	Monolithic breccia with a black silicified matrix and tan clasts. Breccia appears vein-like within dolomite

	rock.
3292-D4-S3R	Fractured dolomite rock. Silicified rock is located in fractured areas. Minor oxidation (red-orange) on dolomite.
3292-D4-S4R	Fractured dolomite rock of 3292-D4-S3R transitions into a monolithic breccia with medium to coarse grained white dolomite clasts. Clasts are subangular. Matrix supported.
3292-D8-S2L	White to grey massive dolomite. Rare fractures, minor oxidation.
3292-D8-S4L	White massive dolomite. Located above a monolithic silicifed breccia. Minor oxidation. Dolomite is fractured. Fractures are no larger than 1 mm across. Oxides and quartz in fractures.
3292-D8-S5L	Monolithic breccia with white dolomite clasts. Located below dolomite rock. Matrix is black and silicified. Clasts are medium grained. Subrounded to subangular.
3292-D8-S6L	Monolithic breccia with a black silicified matrix and coarse grained, white dolomite clasts. Clasts are up to 6 cm in diameter and are angular to subangular.
3292-D8-S7L	Monolithic breccia with a silicified, black matrix and dolomite clasts. Sample is located within dolomite rock. Clasts are coarse grained. Clast supported breccia.
3292-D8-S8L	White to grey fractured, massive dolomite. Fractures are typically less than 1 mm wide.
3292-D8-S9L	Dolomite rock, white in color and a large abundance of fractures. Oxides and clay minerals present in fractures. Rare silicified areas within sample.
3292-D8-S10L	Highly clay altered rock. Very soft. Sample taken adjacent to the dike.
3260-D8-LR-1	Dolomite rock, white in color with fractures less than 1 mm. Fractures contain red oxide minerals. Minor quartz mineralization is rare and located around dolomite fragments.
3260-D8-LR-2	Dolomite rock, white with minor amounts of yellow and red oxidation. Rock is less fractured than 3260-D8-LR-1, but not by much. Fractures have red oxide minerals. Quartz is rare.

3260-D8-LR-3	Classified as a monolithic breccia. Clasts are white dolomite. They are medium grained and angular to subrounded. Matrix supported. Matrix is black in color. No vugs present.
3260-D8-LR-4	Heterolithic breccia with a silicified black matrix and white and minor tan clasts. Clasts are angular to subrounded and are coarse to medium grained. Clast dominated. White calcite has filled in vugs.
3260-D8-LR-5	Heterolithic breccia with a black and brown, silicified matrix and tan, white and black clasts. Matrix supported. Clasts are subangular to rounded and are coarse to fine grained.
3260-D8-LR-6	Monolithic breccia with a soft, yellow to red matrix with black silicifed clasts. Matrix is clay altered and oxidized. Matrix supported. Clasts are fine grained, subrounded to rounded.
3260-D8-LR-7	Heterolithic breccia with tan, grey, and red clasts. Matrix supported. Matrix is silicifed. Grey clasts are dolomite. Clasts are fine grained, angular to subrounded. Majority of clasts are rimmed with oxide minerals. Only sample where this texture has been documented.
3260-D8-LR-8	Monolithic breccia with a black silicified matrix and tan clasts. Clasts are medium grained and rounded. Minor amount of clasts are angular. Matrix supported.
3260-D8-Bacon Clay	Highly clay altered rock, dark orange in color. Located in large clay alteration vein that is approximately 4 feet across. Located adjacent to the dike.
3292-D7-LR-1	Monolithic breccia with a brown, silicified matrix and white dolomite clasts. Matrix has vugs up to 5 mm in diameter and visible oxides. Clasts are fine grained and subangular. Matrix supported. White calcite present.
3292-D7-LR-2	Monolithic breccia with a brown matrix and white clasts. Matrix is silicified and has very fine vugs. Clasts are subangular to rounded. Matrix supported.
3292-D7-LR-3	Monolithic breccia with a red clay matrix and black, white and tan clasts. Matrix supported. Clasts are angular and medium grained. White, dolomite clasts are dominant with minor black, silicifed clasts and trace tan clasts.
3292-D7-LR-4	Monolithic breccia with a red clay matrix and white clasts. Clasts are subrounded to angular, fine to medium grained and low in abundance. Matrix supported.

3292-D7-LR-5	Monolithic breccia with a brown matrix and tan, white and red clasts. Matrix is silicifed with rare white calcite in fractures. Tan clasts are dominant, red clasts are rare. Clasts range from angular to subangular and fine to medium grained. (Up to 5 mm in diameter).
3292-D7-LR-6	Monolithic breccia with a black, silicified matrix and white clasts. Clasts are dolomite, angular to subangular, and fine to coarse grained (up to 1 cm in diameter). Rare vugs present in matrix. Matrix supported.
3292-D7-LR-8	Monolithic breccia with a black silicifed matrix and tan clasts. Clasts are subangular and fine grained. Minor red oxides on Matrix. Vugs present (5-7%) 5 mm in diameter. White calcite present in some vugs.
3292-D7-LR-9	Heterolithic breccia with a yellow, clay matrix and black clasts. Matrix is soft and minor. Clasts supported. Black clasts are silicifed, angular and coarse to fine grained.
3292-D7-LR-10	Clay altered rock. Purple in color. Extremely friable.
3292-D7-LR-11	Monolithic breccia with a silicified, black matrix and tan clasts. Clasts are fine to medium grained and mostly rounded with a few subangular clasts. Rare vugs in clasts. Matrix supported.
3180-W-1	Monolithic breccia with a silicifed, black matrix and tab clasts. Matrix has a minor amount of vugs with minor white calcite. Clasts are subrounded, fine to medium grained. Matrix dominated. Minor oxidation on clasts.
3180-W-2	Highly clay altered rock, no clasts present. Orange in color, soft.
3180-W-3	Clay altered rock with minor fragments. Clasts are fine to medium grained up to 4 mm in length and subangular, black-brown in color, silicifed.
3180-W-4	Highly clay altered rock, orange in color, friable.
3180-W-5	Yellow to orange in color, highly clay altered rock. Very fine grained and rare dolomite clasts
3180-W-6	Highly clay altered rock, dark orange in color. White calcite veins present.
3180-W-7	Monolithic breccia with a black silicified matrix with tan clasts. Matrix has red oxidation in some locations. White calcite present. Large portion of the sample is limestone.

3180-W-8	Dark grey limestone, soft, with tan bands.
3180-W-9	Clay altered rock. Yellow-orange in color. Very rare black silicified clasts.
3180-W-10	Limestone, black to dark grey in color. Tan bands present.

APPENDIX C

EPMA DATA

A JEOL-8900 Electron Probe Microanalyzer (EPMA) at the UNLV EMiL was used to quantify the major, minor and trace element chemistry of texturally and spatially diverse goethite crystals. EPMA analysis focused on identifying native gold and determining the respective chemistries of goethite crystals. Analyzed elements include: Ag, Al, As, Au, Bi, Ca, Co, Cu, Fe, Hg, Mo, Ni, Pb, S, Sb, Se Si, Te, Ti, Tl, and Zn. Since all measurements were taken of goethites, elements excluding Au and Ag, were converted to oxide weight percent to determine the distribution of oxygen in each measured point.

EPMA point name	No.	SeO_2 (wt%)	Ag (wt%)	Au (wt%)	As_2O_3 (wt%)	HgO (wt%)	Tl_2O_3 (wt%)	SiO_2 (wt%)	PbO (wt%)	Bi_2O_3 (wt%)	Al_2O_3 (wt%)
DC-0221-5-a5	5	0.0	0.0	0.0	1.242	0.017	.014	14.59	0.059	0.0	0.186
DC-0221-5-a6	6	0.0	0.0	0.0	1.868	0.015	0.002	5.147	0.052	0.0	0.198
DC-0221-5-a8	8	0.0	0.0	0.0	2.603	0.016	0.008	3.247	0.051	0.089	0.258
DC-0221-5-a9	9	0.0	0.0	0.0	0.776	0.023	0.013	5.423	0.067	0.035	0.664
DC-0221-5-a10	10	0.0	0.0	0.0	1.562	0.003	0.0	2.938	0.069	0.013	0.153
DC-0221-5-a11	11	0.0	0.0	0.0	0.493	0.026	0.011	6.892	0.07	0.016	1.085
DC-0221-5-a14	14	0.0	0.0	0.0	2.190	0.009	0.008	3.301	0.061	0.0	0.121
DC-0221-5-a15	15	0.0	0.0	0.0	1.542	0.011	0.0	13.831	0.056	0.078	0.221
DC-0221-5-a16	16	0.0	0.0	0.0	1.075	0.004	0.0	30.304	0.038	0.024	0.262
DC-0221-5-a17	17	0.0	0.0012	0.0	0.993	0.008	0.008	5.903	0.041	0.087	0.946
DC-0221-5-a18	18	0.0	0.0	0.0	2.150	0.008	0.0	2.723	0.085	0.03	0.194
DC-0221-5-a19	19	0.0	0.0	0.0	1.815	0.005	0.0	7.405	0.054	0.05	0.3
DC-0221-5-a20	20	0.0	0.0	11.6763	0.987	0.25	0.041	1.281	0.025	0.0	0.057
DC-0221-5-a21	21	0.0	0.0	0.0	1.667	0.005	0.038	2.491	0.077	0.07	0.126
DC-0221-5-a22	22	0.0	0.0	0.0	1.853	0.009	0.0	2.438	0.054	0.014	0.109
DC-0221-5-a24	24	0.0	0.0	0.0	1.417	0.019	0.0	2.467	0.062	0.031	0.09
DC-0221-5-b3	27	0.0	0.0	0.0	2.193	0.008	0.0	7.959	0.049	0.039	0.230
DC-0221-5-b6	30	0.0	0.0	0.0	1.967	0.008	0.011	2.473	0.056	0.014	0.083
DC-0221-5-b7	31	0.0	0.0	0.0	1.078	0.009	0.008	3.43	0.048	0.017	0.016
DC-0221-5-b8	32	0.005	0.0	0.0	1.008	0.006	0.0	2.807	0.071	0.031	0.022

EPMA point name	CuO (wt%)	ZnO (wt%)	TeO_2 (wt%)	NiO (wt%)	Sb_2O_3 (wt%)	CoO (wt%)	SnO_2 (wt%)	TiO_2 (wt%)	MoO_3 (wt%)	Fe_2O_3 (wt%)	CaO (wt%)	SO_2 (wt%)	Total (wt%)
DC-0221-5-a5	0.041	0.057	0.0	0.051	6.301	0.095	0.054	0.0	0.046	69.076	0.0	0.082	91.911
DC-0221-5-a6	0.050	0.033	0.0	0.033	5.525	0.102	0.037	0.008	0.056	76.6397	0.072	0.08	89.918
DC-0221-5-a8	0.075	0.0	0.0	0.046	4.709	0.119	0.0231	0.003	0.093	80.292	0.298	0.085	92.015
DC-0221-5-a9	0.010	0.092	0.0	0.033	3.059	0.109	0.0204	0.0	0.02	82.106	0.030	0.029	92.509
DC-0221-5-a10	0.057	0.057	0.0	0.04	5.075	0.128	0.0302	0.0	0.06	79.846	0.301	0.079	90.411
DC-0221-5-a11	0.019	0.089	0.0	0.021	2.499	0.098	0.0088	0.014	0.037	79.476	0.009	0.03	90.894
DC-0221-5-a14	0.115	0.006	0.0	0.044	3.359	0.108	0.0182	0.0	0.059	80.975	0.535	0.064	90.973
DC-0221-5-a15	0.065	0.0	0.0	0.036	4.089	0.134	0.0263	0.0	0.087	74.63	0.251	0.069	95.1263
DC-0221-5-a16	0.044	0.0	0.0	0.021	2.51	0.103	0.0157	0.0	0.069	57.589	0.175	0.094	92.328
DC-0221-5-a17	0.004	0.066	0.0	0.022	3.613	0.0932	0.0146	0.060	0.038	75.635	2.199	0.113	89.845
DC-0221-5-a18	0.105	0.076	0.0	0.036	4.769	0.1023	0.0102	0.004	0.073	79.6	0.418	0.106	90.490
DC-0221-5-a19	0.032	0.003	0.0	0.036	4.535	0.122	0.0208	0.0	0.04	74.522	1.434	0.127	90.501
DC-0221-5-a20	0.101	0.012	0.0	0.021	3.888	0.134	0.0246	0.014	0.0	71.889	0.488	0.074	90.963
DC-0221-5-a21	0.041	0.083	0.0	0.058	6.447	0.123	0.0283	0.003	0.043	79.534	0.143	0.08	91.057
DC-0221-5-a22	0.054	0.0	0.0	0.041	5.779	0.123	0.0337	0.0	0.065	80.358	0.217	0.105	91.253
DC-0221-5-a24	0.024	0.048	0.0	0.038	5.237	0.121	0.0295	0.0	0.079	81.818	0.161	0.122	91.764

EPMA point name	No	SeO_2 (wt%)	Ag (wt%)	Au (wt%)	As_2O_3 (wt%)	HgO (wt%)	Tl_2O_3 (wt%)	SiO_2 (wt%)	PbO (wt%)	Bi_2O_3 (wt%)	Al_2O_3 (wt%)
DC-0221-1-a1	33	0.0	0.0	0.0	2.415	0.0	0.0	3.662	0.174	0.0	0.058
DC-0221-1-a2	34	0.001	0.0007	0.0167	2.462	0.0	0.0	4.134	0.171	0.072	0.030
DC-0221-1-a4	36	0.0	0.0	0.0152	1.312	0.017	0.0	45.532	0..135	0.0	2.801
DC-0221-1-a5	37	0.0	0.0	0.0	2.1	0.01	0.0	2.938	0.138	0.033	0.043
DC-0221-1-a7	39	0.0	0.0	0.0	1.707	0.01	0.0	3.811	0.094	0.062	0.216
DC-0221-1-a8	40	0.0	0.0058	0.0	1.764	0.014	0.0	5.696	0.167	0.079	0.213
DC-0221-1-b2	44	0.005	0.0	0.0	1.743	0.002	0.0	2.092	0.116	0.0	0.071
DC-0221-1-b3	45	0.0	0.0	0.0	1.915	0.004	0.0	3.253	0.129	0.039	0.118
DC-0221-1-b4	46	0.0	0.0004	0.0	2.160	0.0	0.0	4.118	0.154	0.037	0.075
DC-0221-1-b5	47	0.0	0.0	0.0126	2.122	0.027	0.0	4.378	0.159	0.0	1.787
DC-0221-1-c1	48	0.0	0.0	0.0	1.766	0.004	0.0	4.434	0.195	0.0	0.331
DC-0221-1-c2	49	0.0	0.0	0.0	1.656	0.01	0.0	3.543	0.157	0.005	0.142
DC-0221-1-c3	50	0.003	0.0	0.0	1.721	0.006	0.0	4.938	0.128	0.021	0.145
DC-0221-1-d2	52	0.0	0.0	0.0	3.628	0.002	0.0	3.673	0.206	0.063	0.565
DC-0221-1-d3	53	0.0	0.0	0.0	3.46	0.006	0.0	3.433	0.16	0.025	0.536
DC-0221-1-d4	54	0.0	0.0	0.0	1.501	0.0	0.0	48.426	0.104	0.0	0.377
DC-0221-1-d5	55	0.0	0.0	0.0	0.692	0.0	0.0	4.496	0.323	0.0	0.16
DC-0221-1-e2	58	0.004	0.0	0.0	2.003	0.0	0.017	4.959	0.143	0.024	0.408
DC-0221-1-e3	59	0.0	0.0	0.0	2.255	0.01	0.0	4.368	0.179	0.025	0.459
DC-0221-1-b7	64	0.0	0.0	0.0	0.998	0.01	0.0	2.64	0.095	0.034	0.065
DC-0221-1-f1	65	0.01	0.0308	40.4261	0.856	0.792	0.093	8.172	0.0	0.0	0.161
DC-0221-1-g1	67	0.0	0.0	3.2492	2.254	0.114	0.046	2.978	0.197	0.0	0.054
DC-0221-1-g3	69	0.0	0.0	4.7836	2.17	0.175	0.043	2.286	0.129	0.0	0.02

EPMA point name	CuO (wt%)	ZnO (wt%)	TeO_2 (wt%)	NiO (wt%)	Sb_2O_3 (wt%)	CoO (wt%)	SnO_2 (wt%)	TiO_2 (wt%)	MoO_3 (wt%)	Fe_2O_3 (wt%)	CaO (wt%)	SO_2 (wt%)	Total (wt%)
DC-0221-1-a1	0.003	0.109	0.0	0.044	1.102	0.126	0.0081	0.036	0.006	81.655	1.043	0.065	90.506
DC-0221-1-a2	0.02	0.083	0.0	0.041	1.1	0.135	0.0065	0.036	0.008	82.169	1.054	0.058	91.597
DC-0221-1-a4	0.0	0.038	0.0	0.014	0.594	0.053	0.0028	0.038	0.016	40.94	0.564	0.037	91.974
DC-0221-1-a5	0.019	0.064	0.0	0.019	1.03	0.117	0.0091	0.0003	0.0	83.123	0.895	0.076	90.614
DC-0221-1-a7	0.036	0.032	0.0	0.002	0.925	0.132	0.0043	0.01	0.0	82.361	0.897	0.078	90.377
DC-0221-1-a8	0.13	0.051	0.0	0.073	1.158	0.130	0.0073	0.017	0.0	82.644	0.709	0.094	92.952
DC-0221-1-b2	0.017	0.137	0.0	0.042	1.552	0.136	0.0038	0.0	0.021	84.820	0.808	0.0098	91.576
DC-0221-1-b3	0.034	0.093	0.0	0.033	0.991	0.129	0.0023	0.005	0.0	83.821	0.781	0.02	91.367
DC-0221-1-b4	0.015	0.162	0.0	0.022	1.769	0.101	0.0041	0.003	0.031	81.724	0.868	0.063	91.307
DC-0221-1-b5	0.001	0.129	0.0	0.027	1.464	0.121	0.0003	0.006	0.04	78.905	0.823	0.106	90.108
DC-0221-1-c1	0.006	0.335	0.0	0.048	0.936	0.116	0.0077	0.005	0.019	82.332	0.738	0.026	91.299
DC-0221-1-c2	0.059	0.27	0.0	0.036	1.005	0.122	0.0014	0.025	0.033	84.748	0.602	0.0226	92.437
DC-0221-1-c3	0.012	0.345	0.0	0.056	0.985	0.125	0.0089	0.0	0.027	81.823	0.706	0.04	91.090
DC-0221-1-d2	0.08	0.365	0.0	0.015	0.753	0.107	0.0019	0.0	0.031	80.292	1.684	0.023	91.489
DC-0221-1-d3	0.126	0.367	0.0	0.012	0.721	0.117	0.0049	0.0	0.042	77.996	1.954	0.053	89.013
DC-0221-1-d4	0.089	0.089	0.0	0.005	0.450	0.068	0.0126	0.0117	0.025	38.925	1.495	0.042	91.620
DC-0221-1-d5	0.122	0.019	0.0	0.0	0.495	0.148	0.0	0.0022	0.0	84.69	0.498	0.056	91.701
DC-0221-1-e2	0.138	0.123	0.0	0.036	1.176	0.162	0.0046	0.0063	0.0	79.138	2.25	0.062	90.654
DC-0221-1-e3	0.064	0.114	0.0	0.051	1.119	0.162	0.0079	0.0096	0.0	79.475	2.608	0.061	90.968
DC-0221-1-b7	0.021	0.0	0.0	0.01	2.9	0.131	0.0078	0.0	0.013	85.781	0.344	0.086	93.136
DC-0221-1-f1	0.05	0.026	0.0	0.025	0.634	0.069	0.0054	0.0132	0.0	47.518	0.669	0.0	99.551
DC-0221-1-g1	0.057	0.292	0.0	0.027	1.373	0.107	0.0053	0.0	0.002	80.509	1.304	0.1	95.104
DC-0221-1-g3	0.006	0.121	0.0	0.027	1.342	0.113	0.0071	0.0027	0.0	79.581	0.876	0.098	97.701

APPENDIX D

SPECTRAL REFLECTANCE DATA

Two hundred and twenty-two coarse reject samples from underground workings, drill core and outcrop samples were placed within RC-chip trays for Terra Spec 4 standard-resolution mineral analysis to identify clay, oxide and other unknown minerals within samples. Prior to each spectral read-out, chip trays were turned upside-down and shaken allowing for spectral lens to be 100% covered when spectrum was being analyzed. The diameter of the spectral lens is 10 mm. For each reading, the lens was placed on one spot within a chip tray slot. Each chip tray slot is 2.5 cm wide. Spectral data were interpreted using The Spectral Geologist 7 (TSG 7) processing and spectrometer analysis software. The table provides the two most abundant mineral spectrums, absorption features (wavelengths) and white mica crystallinity.

Null = No reading, PX = Poorly Crystalline, WX = Well Crystalline.

Level or Drill	Sample ID	Mineral 1	Mineral 2	Oxide 1	Oxide 2
3292	3292W-BF1	Phengite	Dolomite	Goethite	NULL
3292	3292W-BF2	Phengite	NULL	NULL	NULL
3292	3292W-BF3	Dolomite	Phengite	NULL	NULL
3292	3292W-BF4	Phengite	Ankerite	Goethite	NULL
3292	3260W-BF-16	Siderite	Montmorillonite	NULL	NULL
3292	3260W-BF-21	Phengite	Dolomite	Goethite	NULL
3292	3260W-BF-9	Dolomite	Phengite	Goethite	NULL
3292	3260W-BF-1	Dolomite	Phengite	Goethite	NULL
3292	3260W-BF-2	Dolomite	Kaolinite-PX	Goethite	NULL
3292	3260W-BF-3	Dolomite	Kaolinite-PX	Goethite	NULL
3292	3260W-BF-4	Dolomite	NULL	Hematite	Goethite
3292	3260W-BF-5	Dolomite	Kaolinite-PX	Goethite	NULL
3292	3260W-BF-6	Dolomite	Phengite	Goethite	NULL
3292	3260W-BF-7	Dolomite	NULL	NULL	NULL
3292	3260W-BF-8	Dolomite	NULL	Aspectral	NULL
3260	3260W-BF-10	Phengitic Illite	NULL	Goethite	NULL
3260	3260W-BF-11	Phengite	NULL	NULL	NULL
3260	3260W-BF-12	Calcite	Phengite	Goethite	NULL
3260	3260W-BF-13	Phengite	NULL	Goethite	NULL
3260	3260W-BF-14	Phengite	NULL	Goethite	NULL
3260	3260W-BF-15	Phengite	NULL	Goethite	NULL
3260	3260W-BF-17	Dolomite	NULL	Goethite	NULL
3260	3260W-BF-18	Dolomite	Phengite	Goethite	NULL
3260	3260W-BF-19	Phengite	Ankerite	Goethite	NULL
3260	3260W-BF-20	Phengite	NULL	NULL	NULL
3260	3260W-BF-22	Phengite	NULL	Goethite	NULL

AlOH Wavelength	AlOH Absorption	AlOH Width	Water Absorption	Crystallinity
2218.49	0.0465	29.508	0.0282	moderate
2218.06	0.278	29.804	0.038	excellent
2220.84	0.0605	27.009	0.0266	poor
2218.98	0.129	28.645	0.0284	moderate
2221.09	0.0408	28.031	0.0265	poor
2219.56	0.267	28.894	0.0417	excellent
2219.66	0.0744	29.734	0.0719	poor
2217.35	0.0683	30.912	0.0619	poor
2208.89	0.046	24.903	0.0326	poor
2209.03	0.0474	26.57	0.0289	poor
NULL	NULL	NULL	0.0599	poor
2208.78	0.0891	22.789	0.0385	poor
2214.12	0.13	31.057	0.102	poor
NULL	NULL	NULL	0.234	poor
2224.43	0.0283	31.238	0.0309	N/A
2214.75	0.182	30.943	0.0682	excellent
2216.66	0.101	29.125	0.0436	excellent
2210.14	0.0561	27.504	0.0991	N/A
2214.98	0.158	29.895	0.0399	excellent
2217.14	0.182	29.228	0.0312	excellent
2218.04	0.146	27.965	0.0209	excellent
NULL	NULL	NULL	0.308	poor
NULL	NULL	NULL	0.237	poor
2217.42	0.218	29.903	0.0693	excellent
2217.51	0.394	31.188	0.0845	excellent
2217.44	0.296	30.875	0.111	excellent

Level or Drill	Sample ID	Mineral 1	Mineral 2	Oxide 1	Oxide 2
3260	3260W-BF-23	Phengite	NULL	NULL	NULL
3260	3260W-BF-24	Phengite	NULL	Goethite	NULL
3260	3260W-BF-25	Dolomite	Phengite	Goethite	NULL
3260	326W-BF-26	Ankerite	Montmorillonite	Goethite	NULL
3260	3260W-BF-27	Siderite	Phengite	NULL	NULL
3260	D8-S6L	Phengite	Ankerite	NULL	NULL
3260	D8-S7L	Phengite	Siderite	Goethite	NULL
3260	D8-S8L	Phengite	NULL	Goethite	NULL
3260	D8-S9L	Phengite	NULL	Goethite	NULL
3260	D8-10R	Phengite	Siderite	Goethite	NULL
3220	D8-LO-6	Phengite	Siderite	Goethite	NULL
3180	3180-W-1	Phengite	Ankerite	Goethite	NULL
3180	3180-W-2	Phengite	NULL	NULL	NULL
3180	3180-W-3	Phengite	NULL	NULL	NULL
3180	3180-W-4	Phengite	NULL	Goethite	NULL
3180	3180-W-5	Phengite	Wood	Goethite	Vegetation
3180	3180-W-6	Calcite	Phengite	NULL	NULL
3260	D8-Bacon Clay	Phengite	NULL	Goethite	NULL
3180	3180 W-7	Phengite	Calcite	Goethite	NULL
3180	3181 W-8	Phengite	NULL	NULL	NULL
3180	3182 W-9	Phengite	Calcite	Goethite	NULL
3180	3183 W-10	Calcite	Phengite	Goethite	NULL
3292	3292-D7-LR-6	Kaolinite-WX	Muscovite	NULL	NULL
3292	3292-D7-LR-8	Calcite	Kaolinite-PX	Goethite	NULL
3292	3292-D7-LR-9	Kaolinite-WX	Phengite	Goethite	NULL
3292	3292-D7-LR-10	Phengite	Kaolinite-PX	Goethite	NULL

AlOH Wavelength	AlOH Absorption	AlOH Width	Water Absorption	Crystallinity
2218.27	0.14	28.072	0.0211	excellent
2216.89	0.0778	29.312	0.0336	moderate
2220.12	0.0888	30.874	0.259	poor
2217.79	0.0426	30.116	0.0469	N/A
2213.41	0.0383	31.749	0.0313	N/A
2217.78	0.122	29.234	0.0538	poor
2210.69	0.0608	29.603	0.0417	poor
2218.57	0.158	27.968	0.0383	excellent
2216.57	0.103	31.272	0.0618	moderate
2217.63	0.0677	31.135	0.0407	moderate
2219.74	0.0756	26.168	0.0258	excellent
2218.34	0.17	28.292	0.0287	good
2218.01	0.195	29.02	0.0483	excellent
2217.81	0.207	28.362	0.0224	excellent
2218.22	0.25	29.07	0.0698	excellent
2217.42	0.169	28.685	0.0677	excellent
2217.85	0.0639	27.86	0.0325	N/A
2212.64	0.139	30.69	0.277	moderate
2218.43	0.168	28.14	0.0925	N/A
2218.13	0.097	27.613	0.016	excellent
2217.99	0.198	28.34	0.033	poor
2219.94	0.0475	25.453	0.0908	N/A
2208.45	0.177	20.326	0.0623	poor
2208.36	0.0429	18.157	0.123	N/A
2208.62	0.177	20.354	0.0663	poor
2209.16	0.115	24.622	0.037	moderate

level or drill	sample ID	Mineral 1	Mineral 2	Oxide 1	Oxide 2
3292	3292-D7-LR-11	Phengite	Ankerite	Goethite	NULL
3220	3220-D8-LO-7	Phengite	NULL	NULL	NULL
3220	3220-D8-LO-8	Phengite	NULL	Goethite	NULL
3220	3220-D8-LO-9	Phengite	NULL	NULL	NULL
3220	3220-D8-LO-10	Phengite	NULL	Goethite	NULL
3220	3220-D8-LO-11	Phengite	NULL	NULL	NULL
3260	3260-D8-LR-1	Dolomite	NULL	Goethite	Hematite
3260	3260-D8-LR-2	Dolomite	Phengite	Goethite	NULL
3260	3260-D8-LR-3	Dolomite	Muscovite	Goethite	Hematite
3260	3260-D8-LR-4	Dolomite	Montmorillonite	Aspectral	NULL
3260	3260-D8-LR-5	Dolomite	NULL	Goethite	NULL
3260	3260-D8-LR-6	Phengite	NULL	Goethite	NULL
3260	3260-D8-LR-7	Phengite	NULL	Goethite	NULL
3260	3260-D8-LR-8	Phengite	NULL	Aspectral	NULL
3220	3220-BF-6	Phengite	Kaolinite-PX	Goethite	NULL
3220	3220-BF-7	Phengite	Calcite	Goethite	NULL
3220	3220-BF-8	Phengite	Dolomite	Goethite	NULL
3220	3220-BF-9	Phengite	Dolomite	Goethite	NULL
3220	3220-BF-10	Phengite	Dolomite	Goethite	NULL
3220	3220-BF-7b	Dolomite	Montmorillonite	Goethite	NULL
3220	3220-BF-8b	Phengite	Dolomite	NULL	NULL
3220	3220-BF13-11	Dolomite	Phengite	Goethite	NULL
3220	3220-BF13-12	Dolomite	Phengite	Goethite	NULL
3220	3220-BF13-13	Dolomite	White Marker	Goethite	NULL
3220	3220-BF13-14	Kaolinite-WX	NULL	Goethite	NULL
3220	3220-BF13-15	Dolomite	Montmorillonite	Aspectral	NULL

AlOH Wavelength	AlOH Absorption	AlOH Width	Water Absorption	Crystallinity
2219.17	0.091	28.192	0.0498	poor
2217.97	0.219	29.564	0.0909	excellent
2219.58	0.0823	26.844	0.0237	excellent
2218.56	0.0785	27.993	0.0236	excellent
2218.82	0.204	28.928	0.0527	excellent
2217.18	0.1	29.565	0.0371	excellent
NULL	NULL	NULL	0.306	poor
NULL	NULL	NULL	0.249	poor
2216.72	0.0781	31.749	0.127	poor
2226.47	0.0292	31.176	0.037	poor
NULL	NULL	NULL	0.0789	poor
2211.29	0.121	31.632	0.129	moderate
2219.61	0.131	27.211	0.0307	excellent
2218.5	0.0856	27.934	0.0313	excellent
2211.2	0.15	28.685	0.0234	excellent
2219.61	0.235	28.224	0.0435	good
2212.51	0.112	29.878	0.0343	moderate
2213.41	0.0589	30.652	0.0452	poor
2218.68	0.123	28.929	0.0373	moderate
2218.82	0.0408	30.033	0.034	N/A
2209.65	0.0971	28.703	0.0563	poor
2222.86	0.1	27.655	0.218	poor
2220.72	0.0602	29.267	0.0431	N/A
2211.04	0.105	29.828	0.0828	poor
2207.94	0.308	26.848	0.114	good
2210.55	0.0307	31.489	0.0339	poor
2219.88	0.112	28.132	0.0471	poor

level or drill	sample ID	Mineral 1	Mineral 2	Oxide 1	Oxide 2
3220	3220-BF13-31	Phengite	NULL	Goethite	NULL
3220	3220-BF13-32	Phengite	NULL	NULL	NULL
3220	3220-BF13-33	Phengite	NULL	NULL	NULL
3220	3220-BF13-34	Phengite	NULL	NULL	NULL
3220	3220-BF13-35	Phengite	Dolomite	Goethite	NULL
3220	3220-BF13-36	Phengite	Calcite	NULL	NULL
3220	3220-BF13-37	Phengite	Calcite	NULL	NULL
3220	3220-BF13-38	Phengite	NULL	NULL	NULL
3220	3220-BF13-39	Phengite	NULL	NULL	NULL
3220	3220-BF13-40	Phengite	NULL	NULL	NULL
3220	3220-BF13-41	Phengite	Siderite	NULL	NULL
3220	3220-BF13-42	Phengite	Dolomite	Goethite	NULL
3220	3220-BF13-43	Phengite	NULL	Goethite	NULL
3220	3220-BF13-44	Phengite	NULL	Aspectral	NULL
3220	3220-BF13-45	Phengite	NULL	Goethite	NULL
3220	3220-BF13-46	Calcite	Phengite	NULL	NULL
3220	3220-BF13-47	Dolomite	Phengite	Goethite	NULL
3220	3220-BF13-48	Phengite	Dolomite	Goethite	NULL
3220	3220-BF13-49	Phengite	NULL	Goethite	NULL
3220	3220-BF13-50	Phengite	NULL	NULL	NULL
3220	3220-BF13-51	Phengite	NULL	Goethite	NULL
3220	3220-BF13-52	Phengite	Calcite	Goethite	NULL
3260	3260-BF-1	Phengite	Siderite	Goethite	NULL
3260	3260-BF-2	Phengite	Ankerite	Goethite	NULL
3260	3260-BF-3	Kaolinite-PX	Phengite	Goethite	NULL
3260	3260-BF-4	Phengite	Dolomite	NULL	NULL

AlOH Wavelength	AlOH Absorption	AlOH Width	Water Absorption	Crystallinity
2218.27	0.292	30.206	0.156	excellent
2217.12	0.369	31.59	0.226	excellent
2218.63	0.144	27.781	0.0702	excellent
2217.99	0.0811	28.075	0.0287	excellent
2209.97	0.117	28.129	0.0568	poor
2217.88	0.246	29.399	0.165	moderate
2218.96	0.101	27.659	0.0772	poor
2217.52	0.215	30.038	0.0807	good
2216.94	0.253	31.218	0.146	excellent
2220.18	0.126	26.5	0.0517	excellent
2219.32	0.103	28.864	0.038	moderate
2219.07	0.196	28.134	0.0925	moderate
2219.37	0.207	28.515	0.106	excellent
2217.43	0.0579	28.364	0.0183	moderate
2217.86	0.0819	27.879	0.0348	good
2220.56	0.0868	25.2	0.102	poor
2221.88	0.177	28.665	0.305	moderate
2218.05	0.106	28.667	0.0547	moderate
2217.73	0.339	30.885	0.197	excellent
2217.38	0.201	30.304	0.106	excellent
2215.77	0.125	29.047	0.0559	excellent
2218.55	0.103	26.893	0.16	poor
2218.78	0.0345	28.675	0.0155	poor
2217.26	0.0711	28.688	0.0288	moderate
2208.81	0.112	22.692	0.0395	moderate
2216.99	0.0595	28.731	0.027	moderate

level or drill	sample ID	Mineral 1	Mineral 2	Oxide 1	Oxide 2
3260	3260-BF-5	Dolomite	NULL	GalvanisedIron	Goethite
3260	3260-BF-6	Dolomite	NULL	Goethite	Hematite
3260	3260-BF-7	Phengite	NULL	NULL	NULL
3260	3260-BF-8	Phengite	NULL	Goethite	NULL
3260W	3260W-BF-1	Phengite	NULL	Goethite	NULL
3260W	3260W-BF-2	Phengite	NULL	Goethite	NULL
3260W	3260W-BF-3	Phengite	Siderite	Goethite	NULL
3260W	3260W-BF-4	Phengite	NULL	Goethite	NULL
3260W	3260W-BF-5	Phengite	Marker	NULL	NULL
3260W	3260W-BF-6	Phengite	Ankerite	Goethite	NULL
3260W	3260W-BF-7	Phengite	NULL	NULL	NULL
3260W	3260W-BF-8	Phengite	Ankerite	Goethite	NULL
3260W	3260W-BF-9	Calcite	Phengite	NULL	NULL
3260W	3260W-BF-10	Phengite	Calcite	Goethite	NULL
3260W	3260W-BF-11	Phengite	NULL	Goethite	NULL
3260W	3260W-BF-12	Phengite	Calcite	Goethite	NULL
3260W	3260W-BF-13	Phengite	NULL	NULL	NULL
3260W	3260W-BF-14	Phengite	NULL	Goethite	NULL
3260W	3260W-BF-15	Phengite	NULL	NULL	NULL
3260W	3260W-BF-16	Calcite	NULL	NULL	NULL
3260W	3260W-BF-17	Phengite	Siderite	Goethite	NULL
3260W	3260W-BF-18	Phengite	NULL	Goethite	NULL
3260W	3260W-BF-19	Phengite	NULL	Goethite	NULL
3260W	3260W-BF-20	Phengite	NULL	NULL	NULL
3260W	3260W-BF-21	Dolomite	Phengite	Goethite	NULL
3260W	3260W-BF-22	Phengite	Dolomite	Goethite	NULL

AlOH Wavelength	AlOH Absorption	AlOH Width	Water Absorption	Crystallinity
NULL	NULL	NULL	0.451	N/A
NULL	NULL	NULL	0.376	N/A
2217.69	0.215	29.631	0.109	excellent
2217.37	0.22	29.872	0.12	excellent
2218.32	0.38	30.524	0.197	excellent
2218.63	0.28	29.573	0.148	excellent
2217.98	0.0934	29.576	0.0248	moderate
2217.94	0.277	30.131	0.159	excellent
2218.56	0.0903	28.086	0.0426	good
2218.25	0.0856	27.371	0.0368	moderate
2218.29	0.102	28.208	0.0434	excellent
2217.85	0.113	29.065	0.0423	good
2222.04	0.0483	25.041	0.206	poor
2219.16	0.0879	26.743	0.0501	moderate
2218.44	0.14	27.846	0.0636	excellent
2218.8	0.156	27.386	0.115	moderate
2219.15	0.0745	26.979	0.0277	excellent
2217.99	0.0827	28.632	0.0239	moderate
2219.33	0.158	26.926	0.0816	excellent
2219.59	0.0348	25.57	0.219	N/A
2219.11	0.0732	26.961	0.026	good
2218.71	0.273	29.466	0.132	excellent
2218.78	0.238	29.019	0.138	excellent
2218.34	0.359	30.705	0.198	excellent
2219.39	0.23	28.472	0.245	moderate
2219.14	0.271	29.038	0.121	good

level or drill	sample ID	Mineral 1	Mineral 2	Oxide 1	Oxide 2
3260W	3260W-BF-23	Phengite	Dolomite	Goethite	GalvanisedIron
3260W	3260W-BF-24	PhengiticIllite	NULL	NULL	NULL
3260W	3260W-BF-25	Phengite	Ankerite	NULL	NULL
3260W	326W-BF-26	Phengite	NULL	NULL	NULL
3260W	3260W-BF-27	Phengite	NULL	NULL	NULL
3260W	3260W-BF-28	Phengite	Siderite	Aspectral	NULL
3260W	3260W-BF-30	Phengite	NULL	NULL	NULL
3260W	3260W-BF-31	Phengite	NULL	NULL	NULL
3285	3285-BF-1	Phengite	NULL	NULL	NULL
3285	3285-BF-2	Phengite	NULL	NULL	NULL
3285	3285-BF-3	Phengite	NULL	NULL	NULL
3285	3285-BF-4	Phengite	NULL	NULL	NULL
3285	3285-BF-5	Phengite	NULL	NULL	NULL
3285	3285-BF-6	Phengite	NULL	Goethite	NULL
3285	3285-BF-7	Phengite	NULL	NULL	NULL
3285	3285-BF-8	Phengite	NULL	Goethite	NULL
3292W	3292W-BF1	Phengite	Dolomite	Goethite	NULL
3292W	3292W-BF2	Phengite	NULL	NULL	NULL
3292W	3292W-BF3	PhengiticIllite	Dolomite	Goethite	NULL
3292W	3292W-BF4	Phengite	NULL	Goethite	NULL
3180	3180E-BF-1	Phengite	Dolomite	Goethite	NULL
3180	3180E-BF-2	Phengite	Ankerite	Goethite	NULL
3180	3180E-BF-3	Phengite	Dolomite	Goethite	NULL
3180	3180E-BF-4	Phengite	NULL	NULL	NULL
3180	3180E-BF-5	Phengite	Ankerite	NULL	NULL

AlOH Wavelength	AlOH Absorption	AlOH Width	Water Absorption	Crystallinity
2218.54	0.255	29.906	0.2	moderate
2219.24	0.264	28.869	0.141	excellent
2218.9	0.0532	27.164	0.0394	poor
2217.88	0.126	27.774	0.0568	excellent
2217.94	0.129	28.041	0.0581	excellent
2218.33	0.0374	28.201	0.0207	poor
2218.7	0.15	28.206	0.0666	excellent
2218.54	0.24	29.116	0.122	excellent
2218.25	0.247	29.093	0.134	excellent
2218.88	0.0489	28.868	0.011	poor
2218.98	0.153	27.367	0.078	excellent
2218.66	0.218	28.343	0.108	excellent
2219.52	0.119	26.882	0.0574	excellent
2218.3	0.3	29.794	0.16	excellent
2218.13	0.198	29.393	0.0921	excellent
2219.26	0.133	27.044	0.0649	excellent
2219.16	0.289	28.835	0.209	moderate
2219.11	0.263	28.487	0.143	excellent
2217.37	0.177	29.165	0.0959	moderate
2218.71	0.265	29.579	0.141	excellent
2218.26	0.229	29.723	0.101	moderate
2218.2	0.138	28.333	0.0556	moderate
2218.79	0.307	29.986	0.13	moderate
2217.8	0.292	29.608	0.167	excellent
2218.07	0.236	28.818	0.131	excellent

level or drill	sample ID	Mineral 1	Mineral 2	Oxide 1	Oxide 2
3180	3180E-BF-6	Phengite	NULL	Goethite	NULL
3180	3180E-BF-7	Dolomite	Phengite	Goethite	NULL
3180	3180E-BF-8	Phengite	NULL	Goethite	NULL
3180	3180W-BF-1	Phengite	NULL	NULL	NULL
3180	3180W-BF-2	Ankerite	Phengite	NULL	NULL
3180	3180W-BF-3	Phengite	NULL	Goethite	NULL
3180	3180W-BF-4	Phengite	Calcite	Goethite	NULL
3180	3180W-BF-5	Calcite	Phengite	NULL	NULL
3180	3180W-BF-6	Phengite	Calcite	NULL	NULL
3180	3180W-BF-7	Phengite	Dolomite	Goethite	NULL
3180	3180W-BF-8	Phengite	Calcite	Goethite	NULL
3180	3180W-BF-9	Siderite	Phengite	NULL	NULL
3180	3180W-BF-10	Phengite	Ankerite	NULL	NULL
3180	3180W-BF-11	Phengite	NULL	Goethite	NULL
3180	3180W-BF-12	Phengite	Ankerite	Goethite	NULL
3180	3180W-BF-13	Phengite	Dolomite	Goethite	NULL
3275	3275-BF-1	Dolomite	Marker	Goethite	NULL
3275	3275-BF-2	Phengite	NULL	NULL	NULL
3275	3275-BF-3	Phengite	NULL	Goethite	NULL
3275	3275-BF-4	Phengite	NULL	NULL	NULL
3275	3275-BF-5	Phengite	NULL	Goethite	NULL
3275	3275-BF-6	Phengite	NULL	NULL	NULL
3275	3275-BF-7	Phengite	NULL	NULL	NULL
3275	3275-BF-8	Phengite	NULL	Goethite	NULL
3275	3275-BF-9	Phengite	NULL	Goethite	NULL
3275	3275-BF-10	Calcite	Phengite	Goethite	NULL

AlOH Wavelength	AlOH Absorption	AlOH Width	Water Absorption	Crystallinity
2217.62	0.305	30.465	0.18	excellent
2209.14	0.0932	26.113	0.104	poor
2218.63	0.112	29.66	0.0403	excellent
2218.69	0.186	28.169	0.0956	excellent
2218.71	0.0824	28.15	0.115	poor
2218.83	0.168	27.169	0.0871	excellent
2217.75	0.192	29.301	0.196	poor
2218.11	0.0389	28.557	0.0697	N/A
2217.24	0.139	29.214	0.157	poor
2216.87	0.115	29.466	0.076	moderate
2218.79	0.226	28.388	0.213	poor
2217.42	0.0522	28.451	0.0343	N/A
2218.28	0.142	28.395	0.0918	moderate
2218.92	0.096	26.962	0.0467	excellent
2218.45	0.245	29.517	0.109	good
2218.17	0.216	29.734	0.106	moderate
2218.53	0.0621	29.76	0.117	poor
2219.36	0.255	28.706	0.143	excellent
2218.67	0.235	29.257	0.111	excellent
2218.5	0.186	28.396	0.0934	excellent
2218.13	0.344	30.293	0.191	excellent
2218.76	0.204	28.925	0.0979	excellent
2218.45	0.178	28.552	0.0873	excellent
2218.32	0.196	28.864	0.0886	excellent
2218.53	0.188	27.978	0.1	poor
2216.83	0.0759	30.299	0.127	excellent

level or drill	sample ID	Mineral 1	Mineral 2	Oxide 1	Oxide 2
3275	3275-BF-11	Phengite	NULL	Goethite	NULL
3275	3275-BF-12	Phengite	NULL	Goethite	NULL
3320	3320-BF-1	Phengite	Magnesite	Goethite	NULL
3320	3320-BF-2	Phengite	Siderite	Goethite	NULL
3320	3320-BF-3	Phengite	NULL	NULL	NULL
3320	3320-BF-4	Phengite	NULL	Goethite	NULL
3320	3320-BF-5	Phengite	Dolomite	Aspectral	NULL
3320	3320-BF-6	Phengite	NULL	Goethite	NULL
3260W	3260W-LR-1	Phengite	NULL	NULL	NULL
3260W	3260W-LR-2	Phengite	NULL	NULL	NULL
3260W	3260W-LR-3	Phengite	NULL	NULL	NULL
3260W	3260W-LR-4	Phengite	NULL	NULL	NULL
3260W	3260W-LR-5	Phengite	NULL	Goethite	NULL
3260W	3260W-LR-6	Phengite	NULL	NULL	NULL
3260W	3260W-LR-7	Phengite	NULL	Goethite	NULL
ST02-21	DC02-21-1	Phengite	Ankerite	Aspectral	NULL
ST02-21	DC02-21-2	Phengite	Ankerite	NULL	NULL
ST02-21	DC02-21-3	Phengite	Ankerite	NULL	NULL
ST02-21	DC02-21-5	Phengite	Dolomite	Goethite	NULL
ST02-21	DC02-21-6a	Phengite	Dolomite	Goethite	NULL
ST02-21	DC02-21-6b	Phengite	Magnesite	NULL	NULL
ST02-21	DC02-21-10	Phengite	NULL	NULL	NULL
ST02-21	DC02-21-10	Phengite	NULL	NULL	NULL
ST02-21	DC02-21-9	Calcite	NULL	NULL	NULL
ST02-21	DC02-21-10	Phengite	NULL	Goethite	NULL

AlOH Wavelength	AlOH Absorption	AlOH Width	Water Absorption	Crystallinity
2218.72	0.179	27.769	0.0955	excellent
2218.14	0.161	28.548	0.0741	good
2217.73	0.247	29.967	0.0935	moderate
2218.8	0.0612	28.668	0.0183	good
2218	0.0671	28.507	0.0199	excellent
2218.46	0.203	28.716	0.0874	moderate
2218.66	0.0609	28.124	0.0244	excellent
2218.71	0.316	29.973	0.17	excellent
2219.1	0.11	27.204	0.0419	excellent
2218	0.175	28.929	0.0911	excellent
2218.22	0.127	28.068	0.0537	excellent
2216.88	0.056	29.311	0.0165	excellent
2218.56	0.151	27.621	0.0727	excellent
2219.14	0.107	26.768	0.0438	excellent
2218.3	0.144	28.565	0.0609	excellent
2217.77	0.203	28.922	0.0875	moderate
2217.92	0.166	28.441	0.068	moderate
2218.29	0.183	27.93	0.0774	excellent
2219.44	0.134	26.26	0.0606	good
2218.21	0.107	27.836	0.0526	moderate
2217.93	0.0943	28.279	0.0288	moderate
2217.98	0.217	28.402	0.108	excellent
2218.02	0.2	28.063	0.0985	excellent
NULL	NULL	NULL	0.275	N/A
2216.89	0.402	31.372	0.201	excellent

APPENDIX E

UNDERGROUND MAPS

Underground rib mapping within several drifts of the 144 Zone was completed on various levels to identify the locations of breccia types, their contacts, and the relationships between the breccia types. A modified version of the Anaconda mapping approach was used (Einaudi, 1997). Mine-generated base maps displaying the location and geometry of drifts on each level at a 1:20 scale were used as base maps for the mapping project.

Mapping distinguished two distinct breccia locations adjacent to and away from the dike to the west. Breccia adjacent to the dike is located west of the quartz latite dike and to the east of the Carrara limestone. To the north and south, Bonanza King dolomite encapsulates the breccia. Further away from the dike to the west, the breccia is constrained along the Bonanza King-Carrara contact (Appendix E 1)

Appendix E includes maps of the 3292W, 3260W and 3180W levels not included in Chapter 4: Host Rocks, Breccia Types and Alteration.

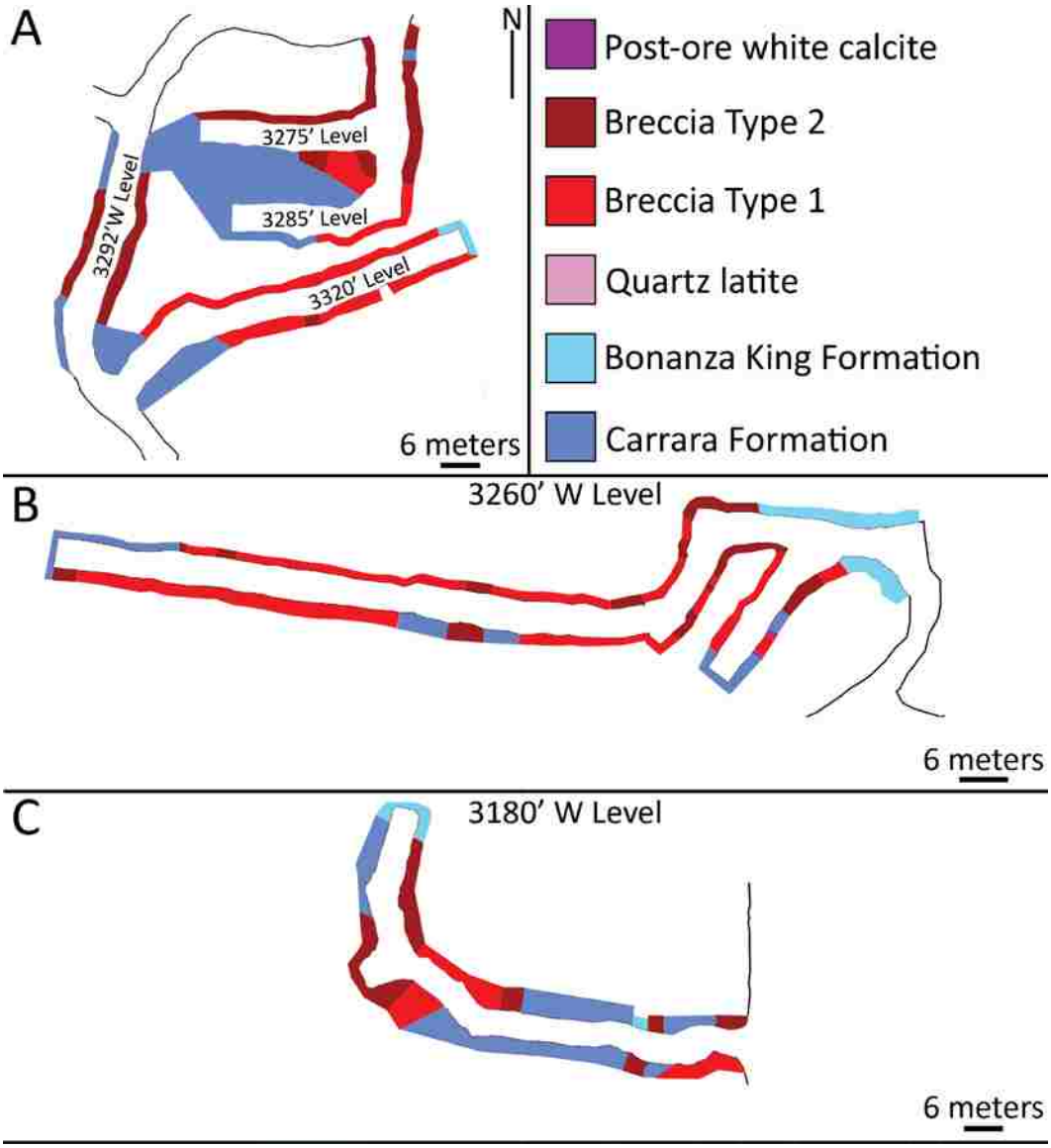

Figure Appendix E 1. Geologic maps of the breccia away from the dike on the 3320' level, 3292' West level, 3285' level, 3275' level (A), 3260' West level (B) and 3180' West (C). Mapped at a scale of 1:20.

REFERENCES

AcmeLabs, *2013,* Acme Price Brochure:. Canada, Accessed: Nov. 2013,, p. 12 & 16.

Armstrong, R. L. and Ward, P.L., 1991, Evolving geographic patterns of Cenozoic magmatism in the North American Cordillera: The temporal and spatial association of magmatism and metamorphic core complexes: Journal of Geophysical Research, v. 96, p. 13,201 – 13,224.

Analytical Spectral Devices, Inc., 2014, Spectroscopy Solutions: Web. 12 Apr. 2014, p. overview, paragraph. 2. <http://www.asdi.com/products/fieldspec-spectroradiometers/fieldspec-4-hi-res>.

Bates, R.L. and Jackson, J.A., 1987, Dictionary of geological terms: American Geological Institute, Virginia, Third edition, 65 p.

Blatt, Harvey, Robert J. Tracy, and Brent Owens., 2006, Petrology: igneous, sedimentary, and metamorphic: New York, Macmillan, Third Edition, 501 p.

Carr, W.J., 1984, Regional structural setting of Yucca Mountain, southwestern Nevada, and late Cenozoic rates of tectonic activity in part of the southwestern Great Basin, Nevada and California: United States Geological Survey, Open-File Report 84-854, 114 p.

Carr, W.J., Byers, F.M. and Orkild, P.P., 1986, Stratigraphic and volcano-tectonic relations of Crater Flat Tuff and some older volcanic units, Nye County, Nevada: United States Geological Survey, Prof. Paper 1, 23 p.

Cas, R., Giordano, G., Balsamo. F., Esposito, A. and Mastro, S., 2011, Hydrothermal breccia textures and processes: Lisca Bianca Islet, Panarea Volcano, Aeolian Islands, Italy: Economic Geology, v. 106, p. 437 – 450.

Castor, S.B. and Weiss, S.I., 1992, Contrasting styles of epithermal precious-metal mineralization in the southwestern Nevada volcanic filed, USA: Ore Geology Reviews, v. 7, p. 193-223.

Cornwall, H.R., 1972, Geology and mineral deposits of southern Nye County, Nevada: Nevada Bureau of Mines and Geology and United States Geological Survey, v. 77 p. 31- 37.

Cornwall, H.R. and Kleinhampl, F.J. 1961, Geologic map of Bare Mountain quadrangle, Nevada 1: United States Geological Survey, p. 3.

Cornwall, H.R. and Kleinhampl, F.J. 1961, Geology of Bullfrog quadrangle and ore deposits related to Bullfrog Hills Caldera, Nye County, Nevada and Inyo County, California: United States Geological Survey, Prof. Paper 1, 32 p.

Einaudi, M.T., 1997, Mapping altered and mineralized rocks. An introduction to the anaconda method: Stanford University, 17 p.

Faulds, J.E., and Christopher, D.H., 2008, Tectonic influences on the spatial and temporal evolution of the Walker Lane: An incipient transform fault along the evolving Pacific-North American plate boundary: Arizona Geological Society Digest, v. 22, p. 437 – 470.

Gillstrom, G., 2006, Technical Report: on the Sterling property 144 Zone: resource summary and exploration proposal: Imperial Metals Corporation, Vancouver, B.C., Canada, 89 p.

Greyback, J. D. and Wallace, A. B., 1991, Gold mineralization at Fluorspar Canyon near Beatty, Nye County, Nevada. In: G.L. Raines, R.E. Lisle, R.W. Schafer and W.H. Wilkinson, eds: Geology and Ore Deposits of the Great Basin, v. 2, p. 935-946.

Hamilton, W. B., 1988, Detachment faulting in the Death Valley region, California and Nevada. Geologic and hydrologic investigations of a potential nuclear waste disposal site at Yucca Mountain, southern Nevada: United States Geological Survey Bulletin 1790, p. 51 – 85

Horton, R.C., 1961, An inventory of fluorspar occurrences in Nevada: Nevada Bureau of Mines and Geology, Report, v. 1 p. 6-8.

Hoisch, T.D. and Heizler, M.T., 1997, Timing of detachment faulting in the Bullfrog Hills and Bare Mountain area, southwest Nevada: Inferences from $_{40}Ar/_{39}Ar$, K-Ar, U-Pb, and fission track thermochronology: Journal of Geophysical Research, v. 102, p. 2815 – 2833.

Jackson, M. R. Jr., 1988, The Timber Mountain magmato-hydrothermal event: an intense widespread culmination of magmatic and hydrothermal activity at the southwestern Nevada volcanic field: Unpublished. M. Sc. Thesis, University of Nevada, Reno, Reno, Nevada, 46 p.

Laznicka, P., 1988, Breccia and coarse fragmentites: Petrology, environments, associations, ores: Developments in Economic Geology, Amsterdam: Elsevier Publishing Co. v. 25 p. 1 – 35 & 363 – 368.

Levy, M., Christie-Blick, N., 1991, Tectonic subsidence of the early Paleozoic passive continental margin in eastern California and southern Nevada: Geological Society of America bulletin, v. 103, p. 1590-1606.

Lincoln, F. C., 1923, Mining districts and mineral resources of Nevada: Newsletter Publishing Company, Nevada City, California. p. 167 – 169.

Mapa, M. R., 1990, Geology and mineralization of the Mother Lode gold mine, Nye County, Nevada. In: R.H. Buffa and A.R. Coyner, eds.: Geology and

Ore Deposits of the Great Basin Symposium, April 1990; Field Trip Guidebook Compendium: Geological Society of Nevada, Reno, NV, p. 1076-1077.

Marvin, R.F., Mehnert, H.H. and Naeser, C.W., 1989, United States Geological Survey: Radiometric Ages– compilation "C" part 3: California and Nevada Isocron/West, New Mexico Bureau of Mines and Mineral Resources, Report, v. 52, p. 3-11.

McCormick, J.E., Evans, L.L., Palmer, R.A. and Rasnick, F.D., 1971, Environment of zinc deposits of the Mascot-Jefferson City District, Tennessee: Economic Geology, v. 66, p. 757 – 762.

Mills Jr., J.G., Saltoun, B. W., and Vogel, T. A. 1997, Magma batches in the Timber Mountain magmatic system, Southwestern Nevada Volcanic Field, Nevada, USA: Journal of Volcanology and Geothermal Research, v. 78, p. 185 – 208.

Meyers, R., Reichmann, M and Brown, C., 2014, North Bullfrog Project, Nevada. Private Report: Corvus Gold Co. North Bullfrog Operation. March, 25th 2014.

Monsen, S.A., Carr, M.D., Reheis, M.C., and Orkild, P.P., 1991, Geologic map and manuscript of Bare Mountain, Nye County, Nevada.: U.S. Department of the Interior, U.S. Geological Survey. Series Map I-2201. p. 1-9.

Morealli, S. and Anderson, T.H., 2008, The Fluorspar Canyon fault: A tilted detachment: Geological Society of America: Cordilleran Section, v. 40, p. 53.

Nevada Bureau of Mines and Geology, 2012, The Nevada mineral industry 2012: Special Publication MI-2012, Mackay School of Earth Sciences and Engineering; Reno, Nevada, 3 p.

Nobel, D.C., Weiss, S.I., and McKee, E.H., 1991, Magmatic and hydrothermal activity, caldera geology, and regional extension in the western part of the southwestern Nevada volcanic field, in G.L., Raines, R.E., Lisle, R.W., Schafer and W.H. Wilkinson, eds.: Geology and Ore Deposits of the Great Basin, v. 2, p. 913 – 934.

Odt, D.A., 1983, Geology and geochemistry of the Sterling gold deposit, Nye County, Nevada. Unpublished. M. Sc. Thesis: University of Nevada, Reno-Mackey School of Mines, Reno, Nevada. 100 p.

Osleger, D. A. and Montanez, I.P., 1996, Cross-platform architecture of a sequence boundary in mixed siliciclastic-carbonate lithofacies, Middle Cambrian, southern Great Basin, USA: Sedimentology, v. 43 p. 197-217.

Palmer, A. R. and Hazzard, J.C., 1956, Age and correlation of Cornfield Springs and Bonanza King Formations in southeastern California and southern Nevada: Bulletin of the American Association of Petroleum Geologists, v. 40 p. 2494 – 2513.

Palmer, A. R. and Halley R. B., 1979, Physical stratigraphy and trilobite biostratigraphy of the Carrara Formation (Lower and Middle Cambrian) in the Southern Great Basin: United States Geological Survey, Government print off (No. 1047). p. 1- 55.

Ransome, F.L., Emmons, W.H. and Garrey, G.H., 1910, Geology and ore deposits of the Bullfrog District, Nevada: United States Geological Survey, Government print off (No. 407). 124 p.

Ren, M., Public Communication. 15 Sept. 2014. Personal Communication.

Sawyer, D. A., Fleck, R. J., Lanphere, M. A., Warren, R. G., Broxton, D. E. 1990, Episodic volcanism in the southwest Nevada volcanic field: New^{40}Ar/Ar^{39} geochronologic results: American Geophysical Union. EOS Transactions, v. 71.43, 1296 p.

Sawyer, D. A., Fleck, R.J., Lanphere, M.A., Warren R.G., Broxton, D.E. and Hudson, M. R., 1994, Episodic caldera volcanism in the Miocene southwestern Nevada volcanic field: Revised stratigraphic framework, 40Ar/39Ar geochronology, and implications for magmatism and extension: Geological Society of America Bulletin, v. 106, p. 1304 – 1318.

Snow, J. K., Asmerom, Y., and Lux, D. R., 1991, Permian-Triassic plutonism and tectonics, Death Valley region, California and Nevada: Geology, v. 19, p. 629-632.

Stewart, J. H., 1966, Correlation of Lower Cambrian and some Precambrian strata in the southern Great Basin, California and Nevada: United States Geological Survey Professional Paper 550, p. C66-C72.

Stewart, J. H., 1970, Late Precambrian Evolution of North America: Plate tectonics Implication: Geology, v. 4(1), p. 11-15.

Taylor, C., McAndless, P., and Rees, C., 2009, Gold-Mineralization in the 144 Zone at Sterling: Stratigraphically and structurally controlled, Carlin-type epithermal gold mineralization in the Southern Walker Lane: Geological Society of Nevada: Great Basin Evolution and Metallogeny, Geological Society of Nevada, Reno, Nevada, v. 2 p. 677-692.

Tingley, J. V., 1984, Trace element associations in mineral deposits. Bare Mountain (fluorine) mining district, Southern Nye County, Nevada: Nevada Bureau of Mines, Prof. Paper, v. 39, p. 28.

Turpault, M.P., Berger, G. and Meunier, A., 1992, Dissolution-precipitation processes induced by hot water in a fractured granite Part 1: Wall-rock alteration and vein deposition processes: European Journal Mineralogy, v. 4, p. 1457-1475.

Wernicke, B, Walk J.D., and Hodges, K.V., 1988, Hanging wall structural evolution of the Tucki Mountain detachment system, Death Valley region, southeastern California: Geological Society of America. Abstracts with Programs. v. 20 p. 242

Wesnousky, S.G., 2005, Active faulting of the Walker Lane: Tectonics. v. 24 p. 1-35.

VITA

Graduate College
University of Nevada, Las Vegas

William T. Fischer
fischerw@unlv.nevada.edu

Degrees:

Bachelor of Science, Geology, 2012
St. Norbert College, De Pere, WI

Thesis Title: Ore classification and breccia formation in the 144 Zone gold deposit: a chemical replacement model Bare Mountain Range, Nevada

Thesis Examination Committee:

Chairperson, Jean S. Cline, Ph. D.

Committee Member, Rodney M. Metcalf Ph. D.

Committee Member, Ganqing Jiang, Ph. D.

Graduate Faculty Representative, Barbara Luke, Ph. D.